

*Digital Comprehensive Summaries of Uppsala Dissertations
from the Faculty of Medicine 2235*

Dynamics of Periprosthetic Bone Metabolism

*Biological Responses to Denosumab and the Clinical
Utility of Metabolic PET/CT Imaging*

CAROLINE SKÖLD



ACTA UNIVERSITATIS
UPSALIENSIS
2026



UPPSALA
UNIVERSITET

Dissertation presented at Uppsala University to be publicly examined in Grönwallsalen, Ingång 70, BV, Akademiska Sjukhuset, Sjukhusvägen, Uppsala, Friday, 10 April 2026 at 09:00 for the degree of Doctor of Philosophy (Faculty of Medicine). The examination will be conducted in English. Faculty examiner: Professor Stephan M H Röhrli (Division of Orthopaedic Surgery, Oslo University Hospital Ullevål (CIRRO), Oslo; Faculty of Medicine, University of Oslo, Oslo, Norway).

Abstract

Sköld, C. 2026. Dynamics of Periprosthetic Bone Metabolism. Biological Responses to Denosumab and the Clinical Utility of Metabolic PET/CT Imaging. *Digital Comprehensive Summaries of Uppsala Dissertations from the Faculty of Medicine* 2235. 128 pp. Uppsala: Acta Universitatis Upsaliensis. ISBN 978-91-513-2750-1.

In four studies, this thesis investigates periprosthetic bone metabolism and the clinical utility of advanced imaging in total joint arthroplasty, with the overall aim of evaluating the biological and densitometric effects of pharmacological bone modulation following total hip arthroplasty (THA) and assessing the diagnostic performance of positron emission tomography/computed tomography (PET/CT) in evaluating painful hip and knee arthroplasties.

Study I examined systemic immunological and bone-related biomarkers after denosumab treatment following THA, finding that denosumab was linked to significant upregulation of receptor activator of nuclear factor κ B ligand (RANKL) and reduced expression of tumour necrosis factor receptor superfamily member 9 (TNFRSF9), suggesting compensatory osteoclastogenesis stimulation potentially driving the ‘rebound phenomenon’ observed after treatment discontinuation.

Study II evaluated the long-term impact of denosumab on periprosthetic bone mineral density (pBMD) following THA. At the five-year postoperative follow-up, no significant differences in femoral or acetabular pBMD were observed between the denosumab and placebo groups. These findings suggest that early densitometric benefits of short-term antiresorptive therapy are transient and do not confer sustained protection against periprosthetic bone loss in this population.

Study III assessed the diagnostic accuracy of fluorine-18 sodium fluoride (18F-fluoride) PET/CT for detecting aseptic loosening in painful hip and knee arthroplasties. The technique demonstrated high accuracy and reproducibility, particularly for THA, but its performance was reduced for certain components in total knee arthroplasty.

Study IV compared 18F-fluorodeoxyglucose (18F-FDG) and 18F-fluoride PET/CT for diagnosing periprosthetic joint infection (PJI) using EBJIS criteria as the reference standard. 18F-FDG PET/CT demonstrated superior diagnostic accuracy, especially for THA stems and tibial components in knee arthroplasties, whereas 18F-fluoride PET/CT showed limited discriminatory capacity. Quantitative SUV_{max} measurements were reproducible across most implant components, supporting their potential role in standardised diagnostic assessment.

In conclusion, short-term denosumab treatment failed to confer sustained preservation of periprosthetic bone after THA. It may induce biological responses—specifically, RANKL upregulation—that contribute to rapid bone loss after treatment discontinuation. PET/CT offers valuable diagnostic support in painful arthroplasties, with 18F-fluoride PET/CT most effective for assessing mechanical loosening and 18F-FDG PET/CT demonstrating superior accuracy for detecting PJI.

Keywords: Periprosthetic bone metabolism, Total joint arthroplasty, Denosumab, Periprosthetic joint infection, PET/CT imaging, Bone mineral density, Diagnostic imaging

Caroline Sköld, Department of Surgical Sciences, Orthopaedics and Handsurgery, Akademiska sjukhuset, ingång 61, Uppsala University, Uppsala, Sweden.

© Caroline Sköld 2026

ISSN 1651-6206

ISBN 978-91-513-2750-1

URN urn:nbn:se:uu:diva-580203 (<http://urn.kb.se/resolve?urn=urn:nbn:se:uu:diva-580203>)

”Motgång danar själen - framgång gör en uppkäftig”

To Jan Bonnerstig and Rolf Andersson, for guiding me toward orthopaedic surgery.

List of Papers

This thesis is based on the following papers, which are cited in the text by Roman numerals.

- I. **Sköld C, Kultima K, Freyhult E, Larsson A, Gordh T, Hailer NP, Mallmin H.** Effects of denosumab treatment on the expression of receptor activator of nuclear kappa-B ligand (RANKL) and TNF-receptor TNFRSF9 after total hip arthroplasty-results from a randomized placebo-controlled clinical trial. *Osteoporos Int.* 2022 Sept;33(9):1–8
- II. **Sköld C, Hailer NP, Mallmin H.** Denosumab prevents early bone-loss in uncemented total hip arthroplasty but gives no long-lasting effects – five-year follow-up of a randomized controlled clinical trial. Re-submitted 2026-01-22
- III. **Sköld C, Sørensen J, Brüggemann A, Hailer NP.** Is 18F-fluoride PET/CT an Accurate Tool to Diagnose Loosening After Total Joint Arthroplasty? *Clin Orthop Relat Res* 2025 March;483(3):415-428
- IV. **Sköld C, Brüggemann A, Lazarinis S, Sørensen J, Hailer NP.** Positron-emission tomography in the diagnosis of prosthetic joint infection: A comparison of 18F-fluorodeoxyglucose with 18F-fluoride. *Manuscript*

Reprints were made with permission from the respective publishers.

Contents

1	Introduction.....	13
1.1	Osteoarthritis	13
1.1.1	Inflammatory changes in OA.....	14
1.1.2	Total hip arthroplasty	15
1.1.3	Total knee arthroplasty.....	16
1.1.4	Inflammatory Responses Following Joint Arthroplasty	17
1.2	Bone Metabolism.....	17
1.2.1	Stress shielding and influence on bone mineral density	20
1.2.2	Aseptic loosening.....	23
1.2.3	“Particle disease”	23
1.2.4	Mechanically induced osteolysis: fluid pressure and supraphysiological loading	24
1.3	Prosthetic joint infection.....	25
1.4	Radiographic outcome measures	27
1.4.1	Radiography	27
1.4.2	Computed tomography.....	28
1.4.3	Dual energy X-ray absorptiometry	28
1.4.4	Positron emission tomography computed tomography.....	29
1.4.5	¹⁸ F-FDG PET/CT – tracer characteristics and differences compared to ¹⁸ F-fluoride	29
1.4.6	PET/CT in diagnosing aseptic loosening.....	31
1.5	Immunological methods to detect proteins from small samples	32
1.5.1	Markers for bone metabolism	32
1.5.2	Enzyme-linked immunosorbent assay	34
1.5.3	Proximity extension assay.....	34
1.5.4	Pharmacological intervention with bone metabolism.....	35
1.5.5	Denosumab.....	36
1.5.6	Rebound phenomenon.....	37
1.5.7	Heterotopic ossification after denosumab treatment.....	37
1.6	DATA study	37
1.7	Outcomes measures	38
1.7.1	EQ-VAS.....	38
1.7.2	Harris Hip Score.....	38
2	Gaps in knowledge.....	39

3	Aims	41
4	Patients and Methods	43
4.1	Ethical considerations	43
4.2	Studies I and II	43
4.2.1	Participants	43
4.2.2	Randomisation and blinding	45
4.2.3	Peri- and postoperative procedures and implants	46
4.2.4	Biochemical markers of bone metabolism	47
4.2.5	Bone mineral density	47
4.2.6	Conventional radiography	47
4.3	Methods specific to study I	48
4.3.1	Analysis of inflammatory response-related proteins	48
4.3.2	Proximity extension assay	48
4.3.3	Enzyme-linked immunosorbent assay	48
4.4	Methods specific to study II	51
4.4.1	Outcome measures	52
4.4.2	Heterotopic ossification	52
4.5	Study III	53
4.5.1	Study Design and Setting	53
4.5.2	Patients	53
4.5.3	Baseline data	53
4.5.4	Surgical Procedures	54
4.5.5	PET Scanning	54
4.5.6	SUVmax evaluation and 18F-fluoride PET/CT analysis	55
4.5.7	SUVmax measurement protocol	55
4.5.8	Primary and secondary study outcomes	57
4.6	Study IV	57
4.6.1	Study design and setting	57
4.6.2	Study population and case selection	58
4.6.3	Reference standard and infection classification	59
4.6.4	PET/CT imaging protocols	59
4.6.5	Image interpretation and SUVmax measurements	62
4.6.6	Outcome measures	62
5	Statistical analysis	63
5.1	Study I	63
5.2	Study II	64
5.3	Study III	64
5.4	Study IV	65
6	Results	67
6.1	Study I	67
6.1.1	Longitudinal change in inflammatory markers	67
6.1.2	ELISA validation of RANKL expression	68

6.1.3	Global mixed-effects model and temporal dynamics of RANKL	69
6.1.4	Temporal pattern of RANKL within the denosumab group	70
6.2	Study II	71
6.2.1	Periprosthetic bone mineral density	71
6.2.2	Longitudinal bone remodelling and radiographic stability	71
6.2.3	Clinical and functional outcomes	74
6.2.4	Safety analysis and complication profile	74
6.3	Study III	75
6.3.1	Quantitative SUV comparisons	75
6.3.2	Diagnostic accuracy and ROC analysis	79
6.3.3	SUV Threshold analysis	80
6.4	Study IV	81
6.4.1	Quantitative SUVmax comparisons for PJI	81
6.4.2	Comparative diagnostic accuracy	82
6.4.3	Radiological FDG-PET/CT interpretation in relation to EBJIS classification	84
7	Discussion	87
7.1	Principal findings	87
7.2	General discussion	88
7.2.1	Study I	88
7.2.2	Study II	91
7.2.3	Study III	93
7.2.4	Study IV	94
7.3	Limitations	97
7.3.1	Study I	97
7.3.2	Study II	97
7.3.3	Study III	99
7.3.4	Study IV	100
8	Conclusion and clinical implications	103
9	Sammanfattning på svenska	107
10	Acknowledgement	109
11	Use of Artificial Intelligence	113
12	References	115

Abbreviations

AP	Anteroposterior
ANCOVA	Analysis of covariance
ASA	American Society of Anesthesiologists
BMD	Bone mineral density
BTM	Bone turnover marker
CFP	Collum femoris preserving
CV	Coefficient of variation
CT	Computed tomography
CTX	C-terminal telopeptide of type I collagen
DATA	Denosumab and total arthroplasty study
DXA	Dual energy X-ray absorptiometry
ECTS	European Calcified Tissue Society
ELISA	Enzyme-linked immunosorbent assay
EQ-5D	EuroQoL – 5 Dimensions
HA	Hydroxyapatite
HCS	Hematopoietic stem cell
HRQoL	Health-related Quality of Life
HHS	Harris hip score
HO	Heterotopic ossification
ICM	International Consensus on Musculoskeletal Infection
IDSA	Infectious Diseases Society of America
IL	Interleukin
KL	Kellgren-Lawrence
LOD	Limits of detection
LRT	Likelihood ratio test
MSC	Mesenchymal stem cell
MSD	Meso Scale Discovery
MSIS	Musculoskeletal Infection Society
NAC	Non-attenuation-corrected
OA	Osteoarthritis
OPG	Osteoprotegin

PACS	Carestream Picture Archiving and Communication System
pBMD	Periprosthetic bone mineral density
PCL	Posterior cruciate ligament
PCR	Polymerase chain reaction
PE	Polyethylene
PET	Positron emission tomography
PEA	Proximity extension assay
PMMA	Polymethyl methacrylate
PINP	Procollagen type I N-terminal propeptide
RA	Reumatoid arthritis
RANK	Receptor activator of nuclear factor kappa-B
RANKL	Receptor activator of nuclear factor kappa-B Ligand
RCT	Randomised clinical trial
ROI	Region of interest
ROS	Reactive oxygen species
SUV	Standardised uptake value
Tc	^{99m} Technetium
THA	Total hip arthroplasty
TKA	Total knee arthroplasty
TNF- α	Tumour necrosis factor alpha
TNFRSF9	Tumour necrosis factor receptor superfamily member 9
XLPE	Cross-linked PE liner
UHMWPE	Ultra-high-molecular-weight polyethylene
WBC	White blood cell
WHO	World Health Organisation
¹⁸ F-FDG	¹⁸ F-fluorodeoxyglucose

1 Introduction

1.1 Osteoarthritis

Osteoarthritis (OA) is a degenerative disease affecting both the articular cartilage in the joint and the underlying subchondral bone. Characterised by the progressive loss of cartilage, joint space narrowing, subchondral sclerosis, and synovial inflammation, OA is increasingly understood as a pathology involving the entire joint unit (Hunter & Bierma-Zeinstra, 2019). Clinical symptoms typically include stiffness, reduced range of motion, and varying degrees of joint pain. Notably, a disjunction often exists between clinical and radiological findings; many patients with radiographic evidence of OA remain asymptomatic, while others experience symptoms that fluctuate in a cyclical pattern. The prevalence of hip OA correlates strongly with age, peaking in the cohort over 85 years, where the disease affects approximately 10% of the population (Danielsson & Lindberg, 1997). While the overall prevalence is similar between sexes, the incidence varies significantly by anatomical location.

Primary OA is a multifactorial, whole-joint pathology characterised by progressive cartilage degradation and remodelling of the subchondral bone. Its aetiology is driven by an interplay of advanced age, genetic predisposition, and obesity. Clinically, primary OA often presents as a polyarticular condition, frequently involving the weight-bearing joints of the hips, knees, and spine, as well as the distal interphalangeal joints of the fingers (Hatzikotoulas et al., 2025).

Secondary OA arises from specific underlying aetiologies or predisposing factors that precipitate joint damage, such as traumatic injury, congenital joint abnormalities, or systemic inflammatory conditions like rheumatoid arthritis. This form of OA is usually localised to specific joints that have been subjected to prior mechanical stress or inflammatory processes (Bijlsma et al., 2011). The first line of OA management prioritises conservative lifestyle interventions, including weight reduction, physiotherapy, and modification of physical activity levels. When necessary, these non-pharmaceutical approaches are supplemented with pharmaceutical treatments, primarily analgesics and anti-inflammatory medications.

1.1.1 Inflammatory changes in OA

Because of the absence of systemic manifestations and the absence of neutrophils in the synovial fluid, OA was historically categorised as a non-inflammatory arthropathy (Vlad et al., 2011). This classification stands in contrast to traditional inflammatory arthritides, such as rheumatoid arthritis (RA). RA is a chronic autoimmune disorder in which the immune system targets the synovium—the inner lining of the joint capsule—precipitating persistent inflammation, progressive joint destruction and, ultimately, significant structural deformity.

In RA, synovitis reflects a chronic autoimmune process in which a loss of immune tolerance triggers persistent immune activation. This state is sustained by an imbalance between pro-inflammatory cytokines—notably tumour necrosis factor [TNF]- α and interleukin [IL]-1—and anti-inflammatory mediators, such as IL-10 and soluble TNF receptors, which collectively drive chronic synovial inflammation and progressive tissue degradation. These pro-inflammatory cytokines are primarily secreted by activated synovial macrophages, especially at the cartilage-pannus junction. As macrophage-derived TNF α is the pivotal mediator of the disease, its neutralisation can effectively reverse synovitis and arrest the progression of structural joint damage (Brennan & McInnes, 2008).

Nevertheless, as previously noted, the presence of a significant inflammatory component—manifesting clinically as joint swelling, stiffness, and pain—is now well recognised in the pathogenesis of OA. Pro-inflammatory cytokines, chemokines, and other inflammatory mediators are synthesised not only within the synovial tissue but also by the chondrocytes themselves; these markers are detectable within the synovial fluid of OA patients (Goldring & Otero, 2011).

At the onset of OA, chondrocytes respond via stress- and inflammation-induced signalling pathways, leading to cellular dysfunction, apoptosis, and the upregulated expression of pro-inflammatory and catabolic genes. These include nitric oxide synthase-2 (NOS2), cyclooxygenase-2 (COX2), matrix metalloproteinase (MMP)-13, and a disintegrin and metalloproteinase with thrombospondin-1 motifs (ADAMTS)- 4 and 5. Simultaneously, synovial inflammation is characterised by the infiltration of mononuclear cells into the synovial membrane and the local secretion of pro-inflammatory mediators, such as IL-1 β and TNF- α (Bondeson et al., 2010; Goldring & Otero, 2011).

Matrix metalloproteinases and cysteine cathepsins B and S, alongside IL-6, are detectable within OA synovial fluid samples. However, their concentrations are significantly lower than those observed in RA patients, a disparity

that demonstrates the more pronounced and aggressive inflammatory processes characteristic of the RA joint environment (Pozgan et al., 2010).

Despite substantial advances in our understanding of inflammatory mediators in OA over the past decade, further research is needed to elucidate how these factors disrupt homeostasis, ultimately leading to matrix destruction and chondrocyte apoptosis. When subjected to stress or inflammatory stimuli, OA chondrocytes synthesise a range of matrix-degrading enzymes, notably metalloproteinases and aggrecanases; the dysregulated expression of these enzymes is a primary driver of cartilage degradation. However, the overlapping signalling pathways shared by inflammatory and biomechanical stress complicate efforts to determine whether inflammatory mediators act as primary or secondary regulators of joint damage. Identifying early biomarkers and novel therapeutic targets remains essential to developing more effective diagnostic and treatment strategies for OA (Goldring & Otero, 2011).

1.1.2 Total hip arthroplasty

In 1961, Sir John Charnley in Wrightington, Manchester, revolutionised the management of end-stage hip OA by introducing the low-friction artificial joint—the first modern total hip arthroplasty (THA) (Charnley, 1960).

1.1.2.1 Design and Fixation Mechanisms

A THA requires two primary components fixed to the host bone: the femoral stem and the acetabular cup. In contrast to Charnley's original monobloc design, contemporary femoral stems are largely modular. This modularity allows for a variety of sizes, caput-collum-diaphyseal (CCD) angles, neck lengths, and offsets, enabling the surgeon to restore the patient's native anatomy with high precision. Fixation of these components is achieved either through bone cement (polymethylmethacrylate, PMMA) or via direct osseointegration. The latter requires a “press-fit” design to ensure primary stability and minimise micromotion during the initial postoperative months.

1.1.2.2 Materials and Osseointegration

Stem and cup designs have evolved significantly to address early challenges such as infection and aseptic loosening. To overcome initial issues with cement failure, porous coatings of cobalt-chrome, stainless steel, and titanium were introduced to facilitate biological fixation. Furthermore, surface materials that mimic bone architecture, such as calcium phosphates, were introduced in the 1980s to promote bone ingrowth and enhance initial stability (Furlong & Osborn, 1991; Geesink et al., 1987). Hydroxyapatite (HA) is a prominent

example of these materials; it may accelerate ingrowth and increase the likelihood of overbridging significant bone-to-implant gaps.

1.1.2.3 Clinical Stability and Complications

The long-term success of the implant is intricately linked to its initial migration pattern. Kärrholm et al. (1997) demonstrated that femoral stem subsidence or proximal migration of the acetabular cup exceeding 1.0–2.0 mm is a strong indicator of an increased risk for early or intermediate-term revision. Despite these advancements, two major complications were identified in early porous and experimental coatings. First, non-circumferential porous titanium coatings were associated with osteolysis—a wear-related process—likely caused by joint fluid and debris infiltrating the medullary canal (Thanner et al., 1999). Additionally, fully coated stems often led to proximal periprosthetic bone loss, a phenomenon known as "stress shielding," in which load is predominantly transferred to the distal bone (Engh et al., 1987, 1992).

1.1.3 Total knee arthroplasty

The modern era of total knee arthroplasty (TKA) began in the mid-20th century, marked by a pivotal transition from constrained, hinged prostheses to less constrained condylar designs. This shift established the fundamental principles underlying contemporary knee replacement surgery (Shiers, 1954; Walldius, 1957). A critical conceptual advancement was the introduction of the "gliding principle," in which a metallic femoral component articulates against a polyethylene (PE) tibial surface. This dual-surface articulation remains the hallmark of modern TKA design, mimicking the knee joint's natural rolling and gliding kinematics.

Contemporary TKA systems involve the resurfacing of the distal femoral and proximal tibial articulating surfaces with distinct, non-linked components. These systems are typically classified according to the management of the posterior cruciate ligament (PCL) and the articulation mechanism, namely fixed-bearing or mobile-bearing designs (Affatato, 2015). Over recent decades, implant development has been primarily directed towards mitigating PE wear, particulate debris, periprosthetic osteolysis, and aseptic loosening. These advancements have been achieved through the refinement of implant geometry and significant innovations in PE material properties, such as the introduction of highly cross-linked polyethylene (Argenson et al., 2012; Buechel & Pappas, 1986; Insall et al., 1982).

Ultra-high-molecular-weight polyethylene (UHMWPE) was established as the standard bearing material, subsequently followed by the introduction of highly cross-linked and antioxidant-stabilised PE. These innovations have

significantly reduced wear-related complications and improved the long-term longevity of the implant (Kurtz et al., 2011).

In TKA, cemented fixation using PMMA remains the gold standard; however, recent evidence suggests that cementless fixation may yield comparable clinical outcomes in selected patient populations (Meneghini & Hanssen, 2008; Prasad et al., 2020). This stands in marked contrast to THA, where cementless fixation has become the predominant approach internationally.

1.1.4 Inflammatory Responses Following Joint Arthroplasty

Although joint replacement surgery has become a highly standardised intervention, our understanding of its systemic and local influence on the inflammatory response remains relatively limited. In a prospective longitudinal cohort study, Cassuto et al. (2018) investigated the inflammatory cascade following THA. Their findings revealed a pronounced initial surge in pro-inflammatory cytokine expression, marking the primary peak in the immediate postoperative inflammatory profile.

Despite these insights into the immediate post-THA inflammatory dynamics, a significant gap remains in the literature regarding the broader, longitudinal impact of joint replacement surgery on inflammatory markers. Further research is needed to elucidate the long-term patterns and clinical implications of chronic inflammation following arthroplasty. Specifically, it remains unclear how these sustained inflammatory profiles may influence critical outcomes, such as biological implant osseointegration, periprosthetic bone resorption, and the subsequent risk of aseptic loosening.

1.2 Bone Metabolism

Bone is a highly dynamic tissue that undergoes continuous remodelling through a precise equilibrium between formation and resorption. This homeostatic balance is essential for maintaining both structural integrity and the metabolic functions of the skeleton. Bone is composed of a cellular component embedded within a calcified extracellular matrix. The three primary cell types include osteoblasts, responsible for bone formation; osteoclasts, which facilitate bone resorption; and osteocytes. The latter are derived from osteoblast lineage and constitute over 90% of the cells in the adult skeleton (Sommerfeldt & Rubin, 2001). Osteocytes function as the primary mechanosensors of bone, orchestrating the spatial and temporal recruitment of cells for remodelling—a regulatory mechanism conceptually described as the

“mechanostat” (Burger & Klein-Nulend, 1999; Frost, 1987). The extracellular matrix comprises approximately 30% organic components (predominantly type I collagen) and 70% inorganic minerals (HA) (Olszta et al., 2007).

According to Wolff’s law, bone architecture adapts dynamically to the mechanical loads to which it is subjected; specifically, mechanical forces exert a significant influence over the processes of bone resorption and formation. Consequently, bone mineral density (BMD) decreases in regions of “unloading” and increases in response to mechanical loading (Frost, 1994). This adaptive remodelling ensures that bone mass is strategically distributed to meet functional demands.

Bone remodelling is a lifelong process that depends on the physiological balance between osteoblastic and osteoclastic activity. An imbalance characterised by predominant osteoclast-mediated resorption leads to a net reduction in bone mass, a phenomenon frequently observed in postmenopausal women and elderly men (osteoporosis). Factors such as systemic osteoporosis (characterised by low BMD) and the biological effects of ageing significantly diminish skeletal strength and increase the risk of fracture (Bolamperti et al., 2022; Cummings et al., 1993; Schott et al., 1998). This remodelling occurs within “basic bone multicellular units” and is notably more metabolic and active in trabecular bone than in cortical bone. Furthermore, osteoblasts initiate this cycle by secreting factors that activate osteoclasts to resorb bone.

The interaction mediates the activation and regulation of osteoclasts through the interaction between receptor activator of nuclear factor kappa-B (RANK) and its ligand, RANKL. Expressed on osteoblasts and stromal cells, RANKL binds to RANK on the surface of osteoclast precursors to promote differentiation. This process is tightly regulated by osteoprotegerin (OPG), a decoy receptor that binds RANKL, preventing RANK interaction and inhibiting osteoclastogenesis.

TNF- α contributes to bone remodelling by enhancing RANKL expression and directly stimulating osteoclast differentiation, thereby increasing bone resorption in inflammatory conditions. In contrast, TNFRSF9 (also known as 4-1BB) is a member of the TNF receptor superfamily that can inhibit osteoclast formation and promote osteoblast differentiation, thus playing a protective role in bone metabolism (Figure 1) (Kong et al., 1999; Lam et al., 2000).

Sclerostin, a glycoprotein produced primarily by osteocytes, negatively regulates bone formation by antagonising the Wnt signalling pathway, which is essential for osteoblast activity. Sclerostin expression is upregulated during mechanical unloading and ageing, contributing to reduced bone formation and an increased risk of fracture (Winkler, 2003).

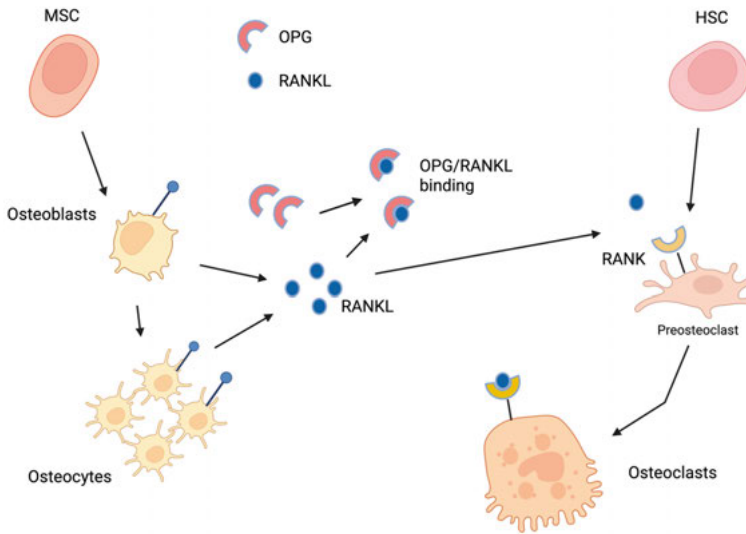


Figure 1 The RANKL/RANK/OPG signalling pathway in osteoclastogenesis. Mesenchymal stem cell (MSC)-derived osteoblasts express RANKL, which binds to its receptor, RANK, on haematopoietic stem cell (HSC)-derived pre-osteoclasts to drive differentiation and activation. Osteoprotegerin (OPG), a decoy receptor secreted by osteoblasts, competitively binds RANKL, thereby inhibiting RANK-mediated osteoclastogenesis and maintaining bone homeostasis.

MSC, mesenchymal stem cell; HSC, haematopoietic stem cell; RANK, receptor activator of nuclear factor κ B; RANKL, receptor activator of nuclear factor κ B ligand; OPG, osteoprotegerin.

During the resorption phase of bone remodelling, coupling factors are secreted to stimulate and recruit osteoblasts to the resorption site to initiate bone formation. Once the absorption lacuna is filled with a volume of bone equivalent to that which was absorbed, the remodelling process concludes with the mineralisation of the new bone matrix (Sommerfeldt & Rubin, 2001).

Periprosthetic BMD (pBMD) loss around the acetabular cup and femoral stem is commonly observed after THA (Digas et al., 2006; Nysted et al., 2011). While initially linked to inflammation resulting from postoperative trauma, this reduction in pBMD is primarily driven by subsequent osteoclast activation. A principal cause is stress shielding, arising from the disparity in stiffness between implant materials and native bone. This altered mechanical loading triggers a cascade that reduces pBMD through osteoclastic bone resorption.

Beyond these mechanical factors, wear represents the gradual abrasion of material from implant surfaces, resulting from mechanical friction and movement between components, particularly in hip and knee prostheses. Over time,

this process generates microscopic debris from materials such as PE, metal, and ceramics, which can trigger a local inflammatory response. These wear particles further exacerbate bone loss by enhancing osteoclastic activity and driving periprosthetic osteolysis.

The type of fixation—whether cemented or uncemented — influences these processes (Sumner, 2015). While the dynamics of pBMD around trabecular acetabular implants remain poorly understood, evidence suggests that pBMD decreases regardless of fixation method (Digas et al., 2006; Lazarinis et al., 2014). In uncemented THA, a clear link exists between periprosthetic osteolysis and acetabular failure, primarily driven by the inflammatory response to PE liner wear debris (Hallan et al., 2006; Thanner et al., 1999). This osteolysis, characterised by localised bone resorption, is triggered by an immune reaction to wear particles; macrophages attempt to phagocytose these particles, inciting chronic inflammation. This, in turn, activates osteoclasts to resorb bone at the bone–implant interface, potentially resulting in aseptic loosening and implant failure (Harris, 1995). Nevertheless, the long-term clinical relevance of proximal pBMD loss and osteolysis specifically around uncemented cups remains unclear (Ollivere et al., 2012).

Proposed regimens to counter pBMD loss include the use of antiresorptive drugs such as bisphosphonates; however, these have shown only transient positive effects on pBMD (Friedl et al., 2009; Muren et al., 2015; Sköldenberg et al., 2006).

1.2.1 Stress shielding and influence on bone mineral density

The load exerted on the leg during weight-bearing is transferred across the joint to the femoral implant and subsequently to the femoral bone. According to Wolff’s law, bone adapts to the mechanical loads to which it is exposed; accordingly, unloaded bone is resorbed through the continuous bone remodelling process, inevitably leading to a loss of BMD. Conversely, the regions of bone that sustain the highest loads will increase in density. Unfortunately, all orthopaedic implants alter load transfer, resulting in specific areas of BMD loss, a phenomenon known as stress shielding. Variations in implant shape and material properties influence this phenomenon to varying degrees, prompting manufacturers to develop designs that minimise stress shielding.

Around the acetabulum, pBMD is commonly assessed using the classification described by Digas et al., which divides the periacetabular bone into five distinct regions known as the Digas zones (Digas et al., 2006). These zones were developed to standardise the evaluation of bone remodelling around the acetabular component following THA, particularly for use with Dual X-ray absorptiometry (DXA) measurements. The five Digas zones are distributed

circumferentially around the acetabular cup and represent anatomically distinct regions of the periacetabular bone. Zone 1 is located superiorly; zones 2 and 3 are positioned anteriorly and posteriorly, respectively, while zones 4 and 5 are situated inferiorly around the acetabular component (Figure 2). This zonal division enables regional assessment of pBMD changes over time and facilitates comparisons among implant designs, fixation methods, and loading conditions.

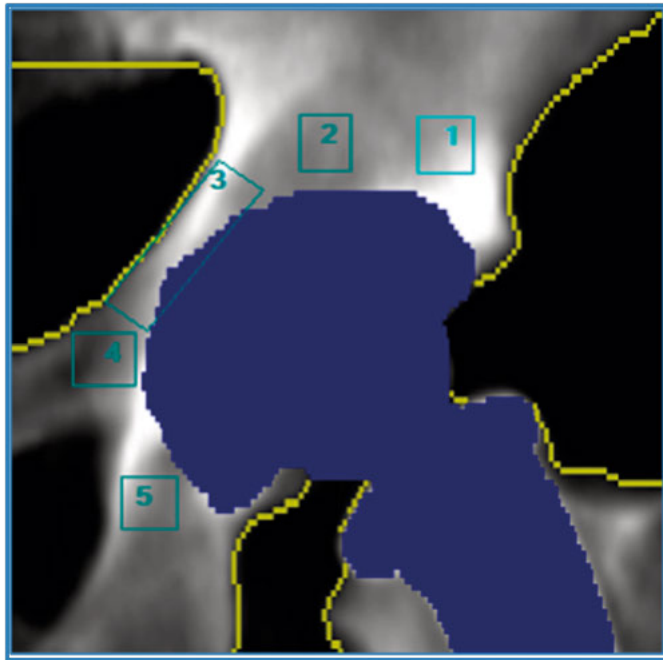


Figure 2 Representative dual-energy X-ray absorptiometry (DXA) scan illustrating the five periprosthetic acetabular regions of interest (ROIs) according to the protocol described by Digas et al. Reprint with permission from Kiritopoulos et al. (2022)

Gruen zones are specific regions around the femoral stem of a hip prosthesis used to assess the implant's fixation and stability on radiographs. These zones were first described by Dr Thomas A. Gruen in 1979 to standardise the analysis of radiographic images following THA. There are seven Gruen zones on the femoral side, numbered from 1 to 7, which are distributed around the femoral stem. The sequence begins at the proximal lateral aspect (zone 1) and moves from the greater trochanter distally along the lateral side of the tip of the stem (zone 4) before continuing medially and proximally towards the lesser trochanter (zone 7) (Figure 3).



Figure 3 Periprosthetic femoral bone mineral density (pBMD) analysis. The dual-energy X-ray absorptiometry (DXA) scan demonstrates the seven periprosthetic regions of interest (ROIs) according to the classification by Gruen et al. Reprinted with permission from Nyström et al. (2019)

Proximal pBMD loss is typically observed in Gruen zones 1, 6, and 7, while gains may occur in zones 3, 4, and 5, as a result of the above-described biological mechanisms (Huiskes, 1990). By altering the proximal coating, manufacturers intend to mitigate the effects of Wolff's law and reduce bone absorption in the proximal femur. Despite these design modifications, calcar stress shielding remains a significant challenge, particularly with uncemented stems (Huiskes, 1990). Minimising stress shielding is a fundamental objective

to preserve the proximal femoral bone stock and facilitate future revision surgery (Sköldenberg et al., 2006).

1.2.2 Aseptic loosening

Aseptic loosening remains the most prevalent indication for revision surgery following THA and TKA (Bozic et al., 2015; Khan et al., 2016). In Sweden, approximately 4,300 THA and total TKA revision procedures are performed annually (W-Dahl et al., 2025). Similarly, in the United States, over 120,000 revision THA and TKA procedures were reported in 2014, with projected increases of 43–70% for revision THA and 78–182% for revision TKA by 2030 (Schwartz et al., 2020). The indications for revision vary over time; while periprosthetic joint infection (PJI) is more prevalent in the early postoperative period, aseptic loosening remains the primary cause of first-time THA revision, according to the Swedish Arthroplasty Register, followed by infection, periprosthetic fracture, and dislocation or instability.

1.2.3 “Particle disease”

Articulating motion in joint prostheses causes wear of implant materials and the subsequent generation of particulate debris. The size, shape, and composition of these wear particles influence the host immune response. Such particles vary not only in material—compromising PMMA, PE, metals, or ceramics—but also in size, ranging from nanometres to micrometres. Each material type and size distribution exerts distinct biological effects on the surrounding tissues.

PMMA particles are typically larger than those generated around uncemented implants. While these larger particles may induce a moderate inflammatory response via macrophage phagocytosis (Sun et al., 2006), the overall osteolytic response to cement debris is generally less aggressive than that elicited by smaller particles, such as those derived from PE. Although cement particles can still lead to bone resorption and subsequent implant loosening, this process tends to progress more slowly. Moreover, the cement mantle distributes mechanical load and reduces micromotion at the bone-implant interface, which may mitigate wear in the short term.

PE particles are highly biologically active, especially in the submicron range (0.1 to 1 micrometre). These particles trigger the innate immune system upon being phagocytosed by macrophages. This phagocytic process induces the release of pro-inflammatory cytokines, including TNF- α , IL-1, and IL-6 (Gallo et al., 2002; Purdue et al., 2007). These cytokines initiate a cascade of inflammatory signals that recruit and activate additional immune cells,

sustaining a persistent, low-grade inflammatory state—a condition often referred to as a chronic foreign body reaction.

Metal particles, particularly those in the nanometre range, can induce both local and systemic inflammatory responses. These are similarly phagocytosed by macrophages, triggering the release of reactive oxygen species (ROS) and pro-inflammatory cytokines. Additionally, metal ions released from these particles may exert toxic effects on surrounding tissues and can induce hypersensitivity reactions in susceptible patients. Larger metal debris can cause direct mechanical damage, further exacerbating wear and particle generation. Metal debris is also associated with clinical conditions such as metallosis, which can lead to extensive tissue necrosis and aseptic loosening (Gallo et al., 2013; Goodman & Gallo, 2019).

Activated osteoclasts resorb bone tissue surrounding the prosthesis, leading to the formation of resorption pits and the subsequent weakening of the bone-implant interface. This progressive bone loss undermines mechanical stability, ultimately leading to aseptic loosening driven by periprosthetic osteolysis. Moreover, inflammatory cytokines not only activate osteoclasts but also impair osteoblast function, thereby suppressing bone formation. This results in a profound imbalance between resorption and deposition, which further exacerbates periprosthetic bone loss. Within this chronic inflammatory environment, fibrous tissue may be deposited in preference to bone; the resulting fibrous membrane lacks the requisite mechanical strength and further compromises the long-term stability of the implant (Carver et al., 2017).

1.2.4 Mechanically induced osteolysis: fluid pressure and supraphysiological loading

In addition to particle-induced osteolysis, mechanical instability has been proposed as a significant contributory mechanism in aseptic loosening. Insufficient primary fixation and early micromotion can generate pressure fluctuations and high interfacial fluid flow; these mechanical stimuli are capable of inducing inflammatory signalling and bone resorption, even in the absence of wear particles (Aspenberg & Herbertsson, 1996; Fahlgren et al., 2010; Skripitz & Aspenberg, 2000).

Transcriptomic analyses have demonstrated that mechanical instability and particulate stimuli elicit largely overlapping inflammatory gene-expression patterns, suggesting convergence on shared osteolytic pathways rather than distinct biological mechanisms (Amirhosseini et al., 2017). At the cellular level, supraphysiological mechanical loading has been shown to promote osteoclastogenic signalling in both murine and human progenitor cells, mediated

in part by fluid shear stress–induced activation of mechanosensitive pathways (Bratengeier et al., 2020, 2022).

Importantly, these mechanobiological mechanisms are considered most relevant in early-stage cases or in specific settings and are unlikely to account for the majority of clinically observed aseptic loosening, which typically develops later and is strongly associated with wear particle–induced osteolysis. Instead, mechanical instability may function as an initiating or permissive factor, increasing susceptibility to subsequent particle-driven bone loss, particularly in uncemented implants.

1.3 Prosthetic joint infection

PJI is a severe complication that occurs when microorganisms—typically bacteria—colonise the surface of a joint prosthesis or invade the surrounding tissue. PJI often leads to debilitating pain, persistent inflammation, and loss of joint function; accordingly, it remains one of the leading causes of failure in joint replacement surgeries.

PJI poses a significant challenge to healthcare systems due to its disabling impact on patients and the requirement for invasive treatments, which carry a risk of serious adverse events. Accurate diagnosis is essential for effective management, and extensive efforts have been made to establish standardised criteria for defining PJI. The Musculoskeletal Infection Society (MSIS) introduced a definition in 2011, which was later refined and subjected to an international consensus review by the International Consensus on Musculoskeletal Infection (ICM) in 2013. That same year, the Infectious Diseases Society of America (IDSA) released diagnostic guidelines developed by an international expert group.

More recently, a new weighted-score definition for PJI was proposed and validated; however, it received support from only 68% of delegates at the 2018 ICM meeting and was not endorsed by the MSIS or the European Bone and Joint Infection Society (EBJIS). While these diverse definitions have underscored the importance of accurate diagnosis and provided reference standards for clinical and diagnostic studies, no single definition has been universally accepted as the ‘gold standard’ in clinical practice. This lack of consensus is likely due to the complexity of diagnostic algorithms, geographical variations in medical practice, the cost of specific tests, and ongoing debates about the accuracy of certain diagnostic methods.

A new definition of PJI, developed by the EBJIS, was recently introduced to enhance diagnostic accuracy and consistency while addressing the limitations of previous criteria (McNally et al., 2021). Designed to be more practical

and adaptable to diverse clinical settings, the EBJIS criteria incorporate both clinical and laboratory findings through a three-tiered diagnostic approach: ‘Infection Confirmed’, ‘Infection Likely’, and ‘Infection Unlikely’. This framework considers factors such as the presence of a sinus tract, microbiological evidence, histopathology, and serum and synovial biomarkers. Ultimately, the EBJIS definition provides a clear, pragmatic tool for diagnosing PJI, thereby improving patient outcomes and facilitating more consistent research comparisons across clinical research (Table 1).

Most recently, a unified international definition was adopted at the 2025 ICM in Istanbul, aiming to harmonise existing diagnostic frameworks and incorporate advances in imaging and microbiology. Under this unified definition, 18F-FDG PET/CT is recognised as a supportive diagnostic criterion for PJI, reflecting the growing evidence that metabolic imaging can detect infection-related inflammatory activity around prosthetic joints. However, PET/CT findings should not be interpreted in isolation; rather, they must be integrated with clinical, microbiological, and histopathological data (*International Consensus Meeting 2025 ICM Istanbul, 2025*).

Table 1 EBJIS definition of periprosthetic joint infection (adapted from McNally et al., 2021). Diagnostic criteria for periprosthetic joint infection according to the European Bone and Joint Infection Society (EBJIS). Infection is categorised as unlikely, likely, or confirmed based on clinical findings, laboratory markers, microbiology, histopathology, and imaging.

Infection likely: requires two positive findings from different diagnostic domains. Infection confirmed: requires any single confirmatory finding.

Abbreviations: ASA = American Society of Anesthesiologists physical status classification; EBJIS = European Bone and Joint Infection Society; CRP = C-reactive protein; PMN = polymorphonuclear neutrophils; HPF = high-power field; WBC = white blood cell; CFU = colony-forming unit.

	Infection unlikely	Infection likely	Infection confirmed
Clinical findings	Alternative non-infectious cause of implant dysfunction	Early radiological loosening (<5 years), wound-healing problems, recent fever or bacteraemia, purulence	Sinus tract communicating with the joint or exposed prosthesis
Serum markers	Normal inflammatory markers	CRP >10 mg/L	—
Synovial fluid (cytology)	Leukocytes ≤1,500 cells/μL PMN ≤65%	Leukocytes >1,500 cells/μL PMN >65%	Leukocytes >3,000 cells/μL PMN >80%
Synovial bio markers	—	—	Positive alpha-defensin (laboratory or lateral-flow assay)
Microbiology	All cultures negative	Single positive culture (aspiration or intraoperative)	≥2 cultures with identical microorganisms
Sonication fluid	No growth	>1 CFU/mL (any organism)	≥50 CFU/mL (any organism)
Histopathology (400×)	No neutrophils	≥2 neutrophils in one HPF	≥5 neutrophils in ≥5 HPFs or visible microorganisms
Nuclear imaging	Negative bone scan	Positive labelled WBC scintigraphy	—

1.4 Radiographic outcome measures

1.4.1 Radiography

Radiography is a medical imaging technique that uses X-ray radiation to visualise the body's internal structures, especially bones. The process involves passing a controlled dose of ionising radiation through the body, which is captured on a detector or film to create an image. Different tissues absorb X-rays to varying degrees; bones, for instance, appear white on radiographs because

of their high density, whereas softer tissues appear in varying shades of grey. This contrast occurs because denser materials absorb more X-ray photons. Radiography remains a fundamental diagnostic tool in orthopaedics, valued for its ability to provide detailed images rapidly and non-invasively.

1.4.2 Computed tomography

Computed tomography (CT) is an advanced imaging technique that uses X-rays to create detailed cross-sectional images of the body. In contrast to standard radiography, which produces a two-dimensional projection, CT uses X-ray sources and detectors that rotate around the patient to capture multiple images from different angles. These data are processed by a computer to generate axial 'slices' and three-dimensional (3D) reconstructions of internal structures (Mayo, 1991). CT is highly valuable for diagnosing a wide range of orthopaedic conditions, including complex fracture patterns, implant positioning, and traumatic soft-tissue injuries, due to its ability to provide high-resolution images of both bone and soft tissue.

1.4.3 Dual energy X-ray absorptiometry

Dual energy X-ray absorptiometry (DXA) is a widely established imaging technique for the assessment of BMD. DXA is based on the differential attenuation of X-ray radiation across two distinct photon energy spectra; this allows discrimination between bone and soft tissue and enables quantification of lean and fat tissue components. Similar to conventional radiography, DXA is a two-dimensional modality that provides areal bone mineral measurements, typically reported as BMD in g/cm^2 .

DXA offers high precision with a minimal radiation dose, typically ranging from 1–5 μSv for scans of the proximal hip or lumbar spine. For comparison, plain radiography of the hip generally results in an effective dose of approximately 0.1–0.6 mSv, while CT of the pelvis typically yields 2–6 mSv, depending on the scan parameters.

The World Health Organisation (WHO) defines osteoporosis based on a DXA-derived T-score of -2.5 or lower. The T-score expresses an individual's BMD in standard deviation (SD) units relative to the mean peak BMD of a healthy young adult reference population. Values between -1.0 and -2.5 are typically categorised as low bone mass (osteopenia), while scores above -1.0 are considered normal. In contrast, the Z-score compares BMD to an age- and sex-matched reference population. It is primarily used for younger individuals and to evaluate potential secondary causes of low bone loss (Kanis, 1994).

DXA is primarily used to diagnose osteoporosis, assess fracture risk, and monitor treatment efficacy in both clinical practice and research settings. The most assessed sites are the lumbar spine and proximal femur, although peripheral skeletal sites and periprosthetic bone are increasingly evaluated. In orthopaedic research, DXA is considered the ‘gold standard’ for the longitudinal monitoring of periprosthetic bone remodelling, as it allows for the precise quantification of mineral changes around both femoral and acetabular components.

1.4.4 Positron emission tomography computed tomography

Positron emission tomography (PET) is an advanced nuclear medicine technology that has become a pivotal tool—not only in research but increasingly in routine clinical diagnostics. The investigation involves administering trace amounts of biologically relevant molecules labelled with radioactive isotopes, such as ¹⁸F-fluoride, and subsequently detecting them via tomography. The resulting images show the regional concentration of radioactivity and can be converted into quantitative measurements of biochemical activity, expressed as standardised uptake value (SUV). When combined with CT (PET/CT), this technique produces 3-D images of bone and its metabolic activity surrounding prosthetic components, such as the femoral stem and acetabular cup.

¹⁸F-fluoride PET/CT measures bone blood flow and metabolic activity, reflecting osteoblastic calcium uptake during bone formation. This imaging method enables visualisation of ongoing metabolic processes associated with bone remodelling. Despite its potential, the application of ¹⁸F-fluoride PET/CT in implant surgery remains limited. Current knowledge about the natural progression of implant fixation, assessed through periprosthetic bone metabolism, is sparse, and the accuracy of this method in this context remains uncertain (Sørensen & Ullmark, 2009; Ullmark et al., 2012, 2013). It is generally assumed that the fluoride isotope is predominantly incorporated by osteoblasts, thereby serving as a marker of osteoblastic activity and new bone formation. Nonetheless, experimental evidence (Bernhardsson et al., 2018) suggests that even non-viable bone may exhibit high tracer uptake, raising questions about the contribution of passive diffusion and the strong affinity of ¹⁸F-fluoride for HA.

1.4.5 ¹⁸F-FDG PET/CT – tracer characteristics and differences compared to ¹⁸F-fluoride

While ¹⁸F-fluoride reflects osteoblastic activity and bone formation, ¹⁸F-fluorodeoxyglucose (¹⁸F-FDG) provides information primarily related to

cellular glucose metabolism. ¹⁸F-FDG is a glucose analogue that enters metabolically active cells via glucose transporters; it is phosphorylated by hexokinase but is not further metabolised, resulting in intracellular trapping proportional to the glycolytic rate.

Within the context of periprosthetic bone and arthroplasty, these two tracers visualise distinct physiological phenomena. ¹⁸F-fluoride uptake reflects bone remodelling and mineralisation, whereas ¹⁸F-FDG accumulation predominantly indicates cellular inflammation, such as macrophage and neutrophil activation. As a result, FDG PET/CT has been proposed as a complementary modality to differentiate aseptic loosening from PJI (Gemmel et al., 2012; Stumpe et al., 2004).

However, the interpretation of ¹⁸F-FDG uptake around implants remains complex. Postoperative inflammatory changes, wear debris-induced synovitis, or mechanical stress can all contribute to increased FDG activity in the absence of infection. Studies have demonstrated that physiologic FDG uptake can persist for several months following arthroplasty, complicating differentiation between infection and aseptic loosening (Kumar et al., 2016b). Alternatively, ¹⁸F-fluoride tends to normalise earlier in uncomplicated cases, as its uptake reflects mineralisation rather than ongoing inflammation (Adesanya et al., 2015).

Although FDG PET/CT demonstrates high pooled sensitivity and specificity for the diagnosis of PJI, substantial inter-study heterogeneity has been reported; this indicates that diagnostic performance varies across clinical settings, thereby limiting its use as a stand-alone confirmatory or exclusionary test (Hu et al., 2022; Kwee & Kwee, 2020). Semi-quantitative approaches using SUVmax or SUV ratios have been explored to improve diagnostic accuracy in differentiating infection from aseptic inflammation. However, no universally accepted cutoff values or standardised interpretation criteria currently exist (Gelderman et al., 2018; Kwee et al., 2018; van Vliet et al., 2018; Wang et al., 2022).

Theoretically, the combined use of ¹⁸F-FDG and ¹⁸F-fluoride PET imaging has the potential to yield complementary insights into periprosthetic metabolism—¹⁸F-FDG reflecting cellular inflammatory activity, while ¹⁸F-fluoride highlights osseous remodelling and fixation processes. Dual-tracer or sequential approaches have therefore been proposed to enhance differentiation between infection, inflammation, and bone turnover around implants, as the tracers target distinct pathophysiological mechanisms. Nevertheless, despite encouraging early experimental and clinical findings, methodological and logistical constraints—including high cost, tracer availability, and lack of standardised protocols—currently constrain the routine clinical application of both

18F-FDG and 18F-fluoride PET/CT in this setting (Kumar et al., 2016b; Lankinen, 2013; Loharkar & Basu, 2023).

1.4.6 PET/CT in diagnosing aseptic loosening

Traditionally, enhanced osteoblastic activity has been assessed using bone scintigraphy following the administration of 99mTechnetium (Tc). Although this technique demonstrates high sensitivity, it is limited by relatively low specificity and modest spatial resolution. Reported diagnostic performance for detecting implant loosening after THA includes a sensitivity of 78%, a specificity of 70%, and an overall accuracy of 74% (Mumme et al., 2005). A large meta-analysis corroborated these findings, reporting pooled sensitivity and specificity values of 85% and 72%, respectively (Temmerman et al., 2005).

To overcome these limitations, indium-labelled white blood cell (WBC) imaging was developed primarily to detect PJI. However, given the restricted diagnostic performance of both Tc-99 bone scintigraphy and indium-labelled WBC scans, more recent nuclear medicine approaches have investigated the use of PET combined with CT, employing the fluoride-18 isotope (18F-fluoride PET/CT), for diagnosing implant loosening. In this technique, fluoride ions exchange with hydroxyl groups in HA on the bone surface, forming fluorapatite at sites of active bone remodelling (Even-Sapir et al., 2007).

18F-fluoride PET/CT has demonstrated acceptable accuracy, with high sensitivity but only modest specificity for aseptic loosening (Sterner et al., 2007). Most studies have relied on qualitative assessment of 18F uptake patterns, while only a limited number have incorporated quantitative analyses (Kobayashi et al., 2011; Koob et al., 2019; Kumar et al., 2016a). Furthermore, intraoperative confirmation of preoperative 18F-fluoride PET/CT findings remains scarce, underscoring the need for more robust validation of this technique.

18F-fluoride was introduced early as a tracer for bone imaging and subsequently used to evaluate hip prostheses (Blau et al., 1962; Creutzig, 1976). It was noted that nonspecific 18F-fluoride uptake typically diminishes between six and nine months after surgery (Creutzig, 1976). Since then, 18 F-fluoride PET, with or without CT, has been used to investigate bone metabolism in osteoporosis—where it has been used to assess treatment-induced changes in bone formation (Berding et al., 1998; Frost et al., 2013; Sheppard et al., 2023)—femoral head necrosis (Schiepers et al., 1998; Ullmark et al., 2011), bone-impaction grafting (Bernstein et al., 2014; Ullmark et al., 2007, 2009), renal osteodystrophy (Messa et al., 1993), and bone malignancies (Araz et al., 2015; Jadvar et al., 2015).

In patients with painful TKAs, 18 F-fluoride PET/CT has demonstrated high sensitivity but limited specificity, with most analyses relying on

qualitative assessment. Moreover, only a subset of patients in these studies underwent revision surgery, thereby limiting the extent of histopathological confirmation of imaging findings (Sterner et al., 2007).

SUVs are commonly used to quantify PET tracer uptake, accounting for the injected dose and patient body weight. Measuring SUV_{max}—the highest SUV within a region of interest (ROI)—around implants may provide a more quantitative approach to analysing 18F-fluoride uptake, potentially improving diagnostic accuracy. However, no study has yet validated the reliability or accuracy of SUV_{max} measurements for diagnosing loosening in total hip or knee arthroplasty. Additionally, increased 18F-fluoride uptake may reflect a range of underlying processes, including infection, which complicates the interpretation of SUV_{max} in the context of implant loosening (Choe et al., 2011; Kobayashi et al., 2011).

Furthermore, although 18F-FDG PET/CT has been increasingly used to detect infection-related inflammatory activity (Basu et al., 2014; Kim & Kim, 2021), its capacity to reliably differentiate PJI from aseptic loosening remains uncertain (Kwee & Kwee, 2020; Verberne et al., 2018). Overlapping inflammatory and bone-remodelling responses may contribute to diagnostic ambiguity (Gelderman et al., 2018; Kiran et al., 2019), and the comparative or complementary value of 18F-FDG and 18F-fluoride PET/CT in differentiating infection from mechanical failure has yet to be clearly established (Kumar et al., 2016a).

1.5 Immunological methods to detect proteins from small samples

1.5.1 Markers for bone metabolism

Biochemical markers are valuable tools for monitoring both bone formation and resorption. They have been widely utilised in basic bone research, epidemiological studies, pharmaceutical development, and randomised controlled trials (RCTs) (Delmas et al., 2000; Kuo & Chen, 2017). Bone turnover markers exhibit a circadian rhythm and are influenced by dietary intake. Therefore, fasting blood samples should be collected in the morning to ensure consistency and reliability.

Type I collagen is the most abundant protein in the human body and is the primary constituent of the extracellular matrix in diverse tissues, including bone, skin, tendons, and ligaments. It is a triple-helix protein composed of three polypeptide chains: two alpha-1 chains ($\alpha 1$) and one alpha-2 chain ($\alpha 2$). These chains coil around each other to form a right-handed helix, creating a

robust and stable structure. A key biochemical marker, serum Procollagen-1 N-Propeptide (PINP), is released during the synthesis of type 1 collagen and serves as a reliable indicator of bone formation. PINP, which is a fragment cleaved from the N-terminal end of the procollagen molecule, is typically analysed using immunochemical electrochemiluminescence. Conversely, the C-terminal telopeptide of type 1 collagen (CTX-1, also known as CrossLaps) is a critical marker of bone resorption and can be quantified via immunoassay (e.g., radioimmunoassay).

At the termini of the collagen molecules, non-helical regions known as telopeptides are present. These regions are essential for the cross-linking of collagen fibres, providing structural integrity to the matrix. CTX-1, or C-terminal telopeptide, is a fragment released during the proteolytic degradation of type 1 collagen. It is located at the C-terminal (carboxy-terminal) end of the collagen molecule (Figure 4).

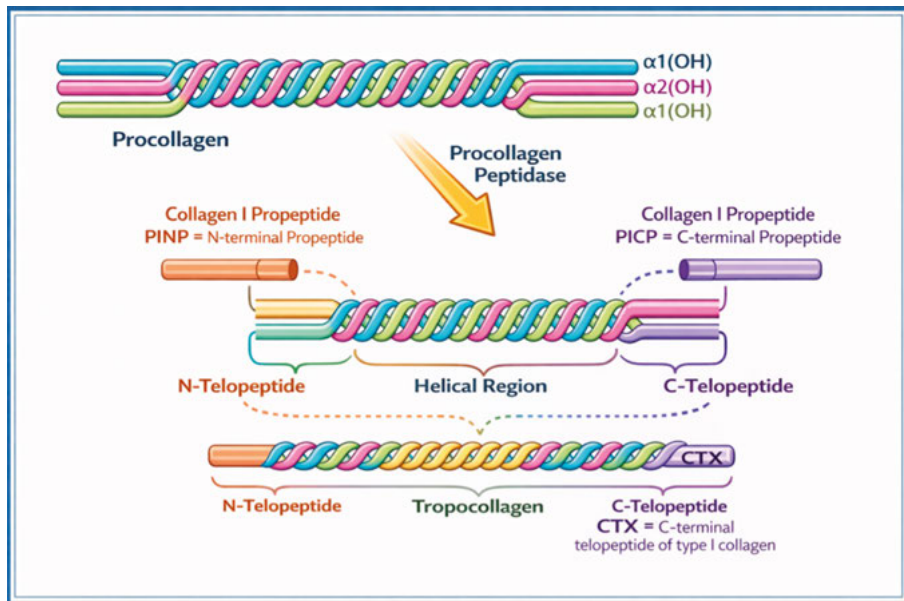


Figure 4 Synthesis and degradation of type I procollagen and the origin of biochemical bone turnover markers. Type I procollagen is synthesised as a triple-helical molecule containing N-terminal and C-terminal propeptides. Extracellular cleavage by procollagen peptidases releases the N-terminal (PINP) and C-terminal (PICP) propeptides, which serve as specific biomarkers of collagen synthesis and bone formation. The resulting tropocollagen molecule comprises a central helical domain flanked by N- and C-telopeptides. During bone resorption, proteolytic degradation of mature, cross-linked type I collagen releases fragments from the C-terminal telopeptide region; these include CTX (C-terminal telopeptide of type I collagen), a highly sensitive and widely utilised marker of osteoclastic bone resorption.

1.5.2 Enzyme-linked immunosorbent assay

Among the four primary types of enzyme-linked immunosorbent assay (ELISA), the sandwich ELISA is the most prevalent. In this method, two specific antibodies—referred to as matched antibody pairs—are employed to ‘sandwich’ the target antigen. The resulting signal is directly proportional to the analyte concentration in the sample. This configuration offers superior sensitivity and specificity, as both antibodies are required to bind the target protein, making it particularly suitable for analysis in complex biological matrices. This procedure is highly effective for quantifying the concentrations of specific biomarkers in clinical samples (Tabatabaei & Ahmed, 2022).

1.5.3 Proximity extension assay

The Proximity extension assay (PEA), developed by Olink Proteomics in Uppsala, Sweden, utilises pairs of antibodies conjugated to oligonucleotides to protein detection and quantification. Upon antibody binding to target proteins, the attached oligonucleotides anneal and are extended by DNA polymerase, generating DNA templates that are subsequently quantified by real-time polymerase chain reaction (PCR) (Figure 5). This technique enables the simultaneous measurement of a large panel of proteins with high specificity and sensitivity—ranging from 92 to 384 biomarkers—while requiring only a few microlitres of biofluid per sample (Assarsson et al., 2014).

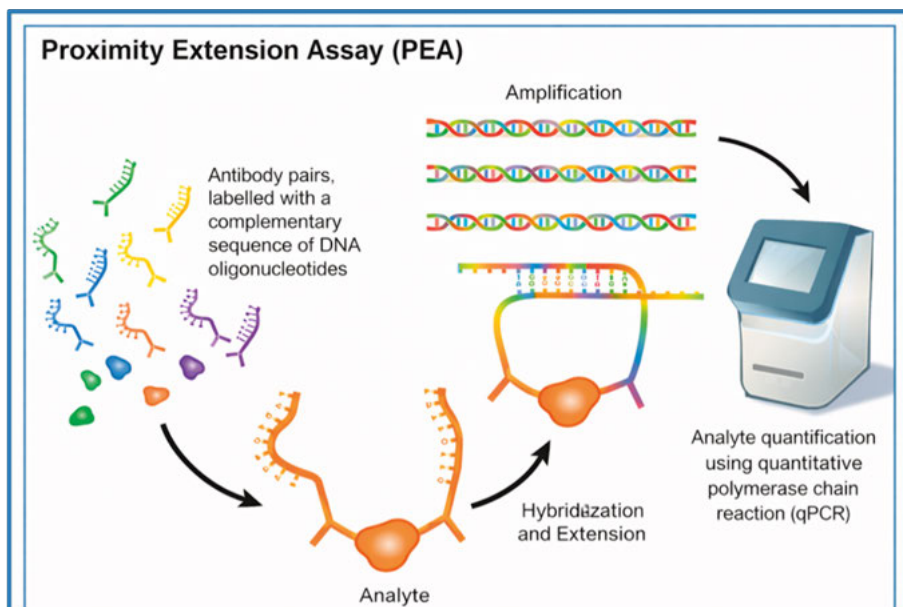


Figure 5 The Proximity Extension Assay (PEA) mechanism for protein detection. Target proteins are recognised by a pair of monoclonal antibodies, each conjugated to a unique, target-specific DNA oligonucleotide. When both antibodies bind simultaneously to the target molecule, their respective DNA tags are brought into close proximity, enabling them to hybridise. Subsequent DNA polymerase-mediated extension forms a stable double-stranded DNA template, which is subsequently amplified and quantified via polymerase chain reaction (PCR). This dual-recognition system ensures high specificity and sensitivity by converting protein concentrations into measurable DNA sequences, thereby minimising the risk of cross-reactivity.

PEA excels at detecting low-abundance proteins that often remain below the detection limit of mass spectrometry. Its multiplexing capacity exceeds that of assays such as Meso Scale Discovery (MSD), which can measure up to 10 biomarkers per well using electrochemiluminescence in 25 μ L samples. The primary advantage of PEA over traditional ELISA and MSD platforms is its ability to quantify a wide range of biomarkers simultaneously from minimal sample volumes.

1.5.4 Pharmacological intervention with bone metabolism

The loss of pBMD is a significant risk factor for implant instability and subsequent revision surgery following total hip and knee arthroplasty (THA/TKA) (Bodén et al., 2006; Sköldenberg et al., 2006). Consequently, pharmacological strategies to modulate bone metabolism have been explored to preserve periprosthetic bone stock and enhance long-term implant fixation.

Bisphosphonates (BPs) are the most widely utilised antiresorptive agents; they bind to bone mineral and are subsequently internalised by osteoclasts to inhibit resorption and promote apoptosis. Clinically, BPs are used to treat osteoporosis by increasing BMD, reducing bone turnover markers, and preventing fractures (Black et al., 2007; Harris et al., 1999; Liberman et al., 1995; Lyles et al., 2007). However, the effects of BP on bone remodelling around orthopaedic implants appear to be transient, with pBMD typically decreasing once treatment is discontinued (Skölden et al., 2011; Venesmaa et al., 2001; Yamasaki et al., 2007).

Beyond bisphosphonates, several other pharmacological agents have been used to modulate bone turnover and increase BMD, including drugs approved for the treatment of osteoporosis and other metabolic bone diseases (Black et al., 2007; Cummings et al., 2009). These agents act through two primary mechanisms: by inhibiting bone resorption or by stimulating bone formation (Kobayashi et al., 2016; Suzuki et al., 2018).

1.5.5 Denosumab

Denosumab, a human monoclonal antibody directed against RANKL, was introduced in 2010. This agent inhibits bone resorption by mimicking the inhibitory effect of OPG on the RANK/RANKL pathway, thereby reducing osteoclast activity and survival. Denosumab is designed to bind specifically to RANKL with high affinity, preventing its interaction with the RANK receptor on the surface of osteoclasts and their precursors. By inhibiting this RANKL-RANK interaction, denosumab effectively suppresses the formation, function, and survival of osteoclasts. This reduction in osteoclastic activity leads to a significant decrease in bone resorption, resulting in diminished bone turnover and a net increase in bone mass and structural strength (Delmas, 2008).

Administered via subcutaneous injection every six months, denosumab significantly improves compliance compared with orally administered BPs (Lekkerkerker et al., 2007). While denosumab increases BMD and reduces fracture risk in postmenopausal women with osteoporosis (Cummings et al., 2009), concerns have been raised regarding a rapid loss of BMD and an increased incidence of vertebral fractures following the discontinuation of long-term treatment. This ‘rebound effect’ necessitates careful clinical management when transitioning patients off the medication to prevent a surge in bone resorption (Tsourdi et al., 2017).

1.5.6 Rebound phenomenon

The ‘rebound phenomenon’ following the discontinuation of denosumab treatment refers to a rapid and marked loss of BMD, accompanied by a heightened risk of fractures (Bone et al., 2011; Miller et al., 2008). Upon discontinuation, bone turnover markers (BTMs) rise substantially, exceeding pretreatment levels. This rebound leads to accelerated bone loss. Hence, BMD frequently returns to or falls below baseline within several months. Furthermore, there is a documented risk of multiple vertebral fractures occurring shortly after treatment termination (Anastasilakis et al., 2017; Cummings et al., 2018).

Current clinical guidelines, including those from the National Osteoporosis Guideline Group (NOGG, UK) and the European Calcified Tissue Society (ECTS), therefore recommend that patients either remain on therapy or be transitioned to bisphosphonates for at least one year following denosumab discontinuation to mitigate this surge in resorption.

1.5.7 Heterotopic ossification after denosumab treatment

Heterotopic ossification (HO) refers to the abnormal formation of lamellar bone within soft tissues, such as muscles, tendons, or other non-skeletal structures. This pathological process frequently occurs following major orthopaedic procedures, traumatic injuries, or specific neurological conditions. Evidence of a potential association between denosumab use and HO development remains sparse (Osaka et al., 2019). However, as HO is a well-recognised complication following THA, it remains unclear whether denosumab could paradoxically stimulate ectopic bone formation in non-osteoporotic patients. Given the drug’s profound influence on bone remodelling, its role in the pathogenesis or prevention of periprosthetic HO warrants further investigation.

1.6 DATA study

The Denosumab and Total Arthroplasty (DATA) study was a placebo-controlled, double-blind RCT involving 64 patients undergoing uncemented THA using the Collum Femoris Preserving (CFP) stem (Waldemar Link GmbH & Co, Hamburg, Germany) and the Continuum cup (Zimmer Co, Warsaw, IN, USA). This phase II study, conducted under the supervision of the Swedish Medical Products Agency, investigated the use of denosumab for this novel indication. The primary outcomes, previously reported by Nyström et al. (2020) focused on changes in femoral pBMD within Gruen zone 7 and the aggregate of Gruen zones 1-7 at 12 months. Secondary outcomes reported by Kiritopoulos et al. (2022) included pBMD changes surrounding the acetabular

cup. The total follow-up period was 24 months, with further secondary outcomes encompassing DXA measurements, biochemical BTMs, and patient-reported outcome measures (PROMs).

The principal finding was that denosumab inhibits pBMD loss around both the stem and the acetabulum 12 months postoperatively. However, this effect diminished following treatment discontinuation, characterised by a rebound in BTMs and a rapid decrease in pBMD during the subsequent year. As there are currently no published long-term data on the use of denosumab to prevent periprosthetic bone loss, further investigation in this field is justified.

1.7 Outcomes measures

PROMs serve as critical endpoints in clinical trials, capturing nuanced data on patient symptomatology, health-related quality of life (HRQoL), and lived experience. Selecting a psychometrically robust, contextually appropriate PROM is fundamental to ensuring the validity and clinical relevance of trial results.

1.7.1 EQ-VAS

The EuroQol Visual Analogue Scale (EQ-VAS) is a standardised, generic instrument designed to provide a quantitative measure of a patient's subjective perception of their overall health status (Rabin & Charro, 2001). Unlike dimension-specific tools, the EQ-VAS captures a global valuation of HRQoL on a vertical, graduated scale.

1.7.2 Harris Hip Score

The Harris Hip Score (HHS) is a clinician-based instrument widely used to evaluate the success of THA by assessing pain, function, absence of deformity, and range of motion (Harris, 1969). Scores range from 0 to 100, with higher values indicating better functional outcomes and less pain. While the HHS is considered the 'gold standard' due to its high validity and responsiveness (Singh et al., 2016), it has faced criticism for a significant 'ceiling effect' (Söderman & Malchau, 2001). In high-functioning postoperative populations, many patients achieve scores at or near 100, which limits the instrument's ability to discriminate between excellent outcomes or to detect further longitudinal improvements (Haverkamp et al., 2008).

2 Gaps in knowledge

The existing literature underscores several critical deficiencies in our understanding of periprosthetic bone management. First, it remains unclear to what extent early pharmacological modulation of osteoclast activity can effectively mitigate the mechanobiological drivers of osteolysis over the long term. Specifically, the capacity for antiresorptive treatment to durably preserve pBMD and significantly alter the longitudinal risk of aseptic loosening following THA remains unproven. Furthermore, the long-term safety profile of denosumab within the arthroplasty context is insufficiently characterised. This includes the potential consequences of treatment discontinuation, such as rebound increases in bone turnover markers and subsequent acceleration of bone loss, which have not been adequately investigated in this specific patient population.

Second, although ¹⁸F-fluoride and ¹⁸F-FDG PET/CT provide quantitative measures of periprosthetic bone turnover and inflammation, respectively, their diagnostic value in defined clinical scenarios remains incompletely characterised. No standardised thresholds for tracer uptake have been established, restricting reproducibility and clinical translation. Moreover, it is uncertain to what extent these modalities can reliably distinguish mechanically driven, particle-induced, and infectious failure mechanisms. Direct comparative studies of ¹⁸F-FDG and ¹⁸F-fluoride PET/CT within the same patient cohorts are lacking, and much of the existing literature predates modern consensus criteria for PJI, thereby limiting its relevance to current practice.

3 Aims

The general aim of this thesis was to improve understanding of biological and diagnostic factors influencing outcomes after total joint arthroplasty, with particular emphasis on periprosthetic bone metabolism and its visualisation. Specifically, the thesis sought to evaluate the potential of denosumab to modulate inflammation and preserve periprosthetic bone stock following cementless total hip arthroplasty, and to assess the diagnostic accuracy of advanced PET/CT imaging modalities in differentiating aseptic loosening from PJI.

- **Study I:** To evaluate whether the capacity of denosumab to modulate the systemic and local inflammatory response following cementless THA in patients with OA.
- **Study II:** To investigate whether postoperative denosumab treatment inhibits late periprosthetic bone loss and to assess the long-term sequelae of treatment discontinuation; specifically, the impact of rebound in bone turnover markers on pBMD, lumbar spine BMD, the contralateral proximal femur, and the incidence of clinical vertebral fractures.
- **Study III:** To determine the diagnostic utility and reliability of 18F-FDG and 18F-fluoride PET/CT as a quantitative measure of periprosthetic bone metabolism in the clinical evaluation of suspected aseptic loosening.
- **Study IV:** To conduct a direct comparison of the diagnostic accuracy of 18F-FDG and 18F-fluoride PET/CT for identifying PJI in patients presenting with symptomatic total hip and knee arthroplasties.

4 Patients and Methods

This thesis presents an extended evaluation of the DATA study (Denosumab in Arthroplasty) cohort. Study I utilises the trial's initial longitudinal data to analyse systemic and local inflammatory markers over the first 24 months post-intervention. Study II provides a long-term follow-up of the same cohort, approximately 60 months after inclusion, and incorporates comprehensive clinical examinations, PROMs, DXA, and conventional radiography to assess late-stage outcomes and the effects of treatment discontinuation.

4.1 Ethical considerations

All studies were conducted in accordance with the principles of the Declaration of Helsinki and adhered to the standards of Good Clinical Practice (GCP). Studies I and II: Ethical approval was granted by the Regional Ethical Review Board in Uppsala, Sweden (Dnr 2011/297/2 and 2007/105/2). For Study II a subsequent amendment was approved by the Swedish Ethical Review Authority (Dnr 2023-04551-02). The DATA study, which served as the source for these studies, was registered at ClinicalTrials.gov (EudraCT 2011-001481-18; NCT01630941). A formal clinical study report was submitted to the Swedish Medical Products Agency in 2018.

Studies III and IV: Ethical approval for Study III was obtained from the Regional Ethics Committee in Uppsala, Sweden (Dnr 2018/338) and the Swedish Ethical Review Authority (Etikprövningsmyndigheten; Dnr 2022-01568-02). Study IV received approval under the same regional framework, with subsequent amendments approved by the Swedish Ethical Review Authority (Dnr 2022-01568-02 and 2025-01499-02).

4.2 Studies I and II

4.2.1 Participants

For Study I, a cohort of 461 patients aged 35–65 years, referred to the Department of Orthopaedics at Uppsala University Hospital, was screened between August 2012 and January 2015. Study II was designed as a *post hoc* analysis

utilising the longitudinal data from Study I and did not require additional patient screening.

4.2.1.1 Inclusion and Exclusion Criteria

Eligibility required radiographic evidence of unilateral hip OA, defined as Kellgren–Lawrence (KL) grade 3–4. Patients were excluded if they presented with contralateral OA exceeding KL grade 1, previous ipsilateral or contralateral THA, or a body weight >110 kg (or BMI >35 kg/m²). Additional exclusion criteria included current or recent treatment with bone-modulating agents or corticosteroids, a history of malignancy, pregnancy, substance abuse, an American Society of Anesthesiologists (ASA) physical class status >3, prior exposure to high-dose radiation, or any comorbid condition considered unsuitable by the investigators. (Baseline data: Table 2)

Table 2 Baseline demographic and clinical characteristics of the study populations in Studies I and II. Data are presented for the denosumab and placebo cohorts participating in the randomised controlled trial.

Characteristic	Denosumab (N=32)	Placebo (N=32)
Age (years), Mean (+/- SD)	58 (5)	59 (5)
Male, n (%)	12 (38)	13 (41)
Body mass index (kg/m ²), Mean (+/-SD)	27 (4)	27 (3)
Kellgren–Lawrence grading, unaffected hip, Median (Min, Max)	1 (0, 1)	1 (0, 1)
Kellgren–Lawrence grading, affected hip, Median (Min, Max)	3 (3, 4)	3 (3, 4)
Harris Hip Score, Median (Min, Max)	58 (28, 81)	51 (33, 77)
CTX (ng/L), Mean (+/- SD), N = 31*	435.9 (192.0)	444.1 (184.2)
P1NP (µg/L), Mean (+/- SD), N = 31*	45.7 (16.2)	44.3 (14.7)
Z-score**, total hip (unaffected hip), Mean (+/- SD)	0.58 (1.13)	0.65 (0.67)
Z-score**, total hip (affected hip), Mean (+/- SD)	0.33 (1.20)	0.33 (0.91)
Z-score**, L1–L4, Mean (+/- SD)	0.91 (1.18)	0.83 (0.91)

A total of 64 participants fulfilled all eligibility criteria and were enrolled in the original RCT. The progression of participants through the study stages is detailed in the flowchart presented in Figure 6.

4.2.2 Randomisation and blinding

Participants were randomised in a 1:1 ratio to receive either denosumab 60 mg (n = 32) or a saline placebo (n = 32). Randomisation was performed using a permuted block design with a fixed block size of four, generated by an independent trial statistician using the PROC PLAN procedure in SAS version 9.4 (SAD Institute Inc., Cary, NC, USA). Sequential treatment assignments were concealed in sealed, opaque envelopes to ensure allocation concealment. The investigators' medicinal products were identical in appearance; consequently, participants, investigators, and outcome assessors remained blinded to treatment allocation throughout the duration of the study.

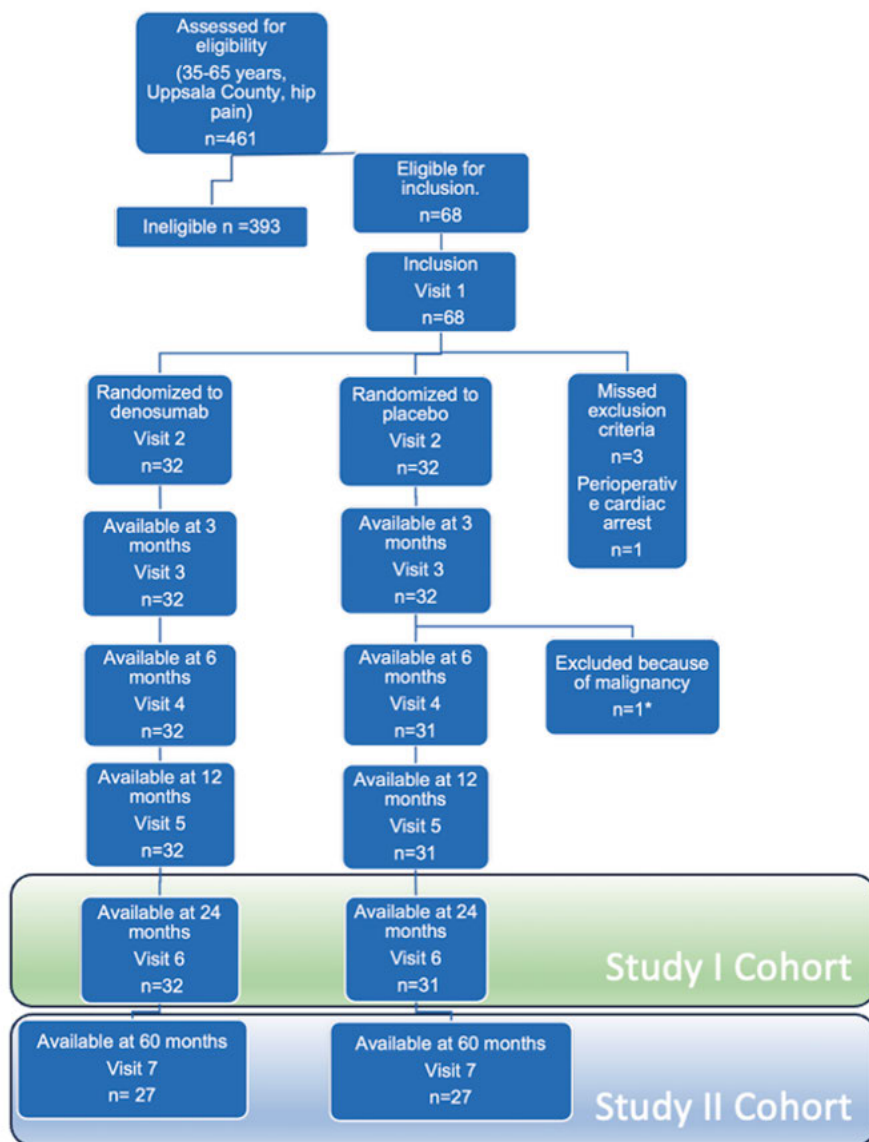


Figure 6 CONSORT flow diagram illustrating the screening, recruitment, and longitudinal follow-up of participants in Studies I and II. The chart shows the distribution of patients between the denosumab and placebo groups from initial inclusion through the five-year final analysis. *EQ-VAS, HHS and biomarkers at 6 months

4.2.3 Peri- and postoperative procedures and implants

All participants underwent cementless THA performed by one of two experienced orthopaedic surgeons. A standardised surgical technique was employed using the Gammer approach (a modified lateral approach). The standardised

implant construct consisted of a Continuum acetabular shell (Zimmer Biomet) fitted with a highly cross-linked PE liner (XLPE), a CFP femoral stem (Waldemar Link, Hamburg, Germany), and a 28-mm cobalt–chromium femoral head. The shell’s apical plug was applied in strict accordance with the manufacturer’s instructions.

The initial subcutaneous injection of denosumab or placebo was administered postoperatively before discharge, followed by a second dose at six months. Baseline DXA scans were performed preoperatively to establish reference BMD. Fasting blood samples were collected 1–3 days after surgery. To ensure calcium and vitamin D₃ homeostasis, all participants initiated daily supplementation (500 mg calcium and 800 IU vitamin D₃) 7–14 days preoperatively. This regimen was maintained for 12 months, corresponding to the active treatment phase of the trial.

4.2.4 Biochemical markers of bone metabolism

Fasting blood samples (1–2 ml) were collected and stored at –70°C until analysis. Two specific biochemical markers were quantified: CTX and PINP, serving as validated indices of bone resorption and bone formation, respectively. Analyses were performed in accordance with ISO 15189 standards, with reported coefficients of variation (CVs) of 3% for PINP and 6% for CTZ.

4.2.5 Bone mineral density

BMD was assessed using a Prodigy Advance DXA system (GE Healthcare, Madison, WI, USA). Preoperative baseline scans included the lumbar spine and both proximal femora in an AP projection. Postoperative assessments, including the 60-month long-term follow-up, quantified pBMD around the femoral stem, in addition to systemic measurements of the lumbar spine and the contralateral (unaffected) hip.

4.2.6 Conventional radiography

AP pelvis and AP/lateral hip projections were obtained preoperatively, with OA severity classified according to the KL system (Kellgren & Lawrence, 1957). Radiographs were repeated at multiple longitudinal follow-up intervals (visits 1, 2, 5, and 7) to assess the periprosthetic interface and identify potential radiographic signs of aseptic loosening, such as progressive radiolucent lines or osteolysis.

4.3 Methods specific to study I

4.3.1 Analysis of inflammatory response-related proteins

Serum samples were analysed using a high-throughput PEA (Olink Proteomics, Uppsala, Sweden). This multiplex platform simultaneously detected 92 inflammation-related proteins. In addition to this proteomic profile, systemic bone turnover markers—specifically P1NP and CTX—were quantified to evaluate the physiological interplay between the inflammatory response and bone metabolism.

4.3.2 Proximity extension assay

Serum samples collected preoperatively and at 3, 6, and 12 months postoperatively were analysed using the Proseek Multiplex inflammation panel (Olink Proteomics, Uppsala, Sweden), a multiplexed PEA immunoassay. This technology facilitates the simultaneous analysis of 92 inflammation-related proteins across 96 samples. (Table 3) For each sample, 1 μ l of serum was incubated overnight in a 96-well plate with 3 μ l of DNA-oligonucleotide-conjugated antibodies.

Following incubation, a PEA enzyme solution containing DNA polymerase was added, enabling the hybridisation of the oligonucleotides to form a unique DNA sequence for each target protein. PCR reagents were then added, followed by a five-minute incubation at room temperature. Quantitative amplification was performed using the BioMark HD System (Standard BioTools, formerly Fluidigm, San Francisco, USA) according to the manufacturer's instructions. Data were normalised on a \log_2 scale using internal controls and a pre-defined correction factor. The limits of detection (LODs) were defined as three standard deviations above the mean background signal.

4.3.3 Enzyme-linked immunosorbent assay

To validate the PEA results for RANKL, serum concentrations were independently measured using a commercial sandwich ELISA (DY626, R&D Systems, Minneapolis, MN, USA). The assay demonstrated a CV of 6%. Testing was performed in a blinded manner, with investigators masked to all clinical data and treatment allocations. ELISA evaluations of RANKL were conducted at all longitudinal intervals, including perioperative baseline and the 24-month follow-up.

Table 3 Comprehensive list of protein biomarkers included in the Olink Target 96 Inflammation panel. *Proteins were analysed using Proximity Extension Assay (PEA) technology as described in Study I.*

UniProt ID	Gene	Protein name
P30203	CD6	T-cell differentiation antigen CD6
P21583	KITLG	Kit ligand
Q14116	IL18	Interleukin-18
Q13291	SLAMF1	Signalling lymphocytic activation molecule
P01135	TGFA	Protransforming growth factor alpha
Q99616	CCL13	C-C motif chemokine 13
P51671	CCL11	Eotaxin
O43557	TNFSF14	Tumour necrosis factor ligand superfamily member 14
Q9GZV9	FGF23	Fibroblast growth factor 23
Q13651	IL10RA	Interleukin-10 receptor subunit alpha
P13236	CCL4	C-C motif chemokine 4
P12034	FGF5	Fibroblast growth factor 5
P42702	LIFR	Leukemia inhibitory factor receptor
Q9NSA1	FGF21	Fibroblast growth factor 21
Q99731	CCL19	C-C motif chemokine 19
Q13261	IL15RA	Interleukin-15 receptor subunit alpha
Q08334	IL10RB	Interleukin-10 receptor subunit beta
Q8N6P7	IL22RA1	Interleukin-22 receptor subunit alpha-1
Q13478	IL18R1	Interleukin-18 receptor 1
Q9NZQ7	CD274	Programmed cell death 1 ligand 1
P01138	NGF	Beta-nerve growth factor
P42830	CXCL5	C-X-C motif chemokine 5
P03956	MMP1	Interstitial collagenase
O14788	TNFSF11	Tumour necrosis factor ligand superfamily member 11
Q969D9	TSLP	Thymic stromal lymphopoietin
P60568	IL2	Interleukin-2
P15692	VEGFA	Vascular endothelial growth factor A
P80098	CCL7	C-C motif chemokine 7
P39905	GDNF	Glial cell line-derived neurotrophic factor
Q9H5V8	CDCP1	CUB domain-containing protein 1
Q9BZW8	CD244	Natural killer cell receptor 2B4
P13232	IL7	Interleukin-7

O00300	TNFRSF11B	Tumour necrosis factor receptor superfamily member 11B
P01137	TGFB1	Transforming growth factor beta-1 proprotein
P00749	PLAU	Urokinase-type plasminogen activator
P05231	IL6	Interleukin-6
P09341	CXCL1	Growth-regulated alpha protein
Q9P0M4	IL17C	Interleukin-17C
Q16552	IL17A	Interleukin-17A
O14625	CXCL11	C-X-C motif chemokine 11
O15169	AXIN1	Axin-1
P50591	TNFSF10	Tumour necrosis factor ligand superfamily member 10
Q9UHF4	IL20RA	Interleukin-20 receptor subunit alpha
Q07325	CXCL9	C-X-C motif chemokine 9
P28325	CST5	Cystatin-D
P14784	IL2RB	Interleukin-2 receptor subunit beta
P01583	IL1A	Interleukin-1 alpha
P13725	OSM	Oncostatin-M
P13500	CCL2	C-C motif chemokine 2
P10145	CXCL8	Interleukin-8
Q8NFT8	DNER	Delta and Notch-like epidermal growth factor-related receptor
Q9NRJ3	CCL28	C-C motif chemokine 28
Q8IXJ6	SIRT2	NAD-dependent protein deacetylase sirtuin-2
Q9NYY1	IL20	Interleukin-20
Q13541	EIF4EBP1	Eukaryotic translation initiation factor 4E-binding protein 1
P02778	CXCL10	C-X-C motif chemokine 10
P80162	CXCL6	C-X-C motif chemokine 6
P49771	FLT3LG	Fms-related tyrosine kinase 3 ligand
P80511	S100A12	Protein S100-A12
P10147	CCL3	C-C motif chemokine 3
P55773	CCL23	C-C motif chemokine 23
P01375	TNF	Tumour necrosis factor
P22301	IL10	Interleukin-10
P09238	MMP10	Stromelysin-2
Q5T4W7	ARTN	Artemin
P35225	IL13	Interleukin-13
Q13007	IL24	Interleukin-24

P29460	IL12B	Interleukin-12 subunit beta
P06127	CD5	T-cell surface glycoprotein CD5
P14210	HGF	Hepatocyte growth factor
P25942	CD40	Tumour necrosis factor receptor superfamily member 5
P01579	IFNG	Interferon gamma
P09603	CSF1	Macrophage colony-stimulating factor 1
P01374	LTA	Lymphotoxin-alpha
P00813	ADA	Adenosine deaminase
P05113	IL5	Interleukin-5
O95630	STAMBP	STAM-binding protein
P50225	SULT1A1	Sulfotransferase 1A1
P78556	CCL20	C-C motif chemokine 20
O43508	TNFSF12	Tumour necrosis factor ligand superfamily member 12
O95760	IL33	Interleukin-33
P20783	NTF3	Neurotrophin-3
P78423	CX3CL1	Fractalkine
O15444	CCL25	C-C motif chemokine 25
Q14790	CASP8	Caspase-8
P80075	CCL8	C-C motif chemokine 8
Q99748	NRTN	Neurturin
P15018	LIF	Leukemia inhibitory factor
P05112	IL4	Interleukin-4
O95750	FGF19	Fibroblast growth factor 19
Q07011	TNFRSF9	Tumour necrosis factor receptor superfamily member 9
P01732	CD8A	T-cell surface glycoprotein CD8 alpha chain

4.4 Methods specific to study II

Study II comprises an exploratory five-year follow-up of the original RCT cohort. Because this longitudinal assessment was not pre-specified in the initial trial registration or study protocol, these mid-term analyses are categorised as *post-hoc* evaluations of secondary and tertiary outcomes. Accordingly, no formal power analysis or additional sample-size calculation was performed for this follow-up phase; rather, the study utilised the maximum available data from the original intention-to-treat population.

4.4.1 Outcome measures

The primary endpoint for Study II was pBMD at 60 months, quantified using DXA within the acetabular ROIs defined by Digas et al. (2004) and the femoral zones described by Gruen et al. (1979). Secondary clinical outcomes included the HHS, EQ-VAS, and implant survival--defined as the absence of any revision surgery involving the femoral stem or acetabular cup. Additionally, back pain was assessed at the 60-month interval. Participants reporting symptomatic back pain underwent thoracolumbar radiography to identify potential vertebral compression fractures.

HO was assessed on AP pelvic radiographs and graded according to the Brooker classification (Brooker et al., 1973). To ensure internal consistency, all radiographic evaluations were performed by a single investigator (CS), who remained blinded to the treatment allocation.

4.4.2 Heterotopic ossification

HO was graded according to the Brooker classification (Brooker et al., 1973) as follows:

- **Grade I:** Isolated islands of bone within the periprosthetic soft tissues.
- **Grade II:** Bone spurs originating from the pelvis or proximal femur, with at least 1 cm remaining between the opposing bone surfaces.
- **Grade III:** Bone spurs from the pelvis or proximal femur, reducing the gap between opposing bone surfaces to less than 1 cm.
- **Grade IV:** Apparent bony ankylosis of the hip, resulting in complete bridging and functional fusion of the joint.

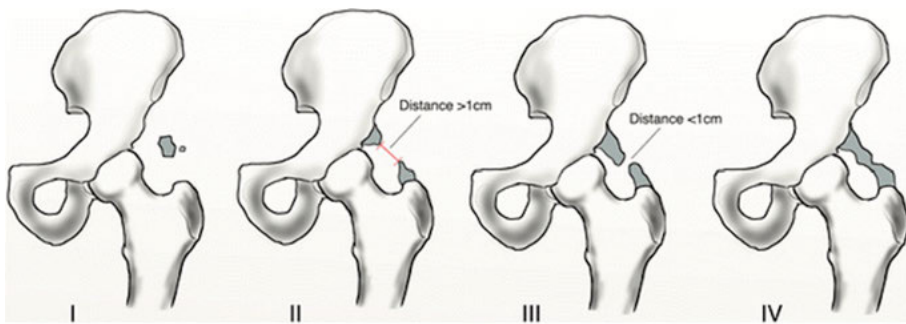


Figure 7 The Brooker classification system for heterotopic ossification. This radiographic grading scale categorises the extent of ectopic bone formation around the hip joint into four stages, ranging from isolated islands of bone (Grade I) to complete bony ankylosis (Grade IV).

Reprinted with permission from Kanakaris and Giannoudis (2015).

4.5 Study III

4.5.1 Study Design and Setting

This was a retrospective diagnostic study evaluating the utility of 18F-fluoride PET/CT in a cohort of 63 patients scheduled for revision total hip or knee arthroplasty between May 2016 and February 2021. The study period was chosen to coincide with the implementation of an updated PET/CT system at the hospital, which enabled standardised and reliable SUV measurements across the entire patient population.

4.5.2 Patients

Within the inclusion period, 689 revision arthroplasties were performed (510 THA and 179 TKA). Of these, 199 patients underwent 18F-fluoride PET/CT as part of the diagnostic work-up for painful THA/TKA. Ultimately, 63 patients met eligibility criteria, having undergone both PET/CT imaging and subsequent revision surgery. Exclusions were primarily due to motion artefacts, bilateral TKA, or technical difficulties in image interpretation. Overall, 9.6% of all revision procedures at the unit were preceded by diagnostic evaluation with 18F-fluoride PET/CT, underscoring its selective but growing role in clinical practice.

4.5.3 Baseline data

The final cohort comprised 41 females and 22 males, with a mean age of 66 years (range: 42-82). Regarding initial implant fixation, 45% were cemented, 32% cementless, and 23% hybrid; all TKAs were cemented. The interval between primary arthroplasty and diagnostic PET/CT assessment ranged from less than 1 year to 23 years, while the duration from PET/CT imaging to subsequent revision surgery varied from 1 month to 36 months. Based on the retrospective evaluation, 81% of cases were classified as 'infection likely', 5% as 'infection likely', and 14% had a confirmed PJI. Demographic and clinical characteristics are summarised in Table 4.

Table 4 Baseline demographic and clinical characteristics of the study population in Study III. Data represent patients undergoing evaluation for symptomatic hip or knee arthroplasty, stratified by final diagnosis.

Characteristic	Hip (N=31)	Knee (N=32)	Overall (N=63)
Gender			
Female, n (%)	61% (19)	69% (22)	65% (41)
Male, n (%)	39% (12)	31% (10)	35% (22)
Age at 18F-fluoride PET/CT (years)			
Mean (range)	67 (42–82)	66 (43–82)	66 (42–82)
Fixation of the revised component			
Cemented, n (%)	45% (14)	100% (32)	73% (46)
Cementless, n (%)	32% (10)	0 (0)	16% (10)
Hybrid, n (%)	23% (7)	0 (0)	11% (7)
Presence of PJI (EBJIS % (n))			
Uninfected	84% (26)	78% (25)	81% (51)
Infection likely	10% (3)	0 (0)	5% (3)
Infection confirmed	6% (2)	22% (7)	14% (9)
Time from original surgery to PET/CT (years)			
Mean (range)	7.8 (0.78–23)	3.7 (0.63–17)	5.7 (0.63–23)
Time from 18F-fluoride PET/CT to revision surgery (months)			
Mean (range)	7.5 (1.0–23)	9.4 (2.0–35)	8.5 (1.0–35)

4.5.4 Surgical Procedures

All revision procedures were performed within the specialised Arthroplasty Unit. Intraoperative assessment of implant stability was conducted by the attending surgeon via direct physical manipulation and visual inspection. To ensure diagnostic consistency, surgical notes were retrospectively reviewed by a senior orthopaedic surgeon. These definitive intraoperative findings served as the reference for the diagnosis of aseptic loosening.

4.5.5 PET Scanning

Imaging was performed on a GE Discovery MI (Digital Photon Counting) PET/CT scanner. A standardised protocol was employed, with an intravenous administration of 3 MBq per kilogram of body weight of 18F-fluoride NaF. For anatomical localisation and attenuation correction, a medium-dose CT scan was performed without intravenous iodine contrast. All images were subsequently archived and analysed using the Carestream Picture Archiving and Communication System (PACS) (Carestream Health, Rochester, NT, USA).

4.5.6 SUVmax evaluation and 18F-fluoride PET/CT analysis

An experienced nuclear medicine physician (JS or colleagues) visually evaluated the 18F-fluoride PET/CT scans as part of routine diagnostics, applying established criteria that focused on the pattern and location of NaF uptake at the prosthesis—bone or cement-bone interface. In addition, two independent observers (CS, orthopaedic surgeon, and AJ, medical student) performed a quantitative assessment of SUVmax values for each implant component (n = 126). Their PET imaging training consisted of a brief structured session led by an experienced nuclear medicine physician (JS), using the Philips Carestream PACS PET/CT viewer routinely employed at the institution. All measurements were documented using archived screen captures, enabling JS to verify them as needed.

4.5.7 SUVmax measurement protocol

The calculation of SUVmax was performed according to the following equation:

$$SUV_{tissue} = \frac{BW * R_{tissue}}{R_{total}}$$

where BW represents the patient's body weight (in grams), R_{tissue} refers to the peak radioactivity concentration measured within the ROI in the tissue (Bq/ml), and R_{total} is the total injected dose of the radiopharmaceutical (Bq). This formula yields a dimensionless index that reflects the relative regional tissue activity normalised to the average radioactivity distribution throughout the body.

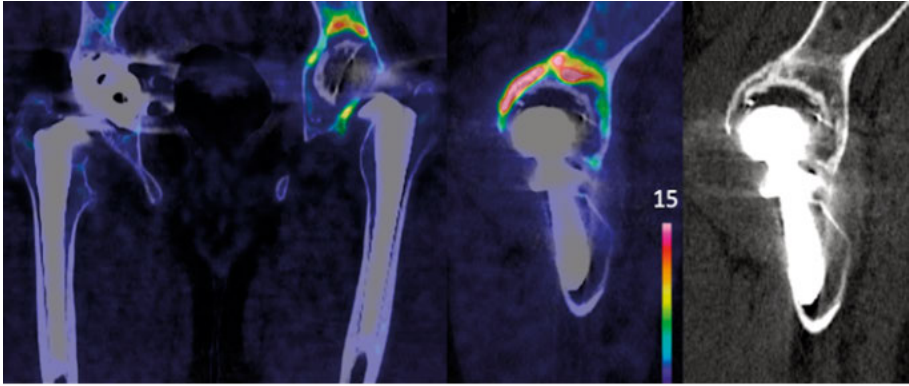


Figure 8 Representative ^{18}F -fluoride PET/CT imaging in total hip arthroplasty. The fused PET/CT image demonstrates focally increased periprosthetic tracer uptake around the acetabular component in a 42-year-old male patient with suspected cup loosening. Quantitative analysis showed higher metabolic activity in the acetabular component (SUVmax 26) compared with the femoral stem (SUVmax 6). The findings are consistent with increased bone turnover associated with acetabular loosening, while femoral stem loosening was reported and later confirmed as well fixed.

Evaluations were performed on attenuation-corrected images, supplemented by a review of potential metal-related artefacts using a non-attenuation-corrected (NAC) window. The initial window for SUVmax was set to 5-80 and was subsequently adjusted based on the specific isotope uptake. Isotope concentrations were colour-coded to facilitate the precise anatomical localisation of the SUVmax.

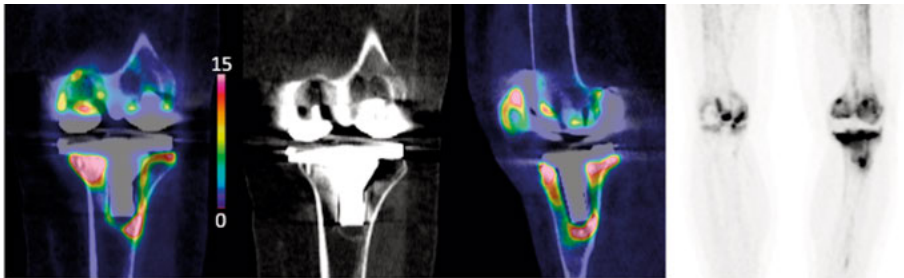


Figure 9 Representative ^{18}F -fluoride PET/CT imaging in total knee arthroplasty. The fused PET/CT image illustrates locally increased periprosthetic bone metabolic activity (tracer uptake) around the femoral component, indicative of accelerated bone turnover. The findings were associated with loosening of both components; infection was clinically suspected but not microbiologically confirmed (EBJIS Infection likely).

Each prosthetic component was systematically examined in the coronal, sagittal, and axial planes. Once the area of the highest periprosthetic uptake was identified, a dedicated ROI was defined. If the SUVmax was localised to the joint component interface, it was interpreted as metabolic activity from arthritic

remnants or synovitis and was deemed irrelevant to the assessment of prosthetic loosening. In such instances, the SUVmax from the next-highest uptake area within the periprosthetic bone was recorded.

All identified SUVmax coordinates were archived via screen captures and stored for future independent verification. The spatial distribution of uptake around the prosthetic components was meticulously documented to identify metabolic patterns suggestive of component loosening. Finally, the diagnostic protocol included SUVmax threshold analysis, in which the two independent observers quantified maximal ¹⁸F-fluoride uptake at the implant-bone interface. This standardised approach was used to differentiate pathologically high uptake associated with loosening from the physiological bone remodelling commonly observed in the residual postoperative period.

4.5.8 Primary and secondary study outcomes

The primary objective was to perform a quantitative comparison of SUVmax values between loose and stable (well-fixed) prosthetic components. Secondary objectives included identifying optimal SUVmax diagnostic thresholds for detecting aseptic loosening and evaluating their diagnostic performance in the subgroup of patients without evidence of PJI.

4.6 Study IV

4.6.1 Study design and setting

Study IV was a retrospective cohort study evaluating the comparative diagnostic performance of two PET/CT tracers—¹⁸F-FDG and ¹⁸F-fluoride—in patients with suspected PJI following THA or TKA. The study was conducted at Uppsala University Hospital, Sweden, where both imaging modalities are routinely used in the clinical workup of symptomatic or diagnostically ambiguous arthroplasties.

Table 5 Patient characteristics by EBJIS infection category (Study IV). Values are presented as mean (SD) or number (%). The cohort comprised 88 patients undergoing PET/CT for evaluation of symptomatic hip or knee arthroplasties, including 69 classified as infection unlikely and 19 as infection likely or confirmed according to EBJIS criteria.

PET/CT = positron emission tomography/computed tomography; THA = total hip arthroplasty; TKA = total knee arthroplasty; EBJIS = European Bone and Joint Infection Society; SD = standard deviation.

Characteristic	Infection unlikely (n = 69)	Infection likely / confirmed (n = 19)	Total (n = 88)
Age at PET/CT, years, mean (SD)	66.8 (10.4)	68.2 (8.9)	67.1 (10.1)
Female sex, n (%)	44 (63.8)	12 (63.2)	56 (63.6)
THA, n (%)	36 (52.2)	9 (47.4)	45 (51.1)
TKA, n (%)	33 (47.8)	10 (52.6)	43 (48.9)
Time from index surgery to PET/CT, years, mean (SD)	3.25 (3.18)	4.09 (5.36)	3.43 (3.74)
Revision surgery, n (%)	24 (34.8)	12 (63.2)	36 (40.9)

4.6.2 Study population and case selection

Patients who underwent both 18F-FDG and 18F-fluoride PET/CT between May 2017 and January 2025 for diagnostic evaluation of suspected arthroplasty complications were identified. To ensure assessment of a consistent underlying biological process, inclusion required both imaging examinations to be performed within a 30-day interval. Eligibility was restricted to patients with either total hip or total knee arthroplasties.

To prevent data interdependence, only one joint per patient was included in the analysis. In cases of bilateral or multiple arthroplasties, the most symptomatic or clinically dominant joint was selected. Where multiple longitudinal paired examinations existed, the chronologically earliest complete pair was retained.

A minor overlap existed between Study III and Study IV. Eleven patients were included in both cohorts. For eight of these patients, the same 18F-fluoride PET/CT examination was used in both studies; SUVmax values were re-extracted and recalculated separately according to each study's specific analysis protocol (Figure 10).

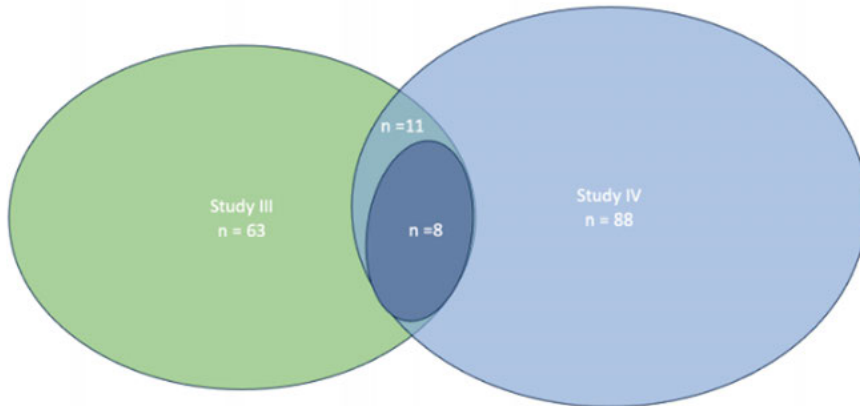


Figure 10 Cohort overlap between Study III and Study IV. Study III included 63 patients and Study IV included 88 patients. Eleven patients were included in both studies (overlapping region). For eight of these patients, the same 18F-fluoride PET/CT examination was used in both studies; SUVmax values were recalculated separately for each study according to the respective analysis protocol.

Examinations performed within six months of the index arthroplasty were excluded to minimise the confounding influence of physiological early postoperative tracer uptake. Furthermore, patients diagnosed with malignancy during the study period or those presenting with periprosthetic fractures were excluded, as these conditions preclude reliable interpretation. Following these exclusions, the final study population comprised 88 patients (45 THAs and 43 TKAs). The participation selection process is detailed in the flowchart presented in Figure 11.

4.6.3 Reference standard and infection classification

Infection status was determined retrospectively according to the EBJIS criteria for PJI. Based on integrated clinical, laboratory, microbiological, and histopathological data, patients were categorised into three tiers: *infection unlikely*, *infection likely*, or *infection confirmed*. To facilitate analysis of diagnostic accuracy and ensure sufficient statistical power, three categories were subsequently dichotomised into ‘Infected’ (*likely* and *confirmed* cases) and ‘Non-infected’ (*unlikely*). This adjudicated classification served as the reference standard for all subsequent evaluations of diagnostic performance.

4.6.4 PET/CT imaging protocols

All PET/CT examinations were performed on a digital PET/CT scanner using standardised clinical protocols. For 18F-FDG PET/CT, patients fasted for at

least six hours, and blood glucose levels were verified before intravenous administration of ^{18}F -FDG (3 MBq/kg). For ^{18}F -fluoride PET/CT, patients received an intravenous injection of ^{18}F -fluoride (3 MBq/kg). Imaging commenced 60 minutes after tracer injection for both protocols. A low- to medium-dose CT scan was acquired for attenuation correction and anatomical localisation, followed by PET acquisition covering the entire prosthetic joint. No intravenous contrast was administered.

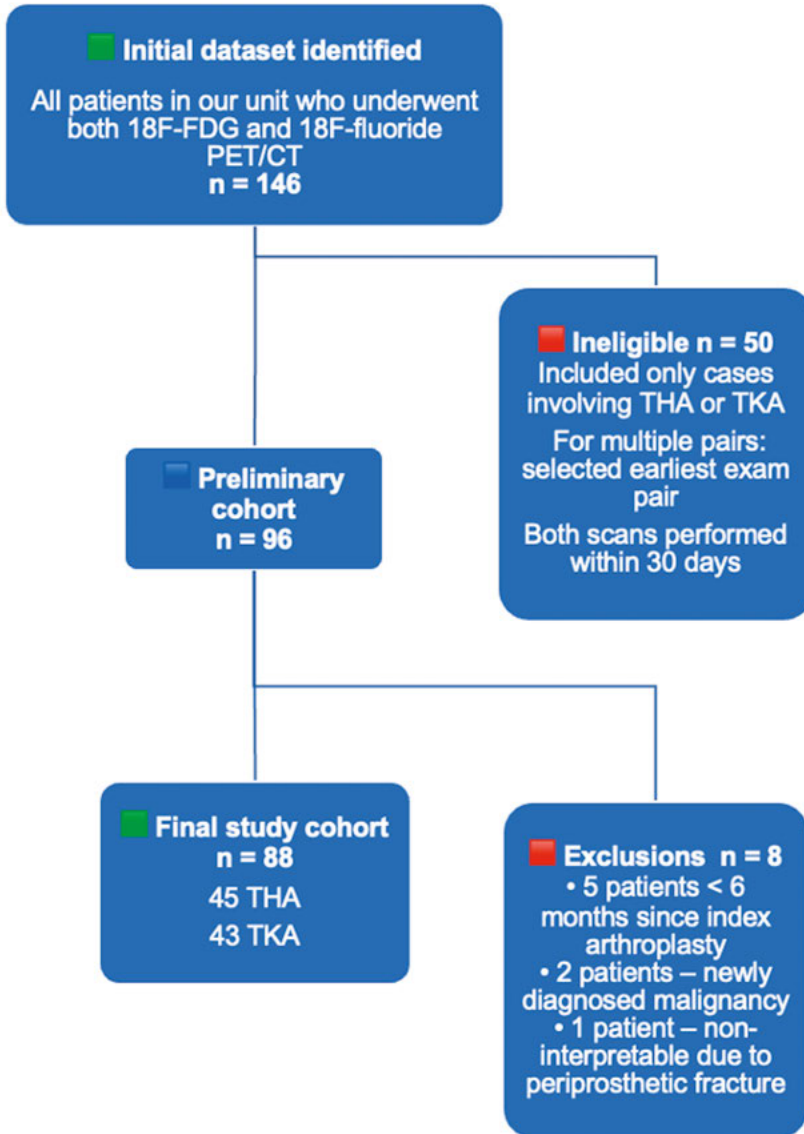


Figure 11 Patient selection process for Study IV. The initial dataset included 146 patients who underwent both 18F-FDG and 18F-fluoride PET/CT scans. After excluding 50 ineligible cases (non-THA/TKA procedures, multiple exam pairs, or scans performed >30 days apart), 96 patients formed the preliminary cohort. Eight additional patients were excluded (five <6 months since index arthroplasty, two with newly diagnosed malignancy, and one with an uninterpretable scan due to periprosthetic fracture), resulting in a final study cohort of 88 patients (45 THA, 43 TKA).

4.6.5 Image interpretation and SUVmax measurements

All PET/CT scans were initially reviewed by consultant nuclear medicine physicians for routine diagnostic purposes. For the specific requirements of this study, semi-quantitative analysis was performed by determining SUVmax. Measurements were meticulously recorded at the bone–implant interface for each prosthetic component: the acetabular cup and femoral stem in THA, and femoral and tibial components in TKA. To ensure diagnostic objectivity, these quantitative assessments were performed by investigators blinded to the final infection status and microbiological findings.

For 18F-FDG PET/CT, measurements were confined to periprosthetic uptake adjacent to the implant, with intra-articular and synovial activity excluded to minimise false-positive findings. For 18F-fluoride PET/CT, regions of increased osteoblastic activity at the bone–prosthesis or cement–bone interface were assessed. All measurements were performed using attenuation-corrected images, while non-corrected reconstructions were systematically reviewed to exclude artefacts.

4.6.6 Outcome measures

The primary outcome of Study IV was the ability of 18F-FDG and 18F-fluoride PET/CT to discriminate between infected and non-infected arthroplasty components based on SUVmax values, using EBJIS classification as the reference standard. Secondary outcomes included diagnostic accuracy assessed by ROC curve analysis and AUC, determination of optimal SUVmax thresholds, correlation between 18F-FDG and 18F-fluoride uptake, and evaluation of intra- and interobserver reliability of SUVmax measurements.

5 Statistical analysis

5.1 Study I

Descriptive statistics were used to compare the baseline characteristics of the trial participants. The proteomic inflammation panel initially quantified 92 proteins; however, Brain-Derived Neurotrophic Factor (BDNF) was excluded due to technical assay inconsistencies, leaving 91 proteins for further analysis. A threshold of 20% was applied for the LOD: 17 proteins exceeding this threshold were excluded from the dataset. Seventy proteins exhibited no values below the LOD and were retained without modification. Four additional proteins had $\leq 20\%$ of values below LOD and were retained, with missing values imputed using the LOD value. The final dataset comprised 74 proteins. Each protein was analysed individually using linear mixed-effects models, with protein levels as the dependent variable. Fixed effects included age, sex, BMI, assay plate, visit, treatment group, and the interaction between visit and treatment. To account for the longitudinal nature of the data, patient identity was incorporated as a random effect.

Likelihood ratio tests (LRTs) were used to evaluate the effects of visit, treatment, and the visit-by-treatment interaction on protein levels, with models adjusted for age, sex, BMI, and platelet count. This analysis yielded global p-values for each protein. To address the risk of type I error inflation from multiple testing, a conservative correction was applied. Recognising the inherent biological interdependence among the 74 inflammation-related proteins, we estimated the effective number of independent tests to be 50 and adjusted the family-wise error rate accordingly.

A Bonferroni correction was subsequently applied, establishing a revised significance threshold of 0.001 (0.05/50). Proteins exceeding this global significance threshold were further examined in *post-hoc* analyses using Tukey's Honest Significant Difference (HSD) test for pairwise comparisons. For these individual comparisons, a $p < 0.05$ was considered statistically significant.

All analyses were conducted using R Statistical Software (version 3.6.3; R Foundation for Statistical Computing, Vienna, Austria).

5.2 Study II

Outcomes were summarised using descriptive statistics and presented as means with standard deviations (SD) or medians with interquartile ranges (IQR), depending on the data distribution. Between-group comparisons at the five-year follow-up were performed using analysis of covariance (ANCOVA). The five-year outcome served as the dependent variable, treatment group as the primary independent variable, and the corresponding baseline measurement was incorporated as a covariate.

Implant revision and the presence of HO were analysed as binary outcomes and summarised descriptively. Between-group comparisons were performed using Pearson's chi-square test or Fisher's exact test, the latter being used where expected cell frequencies were small. Statistical significance for all analyses in Study II was set at $p < 0.05$.

Analyses at the five-year interval were exploratory and were not accounted for in the original sample size calculation. Accordingly, no adjustments for multiple comparisons were made; results should therefore be interpreted with caution, emphasising clinical significance rather than purely statistical thresholds. Missing data at the five-year follow-up were addressed using complete case analysis.

All statistical analyses were conducted using R Core Team software (2021, <https://www.R-project.org>).

5.3 Study III

Data distribution was assessed through visual inspection of histograms and quantile-quantile (Q-Q) plots. Descriptive statistics are reported as means \pm SDs or medians with IQRs, as appropriate. Given that SUVmax values exhibited a predominantly non-normal distribution, the nonparametric Wilcoxon Mann-Whitney U test was used to compare SUVmax between loose and stable (well-fixed) components. These analyses were performed separately for each prosthetic component (acetabular cup, femoral stem, and the femoral and tibial components of the TKA).

Receiver operating characteristic (ROC) curves were constructed to determine the Area Under the Curve (AUC) as a global measure of diagnostic accuracy, with 95% confidence intervals (CIs). Optimal SUVmax thresholds for distinguishing between stable and loose implants were identified using the Youden J statistic, which determines the coordinate on the ROC curve that maximises the combined sensitivity and specificity.

Inter-rater reliability was evaluated using Spearman's rank correlation coefficient (ρ). Furthermore, Bland-Altman plots were generated to assess the

limits of agreement and identify potential systematic bias between the two independent observers. All statistical analyses were conducted using R software (R Core Team; 2021, <https://www.R-project.org>).

5.4 Study IV

Continuous variables were assessed for distributional assumptions via visual inspection of histograms and Q-Q plots; data are reported as means with SDs or medians with IQRs, as appropriate. Given the generally non-normal distribution of SUVmax values for both tracers, non-parametric methods were used for all group comparisons. Differences in periprosthetic tracer uptake between the ‘infection unlikely and the ‘infection likely or confirmed’ cohorts—stratified according to the EBJIS criteria—were analysed using the Mann–Whitney U test at the individual component level.

The diagnostic performance of 18F-FDG and 18F-fluoride PET/CT was evaluated using ROC curve analysis, with discriminative ability quantified by AUC and its 95% CI. Analyses were conducted separately for each arthroplasty component (THA cup, THA stem, femoral TKA component, and tibial TKA component). Exploratory SUVmax thresholds were identified using Youden’s J statistic, but these analyses were interpreted as hypothesis-generating owing to limited subgroup sizes.

Associations between 18F-FDG and 18F-fluoride uptake were examined using Spearman’s rank correlation coefficient to assess the relationship between inflammatory and osteoblastic tracer signals at the bone–implant interface. The reproducibility of SUVmax measurements was evaluated through intra- and interobserver reliability, with intraclass correlation coefficients calculated for each component. Agreement was further examined using Bland–Altman analysis, including estimation of mean bias and limits of agreement.

All statistical tests were two-sided, and statistical significance was set at $p < 0.05$. Given the exploratory nature of the study and the absence of a predefined power calculation for diagnostic accuracy analyses, adjustments for multiple comparisons were not performed: results were therefore interpreted in the context of effect sizes and clinical relevance. Statistical analyses were conducted using IBM SPSS Statistics v 30.0 and R software (R Core Team; 2021, <https://www.R-project.org>).

6 Results

6.1 Study I

6.1.1 Longitudinal change in inflammatory markers

In the proteomic analysis of inflammatory markers following denosumab treatment, two specific proteins—RANKL (TRANCE) and TNFRSF9 (CD137/41BB)—exhibited statistically significant longitudinal changes. Patients receiving denosumab showed a marked, more than twofold increase in systemic RANKL expression at three months compared with the placebo cohort (ratio = 2.10; 95% CI: -0.11; 4.30), $p < 0.001$. This elevated RANKL expression persisted at six months (ratio = 1.50; 96% CI -0.71; 3.70), $p < 0.001$, and remained significantly higher than the control group at the 12-month interval (ratio = 1.47; 95% CI -0.74; 3.67), $p = 0.002$. These findings are illustrated in Figure 12.

By comparison, TNFRSF9 levels in the denosumab group showed an acute postoperative decrease at three months, returning to baseline by six months. In contrast, the placebo cohort showed a transient increase in TNFRSF9 at three months, which then returned to baseline levels. Inter-group comparisons revealed a statistically significant reduction in TNFRSF9 in denosumab-treated patients at three months (ratio = 0.68; 95% CI -1.42; 2.77; $p < 0.001$). This disparity between the treatment and placebo groups remained statistically significant, albeit attenuated, at six months (ratio = 0.83; 95% CI -1.27; 2.92); $p = 0.004$) and persisted through the 12-month follow-up (ratio = 0.86; 95% CI -1.23; 2.96); $p = 0.026$).

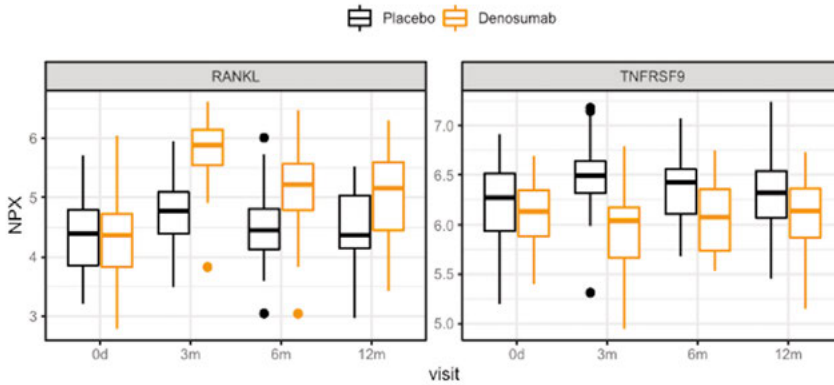


Figure 12 Longitudinal protein levels of RANKL and TNFRSF9 measured using proximity extension assay (PEA) at baseline (0 days) and at 3, 6, and 12 months. Protein levels are expressed as normalized protein expression (NPX), a relative quantification on a log₂ scale. Boxplots summarize the distribution of the data, with boxes representing the interquartile range (first to third quartile) and the horizontal line indicating the median. Whiskers extend to the most extreme values within 1.5 interquartile ranges (IQR) from the box boundaries. Values beyond this range are shown as outliers.

6.1.2 ELISA validation of RANKL expression

To validate the proteomic findings regarding systemic RANKL expression, a cross-platform confirmation was performed using a dedicated enzyme-linked immunosorbent assay (ELISA). Consistent with the PEA results, the ELISA showed a comparable elevation in RANKL protein levels within the denosumab cohort relative to the placebo group. However, a statistically significant peak in RANKL concentration was observed at the three-month postoperative interval; at this time point, RANKL levels were 2.68-fold higher in the denosumab-treated group (ratio = 2.68; 95% CI: -0.45; 5.81) ($p = 0.038$). These findings are depicted in Figure 13.

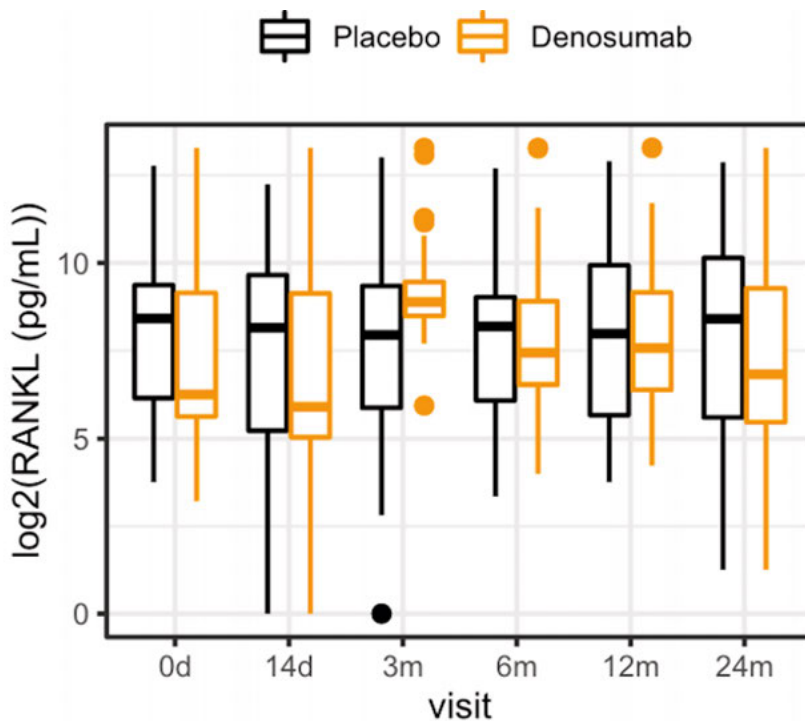


Figure 13 RANKL concentrations measured by ELISA across study visits, presented on a log₂ scale. Boxplots illustrate the distribution of values, with boxes representing the interquartile range (first to third quartile) and the horizontal line indicating the median. Whiskers extend to the most extreme values within 1.5 interquartile ranges (IQR) from the box boundaries. Values beyond this range are shown as outliers (dots).

6.1.3 Global mixed-effects model and temporal dynamics of RANKL

To further characterise the longitudinal behaviour of inflammatory markers, results from the mixed-effects modelling are summarised in Table 6. The global likelihood ratio test demonstrated a highly significant overall effect of denosumab treatment on RANKL trajectory over time, with a pronounced treatment–visit interaction. TNFRSF9 also showed a significant treatment-dependent temporal pattern, although the magnitude of effect was smaller and less sustained.

Table 6 Global mixed-effects model results for proteins significantly affected by denosumab. Values represent p-values from linear mixed-effects models. The global p-value was obtained using a likelihood ratio test comparing the full model (treatment, visit, and treatment×visit, adjusted for age, sex, BMI, and plate) with a reduced model. The remaining columns show Type II ANOVA p-values (Satterthwaite approximation) for the respective fixed effects.

Protein	Global p-value	Treatment × Visit	Treatment	Visit
RANKL	9.48×10^{-35}	1.07×10^{-12}	0.00027	1.95×10^{-28}
TNFRSF9	2.46×10^{-7}	3.02×10^{-6}	0.00021	n.s.

These results confirm that the biological response to denosumab is not static but dynamically modulated over time, with the strongest treatment effect observed early in the postoperative period.

6.1.4 Temporal pattern of RANKL within the denosumab group

Post-hoc pairwise comparisons were performed to quantify the magnitude and timing of RANKL changes within the denosumab-treated cohort (Table 7). The most pronounced shift occurred between baseline and three months, followed by a partial attenuation that nevertheless remained significantly elevated throughout the first postoperative year.

This temporal pattern demonstrates that denosumab induces a rapid and marked perturbation of the RANK–RANKL axis, followed by a sustained but gradually attenuating biological response. The consistency between the global model and post-hoc analyses supports a robust, time-dependent pharmacodynamic effect rather than random variation.

Table 7 Pairwise post-hoc comparisons of RANKL within the denosumab group

Comparison	Estimate	p-value
Baseline → 3 months	-1.46	1.9×10^{-14}
Baseline → 6 months	-0.76	7.0×10^{-13}
Baseline → 12 months	-0.70	3.4×10^{-11}

Denosumab was administered at baseline and repeated at six months, and the observed biological trajectory therefore reflects the combined pharmacodynamic effects of two sequential doses. The most pronounced perturbation occurred within the first three months after treatment, followed by a sustained

but attenuating response. As no intermediate sampling was performed between six and twelve months, the precise temporal evolution of RANKL during this interval cannot be fully characterised; an additional assessment around nine months might have provided further insight into the dynamics of the post-treatment response.

6.2 Study II

The mid-term follow-up for Study II successfully captured data from the majority of the original RCT cohort. All participants were confirmed to be non-osteoporotic at baseline. Comprehensive clinical and radiological assessments were performed at a median interval of 60 months (approximately five years) following the index cementless THA.

6.2.1 Periprosthetic bone mineral density

Quantitative analyses of pBMD demonstrated that the initial protective effects of denosumab were not sustained at the mid-term follow-up. Measurements obtained within both the acetabular and femoral ROIs showed substantial overlap between the denosumab and placebo cohorts. Although denosumab had previously been shown to significantly attenuate early periprosthetic bone loss during the first postoperative year (Aro et al., 2018), this inter-group disparity was no longer present at the mid-term evaluation, indicating convergence of BMD profiles following treatment discontinuation.

6.2.2 Longitudinal bone remodelling and radiographic stability

Across all evaluated regions, pBMD declined gradually over time in both groups, consistent with expected postoperative remodelling. No specific region demonstrated persistent inter-group divergence that would indicate a sustained treatment effect beyond the active dosing period (Figure 14-15, Table 8).

Radiographic evaluation at the mid-term follow-up revealed no evidence of early implant loosening in either the denosumab or placebo cohorts. Furthermore, there were no systematic differences suggestive of pronounced stress shielding between the groups. All implants demonstrated successful osseointegration in the surrounding bone, with a stable periprosthetic interface maintained across both study arms.

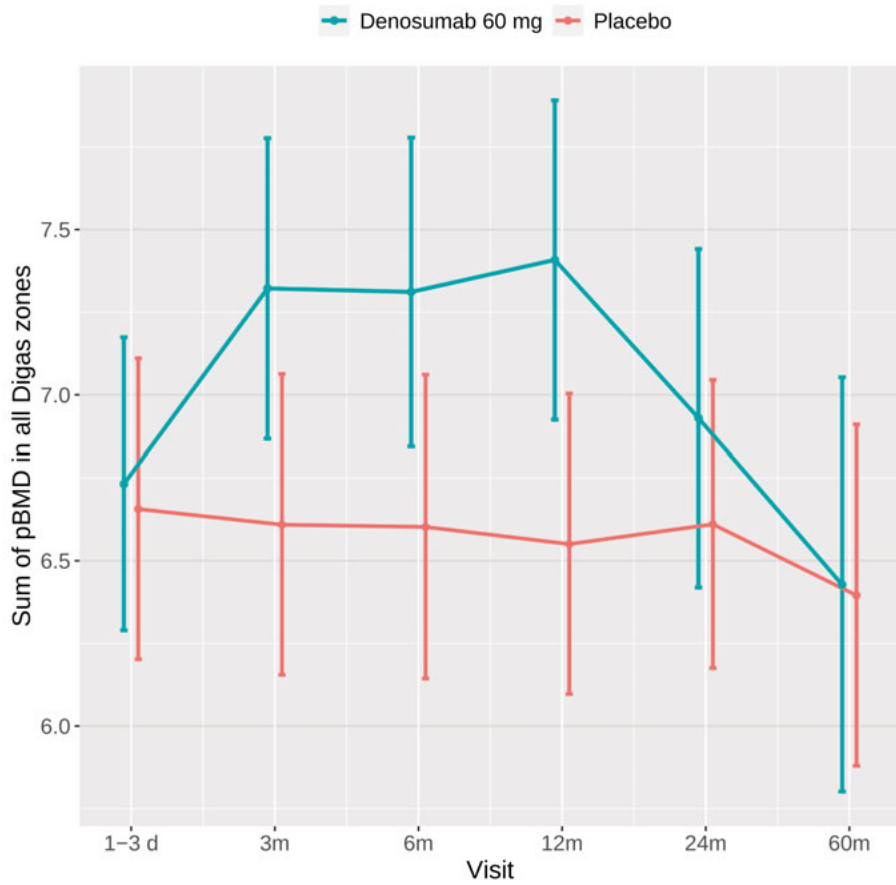


Figure 14 Longitudinal changes in periprosthetic acetabular bone mineral density (pBMD). The graph illustrates cumulative mean pBMD values with 95% confidence intervals (CI) across all five Digas zones surrounding the acetabular cup. At the five-year postoperative follow-up, no significant differences in cumulative pBMD were observed between the treatment groups.

Table 8 Summary median pBMD (g/cm²) of Gruen 7 per timepoint (0, 3, 6, 12,24 and 60 months after surgery).

Visit	Denosumab Median(Q1-Q3) (N)	Placebo Median (Q1-Q3) (N)
2	1.47(1.41-1.67) N =32	1.58(1.42-1.73) N = 31
3	1.56(1.46-1.70) N = 32	1.32(1.15-1.44) N=31
4	1.51(1.37-1.60) N = 32	1.24(1.03-1.41) N = 30
5	1.53(1.42-1.59) N = 32	1.19(1.02-1.37) N = 29
6	1.34(1.10-1.50) N = 31	1.16(1.00-1.34) N = 29
7	1.12(0.86-1.36) N =26	1.06(0.93-1.28) N = 25

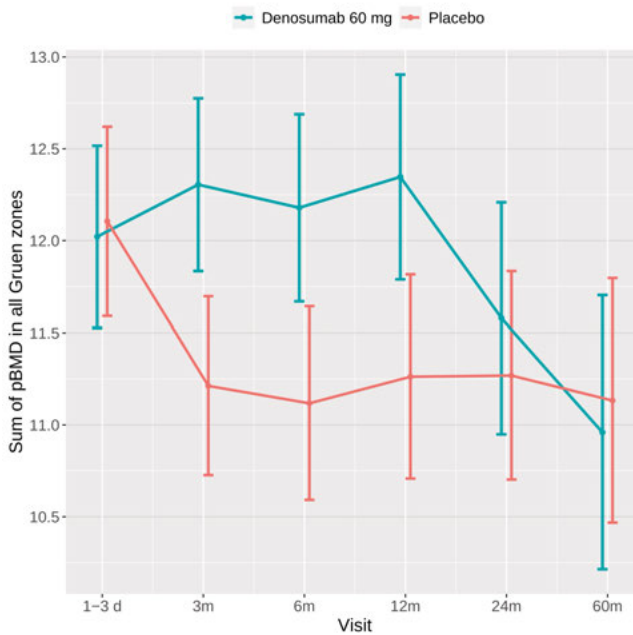


Figure 15 Longitudinal changes in femoral periprosthetic bone mineral density (pBMD). The graph illustrates cumulative mean pBMD values with 95% confidence intervals (CI) across all Gruen zones surrounding the femoral stem. At five years after the index procedure, no significant differences were observed between treatment groups.

6.2.3 Clinical and functional outcomes

Clinical outcome measures followed a comparable trajectory in both arms. Patient-reported hip function (HHS) demonstrated substantial postoperative improvements. These functional gains remained stable throughout the long-term follow-up, with no discernible differences between treatment groups at the mid-term assessment (Figure 16). These data reinforce the notion that while denosumab modulates early bone turnover, it does not appear to influence the primary subjective clinical outcomes of the procedure.

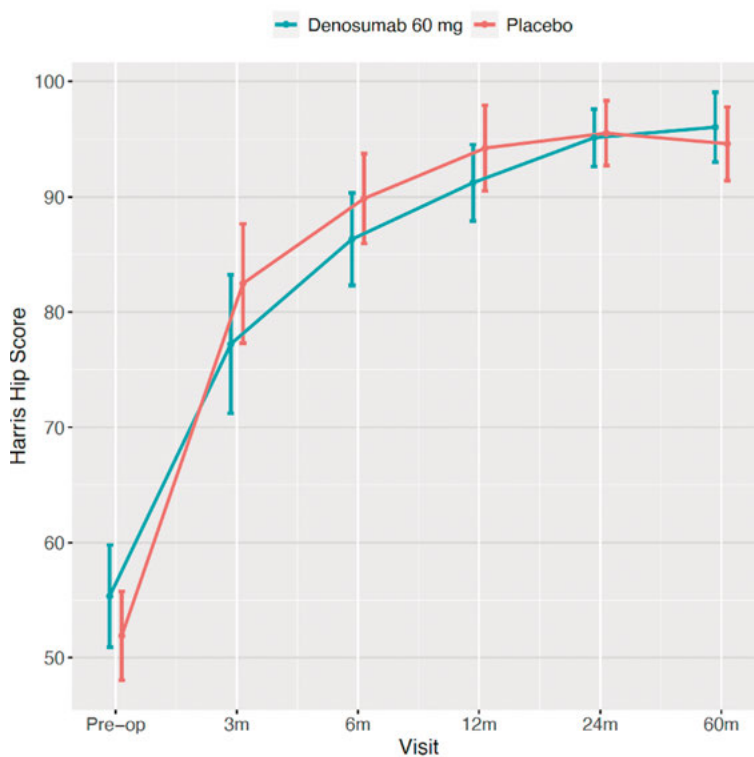


Figure 16 Longitudinal changes in Harris Hip Score (HHS). The graph illustrates mean Harris Hip Score values with 95% confidence intervals (CI) for the denosumab and placebo groups from the preoperative assessment through long-term follow-up. Both groups demonstrated marked postoperative improvement in hip function, followed by sustained stability over time. No clinically relevant differences were observed between treatment groups at mid- or long-term follow-up.

6.2.4 Safety analysis and complication profile

Implant-related adverse events were infrequent. A minimal number of revision procedures occurred during the follow-up period, with an equal distribution between the study groups. HO was a common radiographic finding at the mid-

term assessment; however, its incidence and severity (according to the Brooker classification) were comparable between the denosumab and placebo cohorts (Table 9).

Table 9 Implant revision and heterotopic ossification (HO) rates in the total cohort and treatment subgroups. Rates of implant revision and HO are presented for the overall cohort (n = 64) and stratified by treatment group (denosumab, n = 32; placebo, n = 32). Data are expressed as counts with percentages. P-values for between-group comparisons were calculated using Fisher’s exact test due to small cell counts. Values in brackets indicate the number of patients lost to follow-up.

Variables	Total n = 64	Denosumab n = 32	Placebo n = 32	P* for treatment
HO: 0	21 (37,5%)	11 (39,3%)	10 (35,7%)	0.59
HO: 1	23 (41,1%)	12 (42,9%)	11 (39,3%)	
HO: 2	11 (19,6%)	4 (14,3%)	7 (25%)	
HO: 4	1 (1,8%)	1 (3,6%)	0 (0%)	
HO (≥ 1)	35 (62,5%)	17 (60,7%)	18 (64,3%)	1.00
Revision (Yes)	3 (5,4%)	2 (7,1%)	1 (3,6%)	1.00

No clinical vertebral fractures or other skeletal adverse events attributable to antiresorptive treatment or its subsequent discontinuation were detected during follow-up. Overall, these midterm results demonstrate convergence across structural, radiographic, and clinical outcomes, suggesting that the early physiological benefits of denosumab did not translate into long-term differences in implant stability or patient-reported function.

6.3 Study III

Study III included a cohort of patients undergoing revision of THA or TKA who had received preoperative 18F-fluoride PET/CT as part of the diagnostic evaluation for suspected implant loosening. Definitive intraoperative assessment of component fixation served as the reference standard for all subsequent analyses of diagnostic performance. The study population represented a spectrum of clinical indications, including both septic and aseptic revisions; however, the majority of cases were classified as ‘infection unlikely’ according to the EBJIS criteria.

6.3.1 Quantitative SUV comparisons

Quantitative PET/CT analyses showed significantly higher periprosthetic 18F-fluoride uptake in loose components than around well-fixed components

compared with stable (well-fixed) components across most anatomical regions.

This discriminatory pattern was consistently observed for both the acetabular cups and femoral stems in THA, as well as the tibial component in TKA. In contrast, uptake values surrounding the femoral components of TKA showed substantial overlap between loose and stable implants, indicating a more limited separation in this specific region.

Parallel analyses were performed on the total cohort (Figure 17, Table 10) and were subsequently restricted to the aseptic subgroup to isolate the effects of loosening from potential infectious confounders (Figure 18, Table 11).

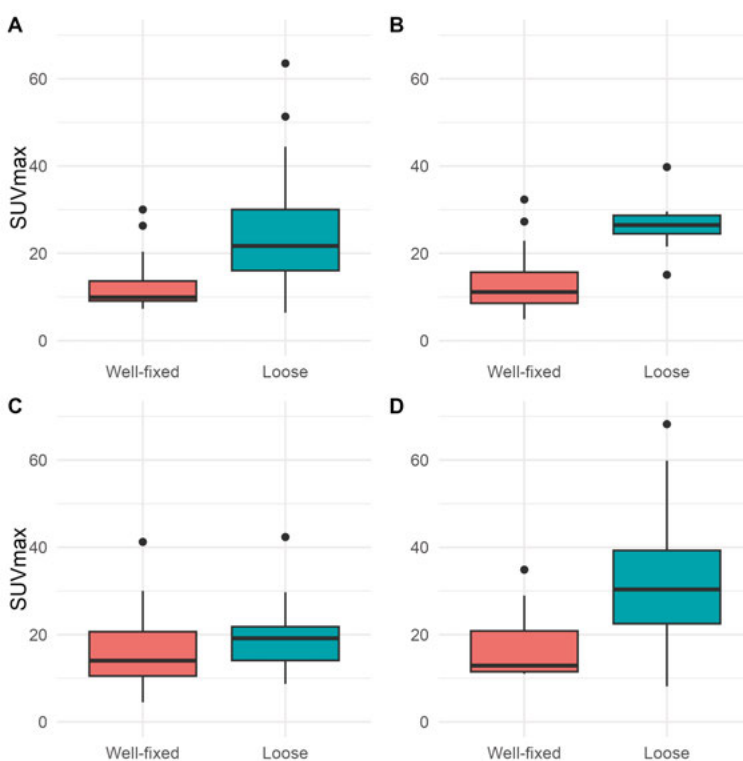


Figure 17 Distribution of ^{18}F -fluoride SUVmax values across implant components. Boxplots illustrate median ^{18}F -fluoride SUVmax values with interquartile ranges (IQR) for all joints ($n = 64$). (A) THA cup ($n = 31$) (B) THA stem ($n = 31$) (C) TKA femoral component ($n = 32$) (D) TKA tibial component ($n = 3$)

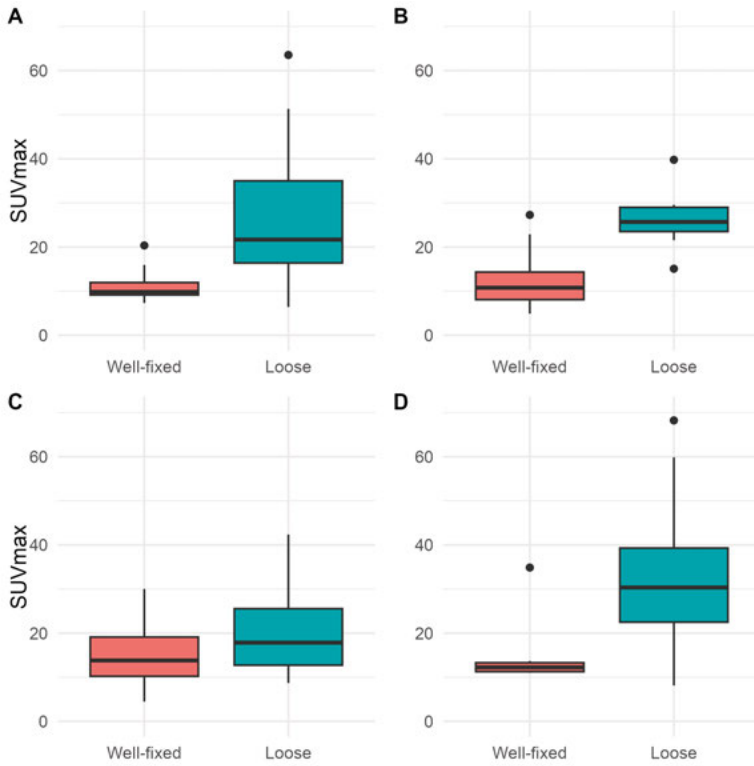


Figure 18 Distribution of ^{18}F -fluoride SUVmax values in aseptic implants. Boxplots illustrate median ^{18}F -fluoride SUVmax values with interquartile ranges (IQR) for all aseptic joints (n = 51). (A) THA cup (n = 26) (B) THA stem (n = 26) (C) TKA femoral component (n = 25) (D) TKA tibial component (n = 25)

Table 10 Diagnostic performance of ¹⁸F-fluoride PET/CT for detecting implant loosening. Test properties of ¹⁸F-fluoride PET/CT in all included patients (n = 63), encompassing both aseptic and septic loosening. Results are presented as the area under the ROC curve (AUC) with 95% confidence intervals (CI), optimal threshold values with corresponding CI, and sensitivity and specificity estimates with 95% CI for each implant component (THA cup, THA stem, TKA femoral component, and TKA tibial component). Note: The optimal threshold in this ROC analysis represents the value that maximises the combined sensitivity (true positive rate) and specificity (true negative rate) for each curve.

	AUC (95% CI)	Best threshold	Threshold 95% CI	Sensitivity (95% CI)	Specificity (95% CI)
THA cup	0.81 (0.64–0.98)	13.9	12.5–21.9	0.93 (0.79–1.0)	0.71 (0.47–0.88)
THA stem	0.90 (0.79–1.0)	17.3	14.0–24.3	1 (1–1)	0.74 (0.57–0.91)
TKA fem comp	0.60 (0.39–0.81)	14.3	8.4–36.3	0.73 (0.45–1.0)	0.55 (0.35–0.75)
TKA tib comp	0.83 (0.66–1.0)	15.8	14.0–36.3	0.95 (0.86–1.0)	0.67 (0.33–1.0)

Table 11 Diagnostic performance of ¹⁸F-fluoride PET/CT for detecting aseptic implant loosening. Test properties of ¹⁸F-fluoride PET/CT in the subgroup restricted to aseptic loosening (n = 52). Results are presented as area under the ROC curve (AUC) with 95% confidence intervals (CI), optimal threshold values with corresponding CI, and sensitivity and specificity estimates with 95% CI for each implant component (THA cup, THA stem, TKA femoral component, and TKA tibial component).

¹ Optimal threshold determined by Youden’s index.

	AUC (95% CI)	Best threshold ¹	Threshold 95% CI	Sensitivity (95% CI)	Specificity (95% CI)
THA cup	0.87 (0.7–1)	14.2	12.5–21.9	0.92 (0.75–1)	0.79 (0.57–1)
THA stem	0.93 (0.84–1)	15.0	14.0–24.3	1.00 (1–1)	0.79 (0.58–0.95)
TKA fem component	0.65 (0.4–0.91)	15.8	8.5–31.6	0.62 (0.25–0.88)	0.71 (0.47–0.88)
TKA: tib component	0.86 (0.67–1)	14.7	14.0–18.0	0.95 (0.83–1)	0.86 (0.57–1)

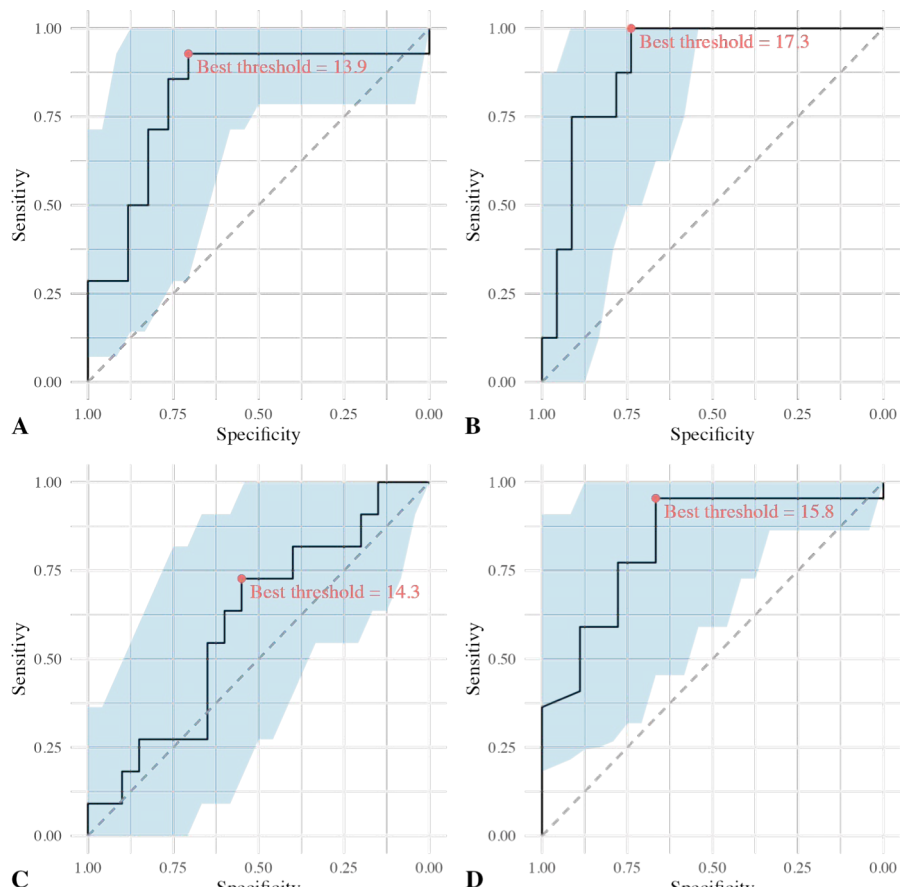


Figure 19 Receiver operating characteristic (ROC) curves for implant components. ROC curves with optimal thresholds are shown for all analyzed joints (n = 64). A) THA acetabular cup (n = 31), (B) THA stem (n = 31), (C) TKA femoral component (n = 32), (D) TKA tibial component (n = 32)

6.3.2 Diagnostic accuracy and ROC analysis

Diagnostic accuracy analyses reflected these site-specific uptake patterns. ROC analyses demonstrated good to excellent discriminatory ability for identifying loosening in acetabular and femoral THA components, as well as the tibial component of TKA. Conversely, the diagnostic performance for the femoral TKA component remained limited (Figure 19). Restricting the analysis to the aseptic subgroup (excluding suspected or confirmed PJIs) further improved diagnostic accuracy for most components. Despite this refinement, the femoral TKA component remained difficult to classify.

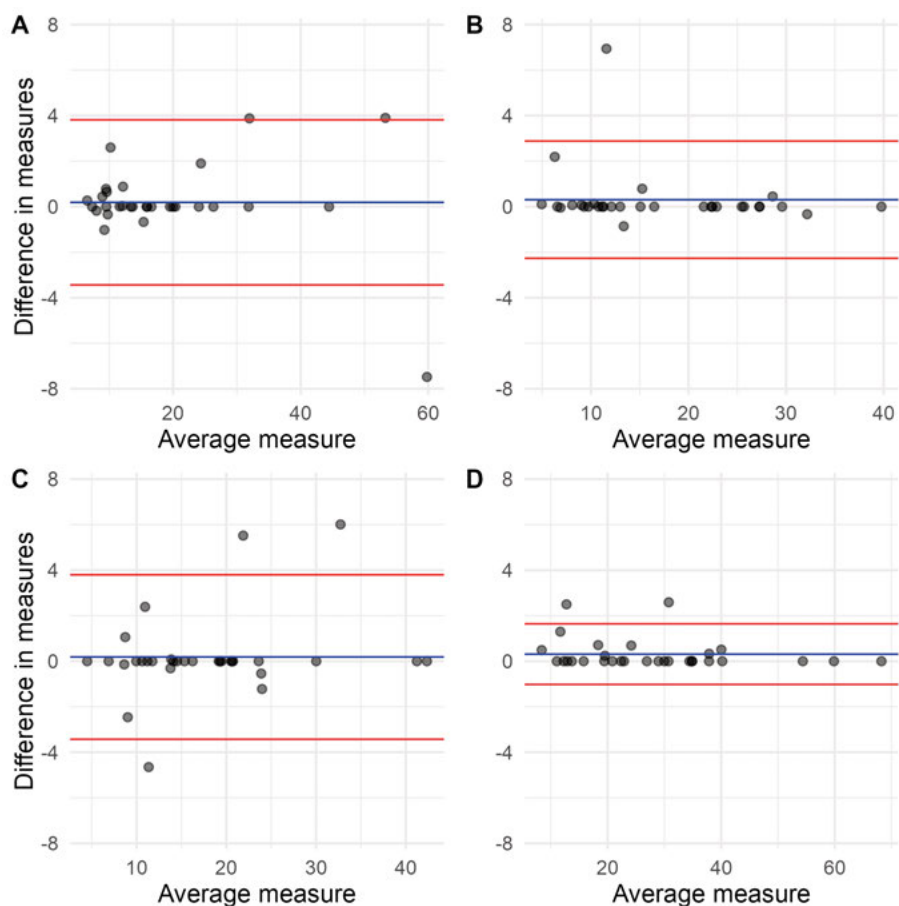


Figure 20 Bland–Altman plots for implant components comparing quantitative SUVmax measurements obtained independently by two blinded investigators. Bland–Altman plots are shown for all investigated components. Blue horizontal lines indicate mean differences, while red horizontal lines represent the limits of the 95% confidence intervals (CI). (A) THA acetabular cup, (B) THA stem, (C) TKA femoral component, (D) TKA tibial component)

6.3.3 SUV Threshold analysis

Exploratory analyses identified component-specific SUVmax diagnostic thresholds that effectively differentiated loose from stable implants on the specific PET/CT system utilised. While these thresholds showed high sensitivity and specificity for most components, the optimal values varied significantly across anatomical regions. Notably, these diagnostic benchmarks were not transferable between components (e.g., from the acetabular cup to the femoral stem), highlighting the necessity for site-specific interpretation in clinical practice.

Reproducibility analyses for SUVmax measurements demonstrated excellent reliability with high intra- and interobserver agreement. Quantitative assessment of 18F-fluoride uptake was found to be a robust methodology, even with limited observer experience (Figure 20). The results indicate that quantitative PET/CT assessment of 18F-fluoride uptake differentiates loose from stable arthroplasty components, but diagnostic performance varies clearly by component.

6.4 Study IV

Eighty-eight patients presenting with symptomatic hip or knee arthroplasties underwent paired 18F-FDG and 18F-fluoride PET/CT within a 30-day interval and were included in the final analysis. Based on EBJIS criteria, approximately one-fifth of cases were classified as ‘infection likely’ or ‘confirmed’ while the remainder were classified as ‘infection unlikely’. Total hip and total knee arthroplasties were represented in comparable proportions across the study population.

6.4.1 Quantitative SUVmax comparisons for PJI

Quantitative PET/CT analyses revealed distinct tracer- and site-specific uptake patterns. For 18F-FDG, SUVmax values surrounding the acetabular cup showed substantial overlap between infected and non-infected components, indicating limited diagnostic separation in this region. In contrast, 18F-fluoride uptake patterns were more distinct at the bone-prosthesis interface, suggesting greater discriminative value.

For 18F-fluoride PET/CT, uptake differences across infection categories were limited. Statistically significant discrimination was observed only for the tibial component of TKA, whereas uptake patterns for the remaining components overlapped considerably between groups.

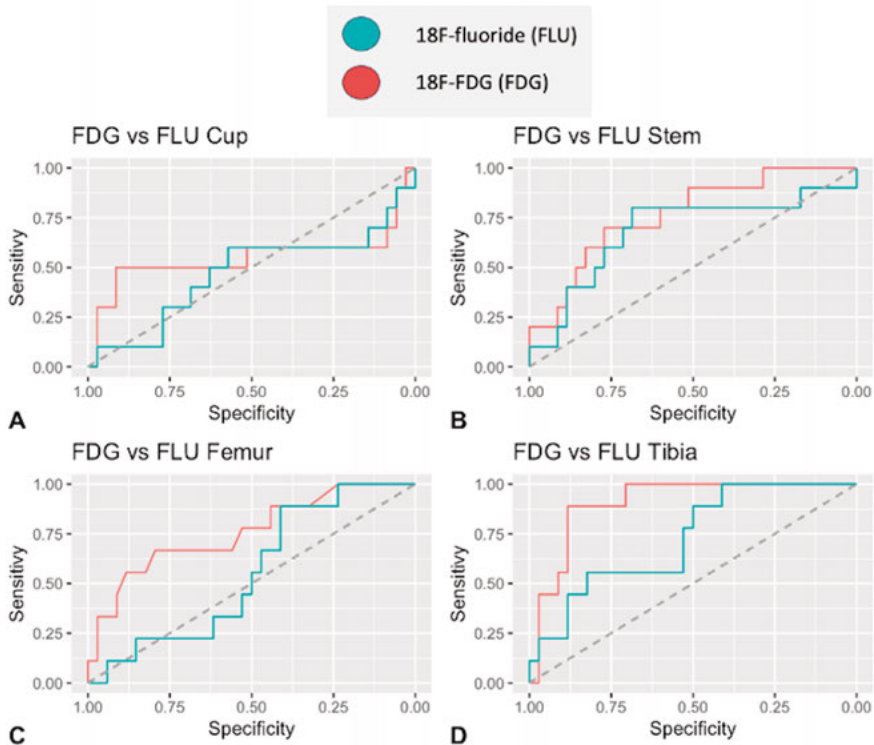


Figure 21 Receiver operating characteristic (ROC) curves for SUVmax measurements. ROC curves compare 18F-FDG (red) and 18F-fluoride (blue) SUVmax measurements for diagnosing periprosthetic joint infection (PJI) according to EBJIS criteria. Curves are shown for each implant component, stratified by infection likelihood (infection unlikely vs. infection likely/confirmed).

6.4.2 Comparative diagnostic accuracy

Diagnostic accuracy analyses reflected the tracer- and site-specific uptake patterns observed in the quantitative comparisons.

For 18F-FDG PET/CT, the highest diagnostic performance was observed for the tibial TKA component (AUC 0.91), followed by the THA stem (AUC 0.77) and the femoral TKA component (AUC 0.76). In contrast, diagnostic performance for the acetabular cup was limited (AUC 0.55).

For 18F-fluoride PET/CT, diagnostic accuracy was consistently lower. Only the tibial TKA component demonstrated modest discriminatory ability (AUC 0.73), whereas the remaining components showed limited performance (AUC 0.47–0.68).

Reproducibility analyses demonstrated excellent intraobserver agreement for SUVmax measurements in the THA cup (ICC 0.999), THA stem (ICC

0.983), and tibial TKA component (ICC 0.974), and good agreement in the femoral TKA component (ICC 0.775). Interobserver agreement was excellent for the tibial TKA component (ICC 0.957), good for the THA cup (ICC 0.916) and THA stem (ICC 0.818), but poor for the femoral TKA component (ICC 0.194). Bland–Altman analyses showed minimal systematic bias across components but wider limits of agreement for the femoral TKA component, consistent with the low interobserver ICC.

Correlation analyses revealed significant positive associations between 18F-FDG and 18F-fluoride SUVmax values across all prosthetic components (Spearman’s rho 0.399–0.702, all $p \leq 0.008$), indicating that increased metabolic activity and bone turnover frequently co-occur within the periprosthetic environment despite their differing diagnostic performance in PJI detection.

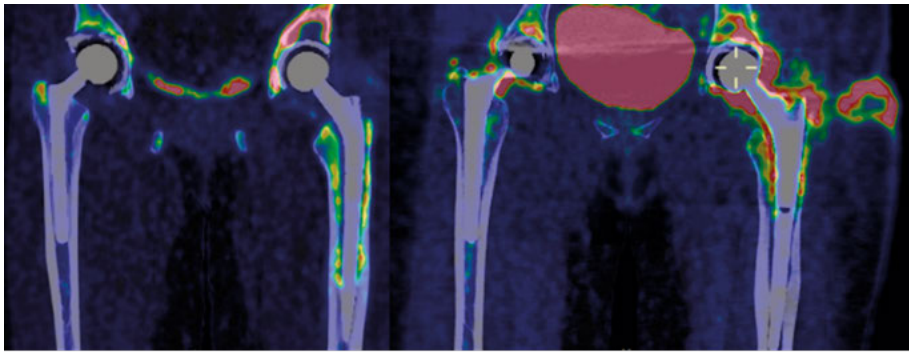


Figure 22 Comparative 18F-fluoride and 18F-FDG PET/CT imaging in periprosthetic joint infection (Study IV). 55-year-old female patient 3 yrs after index procedure. The left panel (18F-fluoride PET/CT) demonstrates increased periprosthetic tracer uptake reflecting enhanced bone turnover around the prosthetic components. The right panel (18F-FDG PET/CT) shows intense metabolic activity consistent with inflammatory response at the bone–implant interface. The case represents EBJIS-confirmed periprosthetic joint infection, with coagulase-negative staphylococci verified by intraoperative tissue cultures.

Table 12 Patient characteristics and microbiological findings Patient-level data including joint type, ASA classification, EBJIS diagnostic category, and microbiological results. Pathogens are listed with corresponding sample sources; multiple pathogens and sources are reported where applicable. Within the EBJIS definition, infection may be classified as likely despite negative cultures, as diagnostic criteria also incorporate clinical findings, inflammatory markers, and histology, acknowledging the possibility of culture-negative infection.

Abbreviations: Sex: F = female, M = male; Joint: H = hip, K = knee; ASA = American Society of Anesthesiologists physical status classification; EBJIS = European Bone and Joint Infection Society diagnostic category; CoNS = coagulase-negative staphylococci; Strep. = streptococci; Coryne. = *Corynebacterium* spp.; Cutib. = *Cutibacterium* spp.; Kleb. = *Klebsiella* spp.; S. aureus = *Staphylococcus aureus*; E. corrodens = *Eikenella corrodens*. Sample sources: SF = synovial fluid, T = tissue, SON = sonication fluid, B = blood.

P no	Joint	ASA	EBJIS	Pathogen 1	Source 1	Pathogen 2	Source 2
1	K	3	1	CoNS	SF		
2	K	2	1	CoNS	T		
3	K	3	1	S. aureus	B		
4	K	3	1				
5	H	4	1	Strep.	SF	CoNS	SF
6	K	2	1		SON		T
7	K	2	1		SF		
8	H	2	1				
9	K	3	1		SON		T
10	K	3	1	Strep	SF	E. corrodens	T
11	H	3	2	Coryne.	T/SON	CoNS	SON
12	H	3	2	CoNS	T	CoNS	T
13	H	3	2	CoNS	SON	CoNS	T
14	H	3	2	CoNS	SF		
15	H	3	2	CoNS	SON	Cutib.	T
16	H	4	2	CoNS	SF	Kleb.	B
17	H	2	2	CoNS	SON	CoNS	T
18	H	3	2	CoNS	T	CoNS	SF
19	K	3	2	Kleb.	SON	Kleb.	T/SF

6.4.3 Radiological FDG-PET/CT interpretation in relation to EBJIS classification

When radiological interpretation of 18F-FDG PET/CT was evaluated according to the EBJIS classification, a significant association was observed, demonstrating moderate agreement between methods and an overall diagnostic profile characterised by moderate sensitivity and high specificity for both hip and knee prostheses (Table 9). Diagnostic performance was broadly comparable between THA and TKA, with slightly higher negative predictive values

observed for knee prostheses. Cohen's κ indicated moderate concordance with the reference classification.

Table 13 Diagnostic performance of radiological FDG-PET/CT interpretation versus EBJIS classification

	THA	TKA
Sensitivity	67% (8/12)	71% (5/7)
Specificity	83% (33/40)	86% (25/29)
Positive Predictive Value (PPV)	53% (8/15)	56% (5/9)
Negative Predictive Value (NPV)	89% (33/37)	93% (25/27)
Accuracy	79% (41/52)	83% (30/36)
Cohen's κ	0.45	0.52

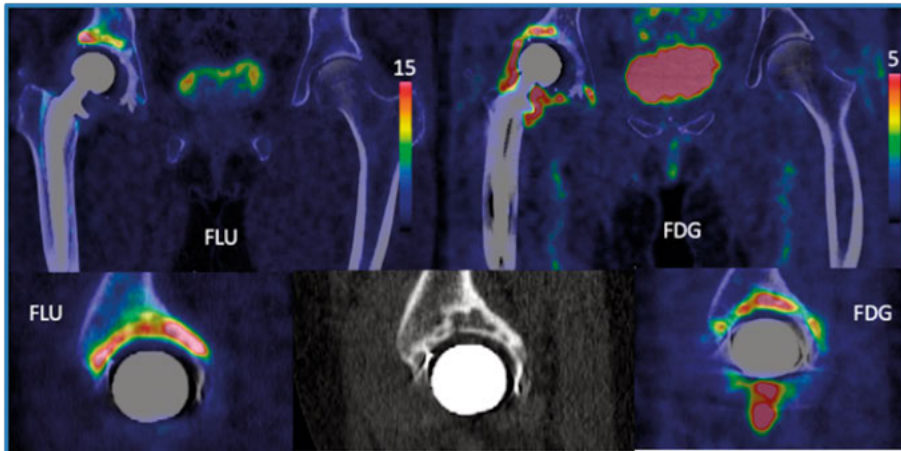


Figure 23 Comparative 18F-fluoride and 18F-FDG PET/CT imaging in suspected isolated acetabular infection (Study IV). The left panel (FLU: 18F-fluoride PET/CT) demonstrates increased periprosthetic tracer uptake around the acetabular component, reflecting elevated bone turnover (SUVmax 26.9). The right panel (FDG: 18F-FDG PET/CT) shows moderate metabolic activity at the same location (SUVmax 7.5). The case represents a 58-year-old patient with a prosthesis in situ for 13 years and in retrospect suspected isolated cup infection; however, EBJIS classification was negative (infection unlikely). At revision surgery the acetabular component was found to be loose, but unfortunately no intraoperative cultures were obtained from this region.

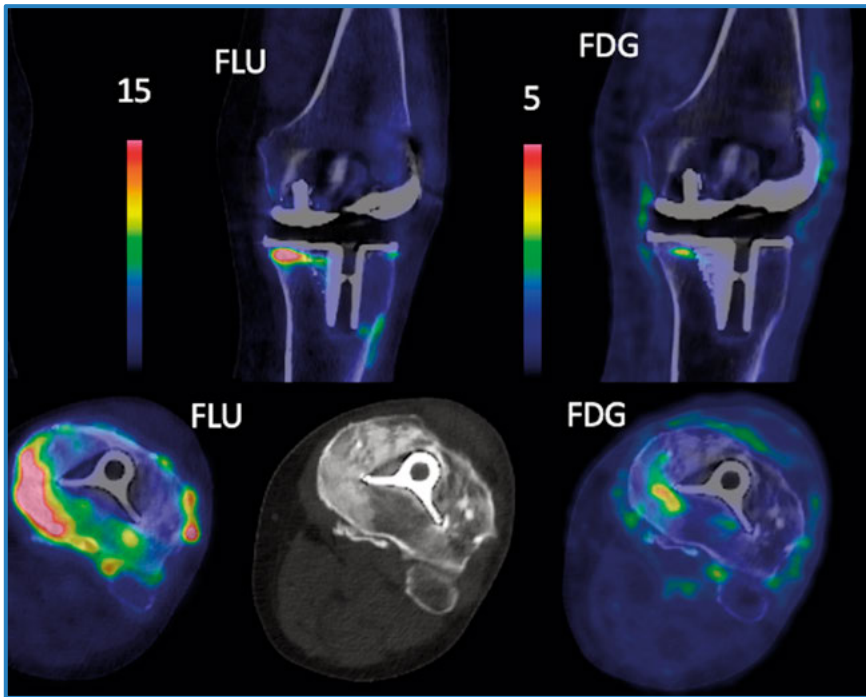


Figure 24 Comparative 18F-fluoride and 18F-FDG PET/CT imaging in periprosthetic joint infection (Study IV). The upper panels show coronal fused PET/CT images and the lower panels axial views. The left images (18F-fluoride PET/CT) demonstrate increased periprosthetic tracer uptake around the tibial component, consistent with elevated bone turnover (SUVmax 26.4). The corresponding 18F-FDG PET/CT images (right) show moderate metabolic activity in the same region (SUVmax 4.4). The case represents a 77-year-old male patient one year after primary knee arthroplasty, initially suspected to have tibial component loosening. One isolated joint aspiration yielded coagulase-negative staphylococci, and the case was therefore classified as EBJIS infection likely.

7 Discussion

7.1 Principal findings

The principal findings of this thesis can be summarised as follows. First, pharmacological modulation of bone metabolism with denosumab effectively attenuates early periprosthetic bone loss following uncemented THA. However, this effect is transient and does not translate into the sustained preservation of pBMD or superior implant-related outcomes at the mid-term follow-up (Studies I and II). In Study I, denosumab treatment suppressed bone turnover and induced sustained RANKL upregulation alongside transient TNFRSF9 downregulation. This molecular profile suggests the activation of compensatory osteoclast-regulatory pathways, which likely contribute to the previously observed post-treatment rebound in bone remodelling. Ultimately, these findings indicate that while early postoperative bone remodelling is susceptible to pharmacological intervention, the long-term periprosthetic bone landscape is predominantly governed by mechanobiological factors (e.g., stress shielding).

Second, quantitative assessment of ¹⁸F-fluoride PET/CT uptake primarily reflects pathological bone remodelling associated with mechanical instability, enabling differentiation between loose and well-fixed arthroplasty components in patients undergoing revision surgery. Diagnostic performance varied by component: uptake patterns were most informative for cup and stem in THA and for tibial components in TKA, whereas femoral components in TKA demonstrated limited discriminatory capacity. Collectively, these findings support the use of ¹⁸F-fluoride PET/CT as a marker of mechanically driven bone remodelling rather than infection.

Third, comparative dual-tracer PET/CT imaging demonstrated that ¹⁸F-FDG provided superior discrimination between infected and non-infected arthroplasty components compared with ¹⁸F-fluoride in patients with suspected PJI (Study IV). Although ¹⁸F-fluoride uptake was frequently increased in infected cases, its diagnostic performance was limited, and substantial overlap was observed in aseptic conditions, particularly in hip arthroplasty. In contrast, elevated ¹⁸F-FDG uptake was consistently associated with infection across most components, except for acetabular cups. These findings highlight the value of ¹⁸F-FDG PET/CT as a more reliable imaging marker for infection in the revision arthroplasty landscape.

Taken together, these findings indicate that ¹⁸F-fluoride PET/CT primarily reflects periprosthetic bone turnover and mechanical adaptation, whereas ¹⁸F-FDG PET/CT more accurately captures infection-related inflammatory activity. This conceptual separation underscores the importance of aligning tracer selection with the underlying clinical question—mechanical loosening or suspected infection—rather than applying the tracers interchangeably.

7.2 General discussion

7.2.1 Study I

In a secondary endpoint analysis of a previous RCT investigating the effects of denosumab on pBMD, serum inflammatory markers were analysed. RANKL levels were significantly upregulated in patients treated with denosumab, with the largest increase observed three months post-treatment. In contrast, TNFRSF9 levels were downregulated at three months but returned to baseline by six months. Other inflammatory markers showed no significant differences between the denosumab and placebo cohorts. These findings suggest that denosumab modulates specific inflammatory pathways without broadly altering systemic inflammation in hip OA treated with THA. Moreover, improvements in patient-reported outcomes following THA were not associated with changes in the selected inflammatory markers from the Olink Proseek Multiplex inflammation panel.

Denosumab's elimination half-life (15-32 days) (Chen et al., 2018; Narayanan, 2013) suggests that the drug would be largely eliminated by three months; yet elevated RANKL levels persisted. This persistence may reflect anti-idiotypic antibody responses or immune complex formation accelerating denosumab clearance. Notably, PEA data were limited to four time points, and additional measurements—particularly at 24 months—would have provided greater insight into these dynamics.

Our findings highlight the need for further studies to clarify assay specificity for different RANKL isoforms. Compared with prior studies, the RCT design represents a major strength, in contrast to many retrospective analyses. The use of multiplexed PEA enabled simultaneous assessment of numerous inflammation-related molecules, though it was limited to relative quantification. Cassuto et al. reported marked changes in inflammatory markers following THA, including a primary peak in pro-inflammatory cytokine expression that was not replicated in the current study (Cassuto et al., 2018). They also observed increased RANKL levels at five years post-THA, though they remained below baseline until then. These early findings align with observations

in the placebo group in the present study, accentuating the importance of long-term follow-up when evaluating inflammatory responses after THA.

Fassio et al. (2019) conducted a prospective cohort study examining the effects of denosumab discontinuation after long-term use. They observed increased levels following discontinuation, in contrast to the present study, which found RANKL upregulation during treatment. However, Fassio et al.'s study was limited by the absence of baseline and on-treatment serum marker measurements, a small sample size, and the lack of a control group. Their findings suggest that the rebound phenomenon seen after denosumab discontinuation may be due to osteoclast hyperstimulation.

Importantly, the proteomic response was highly selective, with no broad activation of inflammatory pathways. This suggests that denosumab primarily modulates osteoimmune signalling through targeted effects on the RANK–RANKL axis rather than inducing a generalised inflammatory response.

Additionally, recent research by McDonald et al. (2021) revealed that osteoclasts may undergo fission into osteomorphs rather than undergo apoptosis, and that RANKL inhibition blocks their recycling into osteoclasts. (Figure 20) This process could lead to osteomorph accumulation during denosumab treatment. The current study supports this mechanism, showing that RANKL upregulation began immediately after denosumab initiation and persisted throughout treatment, potentially predisposing to increased bone resorption if denosumab is discontinued.

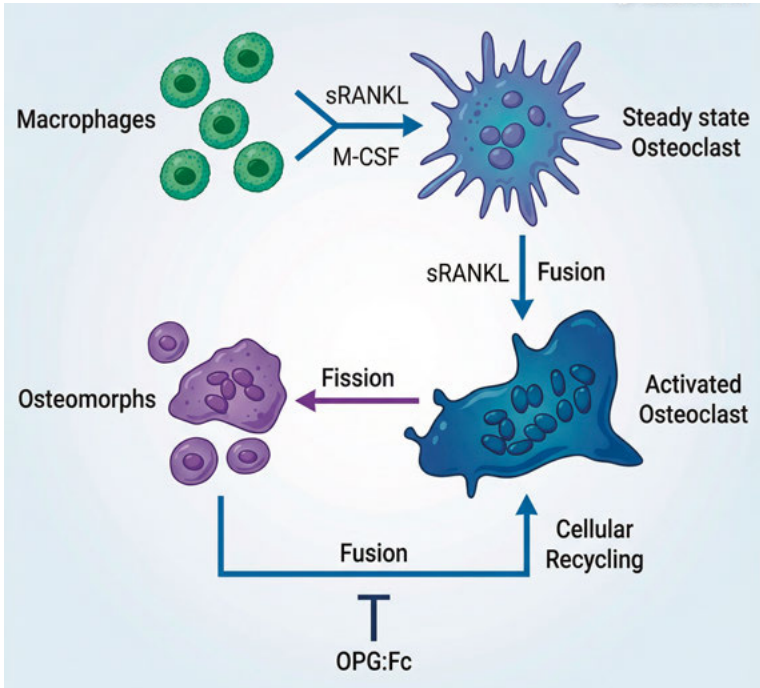


Figure 25 Osteoclast fission and formation of osteomorphs Osteoclasts differentiate from macrophages under the influence of macrophage colony-stimulating factor (M-CSF) and soluble receptor activator of nuclear factor κ B ligand (sRANKL). Activated osteoclasts may undergo fission to form osteomorphs, which retain the capacity to fuse and regenerate osteoclasts. Osteoclast formation and fusion are inhibited by osteoprotegerin–Fc (OPG: Fc). Illustration inspired from McDonald et al. (2021).

The temporal pattern observed is consistent with the administration of two denosumab doses at baseline and six months, indicating a sustained pharmacodynamic suppression followed by biological rebound activation of the RANK–RANKL axis. The absence of intermediate sampling between six- and twelve-months limits precise characterisation of this transition phase but supports a time-dependent rather than random biological response.

Our study also noted that TNFRSF9, a receptor implicated in RANKL-mediated osteoclastogenesis, was downregulated in the intervention cohort, suggesting that denosumab may modulate osteoclastogenesis through feedback regulation. Bidirectional signalling between RANKL and TNFRSF9 may help maintain cellular homeostasis and regulate osteoclast activity. These findings draw attention to the need for further mechanistic studies to clarify the pathways underlying these observations.

7.2.2 Study II

The principal finding of Study II is that short-term denosumab treatment following uncemented THA does not result in sustained preservation of pBMD at the mid-term follow-up. Although denosumab effectively attenuated early periprosthetic bone loss during the first postoperative year—as previously reported in this RCT—this protective effect was not maintained after treatment cessation. Instead, pBMD values gradually converged with those observed in the placebo group over time (Kiritopoulos et al., 2022; Nyström et al., 2020; Sköld et al., 2021). This longitudinal convergence suggests that the biological ‘window of opportunity’ to pharmacologically inhibit stress shielding may be limited unless the antiresorptive stimulus is sustained or followed by sequential therapy.

Importantly, the absence of a long-term between-group difference does not negate the pharmacological efficacy of denosumab. As a potent inhibitor of osteoclast-mediated bone resorption through RANKL blockade, denosumab increases trabecular and cortical BMD (Curtis et al., 2024; Miller et al., 2008). The present findings instead highlight the transient nature of antiresorptive modulation within a biological environment primarily governed by mechanical loading, stress shielding, and implant-related load transfer. In uncemented THA, early postoperative bone loss appears amenable to pharmacological intervention, whereas long-term periprosthetic remodelling is largely determined by biomechanical factors.

These results are consistent with previous randomised trials of antiresorptive therapy in cementless THA. Several studies have demonstrated a reduction in early periprosthetic bone loss with bisphosphonates or denosumab, but have not sustained bone preservation or improved implant fixation after treatment discontinuation (Aro, 2021; Aro et al., 2019; Nyström et al., 2020; Sköldenberg et al., 2011).

Moreover, randomised studies have failed to show a consistent association between preserved periprosthetic bone density and reduced early implant migration or subsidence, suggesting that pBMD may be an imperfect surrogate for implant stability in non-osteoporotic patients (Aro, 2021; Aro et al., 2019; Sköldenberg et al., 2011). These findings underscore the need to interpret changes in pBMD cautiously and in the context of long-term biomechanical outcomes.

Increasing attention has been directed toward the rebound phenomenon following denosumab discontinuation, characterised by accelerated bone turnover, BMD loss below pretreatment levels, and heightened risk of vertebral fractures (Kim et al., 2022; Lamy et al., 2017; Martín-Pérez et al., 2025; Sølling et al., 2021; Tsourdi et al., 2017). In the present cohort, no evidence of a

clinically relevant rebound phenomenon—defined as back pain and radiographically verified vertebral fractures/compression—was observed. This finding should be interpreted in light of the study's specific clinical and biological context: participants were non-osteoporotic, exposure to denosumab was limited to two doses, and follow-up primarily examined a localised periprosthetic bone compartment rather than systemic skeletal sites. These considerations stress the importance of the patient population and treatment duration when evaluating rebound risk.

Following treatment cessation, pBMD declined gradually and approached placebo levels without dropping below baseline values. Importantly, no vertebral fractures or serious skeletal adverse events were observed. Clinically relevant rebound phenomena have predominantly been described in skeletally fragile populations exposed to prolonged RANKL inhibition, where rapid post-cessation increases in bone turnover coincide with pre-existing microarchitectural vulnerability and translate into excess fracture risk (Kim et al., 2022; Lamy et al., 2017; Martín-Pérez et al., 2025; Sølling et al., 2021; Tsourdi et al., 2017). The biological prerequisites for such events were not present in the current study population.

From a clinical perspective, the absence of a sustained pBMD benefit is particularly noteworthy. Preservation of periprosthetic bone density has been suggested as a surrogate marker for enhanced implant fixation and a reduced risk of aseptic loosening. However, both the present study and previous randomised trials demonstrate that pharmacologically induced changes in pBMD do not necessarily translate into improved implant survival or lower revision rates in non-osteoporotic patients undergoing uncemented THA (Aro, 2021; Aro et al., 2019; Nyström et al., 2020; Sköldenberg et al., 2011). This observation points to the limitation of pBMD as a standalone surrogate outcome and emphasises the predominant importance of mechanical stability and initial fixation in ensuring long-term implant success.

Consistent with this interpretation, Mjöberg proposed that insufficient primary fixation may serve as an initiating factor in aseptic loosening. According to this concept, early micromotion at the bone–implant interface can trigger bone resorption and progressive loss of fixation, even in the absence of substantial wear debris (Mjöberg, 1994, 1997, 2018).

No differences were observed between treatment groups in clinical outcome measures, implant survival, or HO. These outcomes were exploratory, and the study was not powered to detect between-group differences. Nevertheless, the revision rates observed were consistent with national registry data. In the Swedish Arthroplasty Register, the LINK Collum Femoris Preserving (CFP) stem has shown an increased relative risk of revision in consecutive

annual reports (HR 3.76, 95% CI 1.75–8.05 in 2023; HR 3.56, 95% CI 1.29–9.86 in 2024), although interpretation is limited by small sample size and wide confidence intervals. The Continuum acetabular cup shows a corresponding cumulative revision risk of approximately 4.4% at 5 years and 5.4% at 10 years (W-Dahl et al., 2025. The revision rates reported in the present study fall within these ranges, supporting the external validity of the findings). Taken together, the results do not support a clinically meaningful benefit of short-term denosumab treatment in the routine management of non-osteoporotic patients undergoing uncemented THA.

7.2.3 Study III

The primary aim of this study was to evaluate the quantitative analysis of periprosthetic ¹⁸F-fluoride uptake using ¹⁸F-fluoride PET/CT for the diagnosis of implant loosening. The findings indicate that quantitative measurement of ¹⁸F-fluoride uptake is reliable and reproducible. The maximum uptake, expressed as SUVmax, was able to differentiate between loose and well-fixed THA and TKA components, although this distinction was not observed for femoral TKA components. Notably, diagnostic accuracy improved when patients with probable or confirmed PJI were excluded. Specific SUVmax threshold values and uptake ratios were established as potential indicators for detecting implant loosening, providing a basis for further clinical validation.

We observed increased ¹⁸F uptake around loose compared with well-fixed components in all cases except for femoral TKA components. This finding has important clinical implications for pre-revision diagnostics, particularly for patients with painful THA or TKA when conventional assessments are inconclusive. Although the application of ¹⁸F-fluoride PET/CT in diagnosing aseptic implant loosening remains relatively underexplored, Koob et al. (2019) provided supportive evidence in a retrospective study of 26 patients with 37 implants. In their cohort, 18 implants were revised and 11 were considered "clinically silent." Rather than relying on quantitative SUV measurements, they employed a qualitative assessment of uptake patterns to identify loosening, reporting an overall sensitivity of 95% and specificity of 87%.

One challenge with SUV measurement is its dependency on image reconstruction settings and scanner resolution, which complicates direct comparisons across different PET/CT devices. Of note, the femoral TKA component appears to behave differently from other components, posing unique challenges for evaluation with ¹⁸F-fluoride PET/CT. The underlying cause of this phenomenon remains unclear and warrants further investigation. One hypothesis is that differences in biomechanical load distribution may lead to higher, more nonspecific uptake beneath the femoral shield. Supporting this, Duus et

al. (1990) reported prolonged uptake on bone scans up to two years post-TKA, which may account for this pattern. Similarly, Son et al. (2016) observed that the ¹⁸F-fluoride uptake pattern in asymptomatic joint reconstructions differs between THA and TKA, with TKA showing prolonged curvilinear uptake persisting up to 15 months postoperatively. Another possibility is that the femoral component absorbs more photons, thereby producing pronounced SUV artefacts when CT-based attenuation correction is applied.

We observed that ROC analyses showed good to excellent AUC values when distinguishing between loose and well-fixed arthroplasty components, except for femoral TKA components. Moreover, this method maintained high diagnostic accuracy even when applied to a heterogeneous cohort that included both aseptic and septic loosening cases. Similarly, Kobayashi et al. (2011) generated ROC curves and identified an SUV_{max} threshold of 6.9 for infection, yielding 81% sensitivity and 80% specificity (AUC 0.87). For aseptic loosening, they set a threshold at an SUV_{max} of 4.9, with 95% sensitivity and 82% specificity (AUC 0.96). Both their ROC analysis and ours demonstrate sensitivity and specificity levels that provide high diagnostic accuracy. However, unlike their findings, our thresholds for aseptic loosening ranged from SUV_{max} values of 14 to 20, underlining the need for individual calibration for each PET/CT device to ensure reliable interpretation.

7.2.4 Study IV

Study IV extends the diagnostic framework established in Study III by directly comparing two PET tracers with distinct biological targets in patients with suspected PJI. The results demonstrate that tracer selection substantially influences diagnostic performance, as ¹⁸F-FDG and ¹⁸F-fluoride capture fundamentally different aspects of the periprosthetic biological environment. This distinction is consistent with the established biological mechanisms of tracer uptake. ¹⁸F-FDG reflects cellular inflammatory activity, whereas ¹⁸F-fluoride reflects osteoblastic activity and bone turnover (Basu et al., 2014; Czernin et al., 2010; Even-Sapir et al., 2007; Kim & Kim, 2021).

A key finding of Study IV is the superior ability of ¹⁸F-FDG PET/CT to discriminate between infected and non-infected arthroplasty components compared with ¹⁸F-fluoride PET/CT when EBJIS criteria are used as the reference standard. Elevated ¹⁸F-FDG uptake was consistently associated with infection across most components, reflecting increased glucose metabolism in activated immune and inflammatory cells at the bone-implant interface. This observation aligns with previous studies demonstrating the diagnostic value of ¹⁸F-FDG PET/CT in prosthetic joint infection, although reported accuracy has been found to vary depending on interpretation criteria and reference

standards (Basu et al., 2014; Kim & Kim, 2021; Kwee et al., 2018; Verberne et al., 2018). Taken together, these findings highlight the importance of tracer selection in PET/CT imaging for suspected PJI. While 18F-fluoride provides valuable information on bone turnover and osteoblastic activity, its diagnostic utility in infection appears limited compared with 18F-FDG. The complementary biological information captured by these tracers suggests that a combined or sequential imaging approach could potentially enhance diagnostic accuracy, particularly in complex cases where conventional assessments remain inconclusive.

Using EBJIS as the reference standard, FDG PET/CT demonstrated a diagnostic profile characterised by relatively higher specificity than sensitivity. This contrasts with several earlier studies and suggests that FDG uptake in this cohort may reflect more infection-specific inflammatory activity rather than nonspecific postoperative or aseptic inflammation.

In contrast, although 18F-fluoride uptake was frequently elevated in infected cases, its diagnostic performance was limited by substantial overlap with aseptic conditions. This observation is biologically plausible, as 18F-fluoride uptake reflects osteoblastic activity and bone remodelling, processes that may be increased in multiple non-infectious conditions, including mechanical instability, stress redistribution, and ongoing physiological remodelling around well-fixed implants (Adesanya et al., 2015; Czernin et al., 2010; Koob et al., 2019; Ullmark, 2020). Therefore, increased 18F-fluoride uptake cannot be interpreted as infection-specific, particularly in the absence of clear mechanical loosening.

The results of Study IV also provide important context for the findings of Study III. In the revision setting, 18F-fluoride PET/CT differentiated loose from well-fixed components with good diagnostic accuracy, supporting its role as a marker of mechanically driven bone remodelling (Koob et al., 2019; Sköld et al., 2025; Ullmark, 2020). However, when the clinical question shifts from loosening to infection, as in Study IV, the same tracer shows limited discriminatory capacity. Together, these findings indicate that 18F-fluoride PET/CT is primarily informative for mechanical complications, whereas 18F-FDG PET/CT is better suited for identifying infection-related inflammatory activity.

When radiological FDG-PET/CT interpretation was evaluated according to EBJIS classification, diagnostic performance was characterised by moderate sensitivity and consistently high specificity, resulting in a high negative predictive value. This pattern closely mirrored the findings from quantitative SUVmax analyses, where discrimination was strongest for certain anatomical components and limited for others. The concordant strengths and weaknesses

observed for radiological interpretation and SUVmax suggest that both methods reflect similar underlying biological signals rather than independent diagnostic phenomena. A notable contrast to the findings of Kiran et al. (2019) is the different balance between sensitivity and specificity. Whereas that study reported very high sensitivity but low specificity for FDG-PET when evaluated according to MSIS criteria, the present study demonstrated more moderate sensitivity but higher specificity within the EBJIS framework. This difference likely reflects variations in reference standard, analytical approach, and the biological nature of FDG uptake, which reflects inflammatory activity rather than infection per se. Importantly, both studies demonstrated a similarly high negative predictive value, supporting the role of FDG-PET primarily as a tool to exclude infection rather than confirm it.

Diagnostic performance varied by anatomical component. Both tracers showed limited ability to discriminate infection in acetabular cups, illustrating the importance of cautious interpretation of PET/CT findings in this region and integration with clinical and surgical context. Reduced discrimination behind the acetabular cup may partly reflect the heterogeneous anatomical distribution of PJI, since infection does not involve all implant interfaces. In contrast, involvement of the femoral side may be more readily detected in some cases. The intramedullary environment of long bones may facilitate microbial persistence and spread, although evidence comparing anatomical distribution remains limited. Technical and biological factors—including implant fixation, local inflammatory response, and tracer-specific uptake mechanisms—likely also contribute to the observed differences in diagnostic performance.

Reduced performance for femoral components in TKA likely reflects a combination of postoperative bone adaptation, implant design, and technical challenges related to partial volume effects and metal artefacts (Gelderman et al., 2018; Mayer-Wagner et al., 2010; Sterner et al., 2007). These component-specific limitations reinforce the importance of interpreting PET/CT findings in conjunction with implant type, anatomical location, and clinical context rather than applying uniform diagnostic thresholds. Careful integration of imaging results with surgical history, implant characteristics, and patient-specific factors is therefore essential to avoid misclassification and to optimise diagnostic accuracy.

From a clinical perspective, the findings of Study IV support the targeted rather than generic use of PET/CT in evaluating painful arthroplasties. When infection is suspected, ¹⁸F-FDG PET/CT provides more clinically relevant information than ¹⁸F-fluoride PET/CT. In contrast, increased ¹⁸F-fluoride uptake should be interpreted with caution in this setting, as it may reflect non-infectious bone remodelling rather than infection. These results are consistent

with current EBJIS and consensus-based diagnostic approaches, which emphasise that imaging should serve as an adjunct rather than a standalone diagnostic test (*International Consensus Meeting 2025, ICM Istanbul, 2025*; McNally et al., 2021).

Notably, semi-quantitative SUVmax analysis performed by an orthopaedic surgeon demonstrated diagnostic performance comparable to expert radiological interpretation, suggesting that structured quantitative assessment may reduce observer dependency and increase the clinical accessibility of PET/CT in orthopaedic practice.

Across analyses, 18F-FDG PET/CT consistently demonstrated high negative predictive value, supporting its primary clinical role as a tool to exclude rather than confirm infection.

Collectively, Study IV clarifies the complementary but non-interchangeable roles of PET tracers in evaluating arthroplasty complications. The findings support a pathophysiology-driven selection of imaging modalities, in which tracer choice is guided by the dominant clinical question—mechanical instability or suspected infection—rather than by availability alone.

7.3 Limitations

7.3.1 Study I

Our study was limited by its *post hoc* analysis and by a sample size initially designed to investigate pBMD rather than inflammatory markers. These limitations may have led to type II errors, as most inflammatory markers showed no significant differences between treatment groups. We validated the PEA-derived findings for RANKL through ELISA, confirming substantial RANKL upregulation with denosumab treatment, particularly at three months. TNFRSF9 was temporarily downregulated at three months but returned to baseline levels by six months. Unexpectedly elevated RANKL levels suggest potential interference with PEA measurement, although PEA technology generally prevents cross-reactivity due to its unique DNA-binding mechanism (Assarsson et al., 2014).

7.3.2 Study II

Study II has several limitations that should be considered when interpreting the findings. First, the five-year follow-up represents an exploratory extension of a previously conducted RCT and was not pre-specified in the original study protocol or trial registration. Consequently, no formal sample size calculation was performed for the mid-term analyses, and the study was not powered to

detect small between-group differences in pBMD or rare clinical events. The absence of statistically significant differences should therefore be interpreted in the context of limited statistical power.

Second, the study population was highly selected. Inclusion was restricted to non-osteoporotic patients <65 years, with unilateral hip OA and a relatively low comorbidity burden. While this reflects clinical practice for uncemented THA at the time of study initiation, it limits the generalisability of the findings to older patients, individuals with osteoporosis, those with bilateral disease, or individuals at higher fracture risk. These restrictions may also have reduced the likelihood of detecting clinically meaningful effects of antiresorptive treatment.

Third, denosumab exposure was limited to two doses administered during the first postoperative year. This short treatment duration was sufficient to demonstrate a clear early pharmacological effect on periprosthetic bone loss but may have been inadequate to influence longer-term bone remodelling. The study design did not include a predefined post-treatment strategy, such as sequential anti-resorptive therapy, which is now recommended in other clinical contexts following denosumab discontinuation (Kim et al., 2022; Lamy et al., 2017; Martín-Pérez et al., 2025; Sølling et al., 2021; Tsourdi et al., 2017). Whether alternative treatment durations or sequential regimens could modify long-term periprosthetic bone preservation cannot be addressed by the present data.

Fourth, pBMD was used as the primary outcome measure. Although pBMD is a well-established and reproducible surrogate marker, its relationship with clinically relevant endpoints, including implant fixation, migration, and long-term revision risk, remains uncertain. The study did not include radiostereometric analysis, which could have provided more sensitive information on early micromotion and implant stability. Radiostereometric analysis was not performed due to concerns regarding cumulative radiation exposure in participants who also underwent PET examinations during the early follow-up period.

Fifth, clinical outcomes such as implant revision, HO, and vertebral fractures were secondary or exploratory endpoints. The study was not powered to detect differences in these outcomes, and a systematic assessment of vertebral fractures was not part of the protocol. Thoracolumbar spine radiographs were only obtained in participants reporting back pain, meaning that asymptomatic non-clinical vertebral fractures may have gone undetected.

Finally, under ethical approval, registry data or medical records of participants lost to follow-up could not be accessed. As a result, no outcome data are available for these individuals, and potential differences between participants who attended the five-year follow-up and those who did not cannot be excluded.

7.3.3 Study III

This retrospective study evaluated the diagnostic accuracy of 18F-fluoride PET/CT for detecting implant loosening, with surgical confirmation as the reference standard. Surgeons were not blinded to the PET/CT results, which may have influenced their intraoperative assessment. This lack of blinding, combined with varied reasons for revision surgery, introduces a potential confirmation bias that could be mitigated in a prospective, blinded study.

All revisions were performed at a single unit by experienced surgeons; however, the retrospective nature of the study led to inconsistencies in documenting implant stability during surgery. Detailed categorisations of implant stability were lacking, and our interpretation of the operative notes was likely less precise than that of standardised protocols.

The small cohort size led to substantial uncertainty in the estimates of sensitivity and specificity, particularly for SUVmax thresholds. The absence of significant differences in SUVmax for femoral TKA components may be attributable to the small sample size. Moreover, SUVmax values are not universally comparable across different PET/CT devices, although technical calibration can mitigate this issue (De Luca & Habraken, 2022).

The study included various implants and fixation methods, which affected results due to differences in bone metabolism around cemented versus cementless implants. The lower accuracy of SUVmax around femoral TKA components, typically made of cobalt-chromium alloys, may be due to greater photon attenuation by these denser materials than by titanium (Konishi et al., 2021; Suh et al., 2020).

Including both PJI and non-PJI patients was a potential limitation. Sensitivity analysis excluding PJI patients improved diagnostic accuracy, supporting the method's validity for non-infected cases. However, distinguishing between infected and non-infected patients is challenging (Adesanya et al., 2015), and some low-grade infections may have been misclassified.

SUVmax measurements were performed by novice observers, trained by an expert, which, despite excellent reliability, represents a limitation. Another concern was the inconsistent intervals between PET/CT scans and revision surgeries; in one instance, the interval was three years. This variability complicates comparisons, as implant loosening might progress to infection over time, or well-fixed implants may eventually become loose.

Lastly, the timing of PET/CT relative to the initial arthroplasty varied: two scans were performed less than a year post-surgery, which may reflect post-operative bone metabolism rather than implant loosening. Further studies are needed to refine these findings and address the noted limitations.

7.3.4 Study IV

A small cohort overlap between Study III and Study IV ($n = 11$) constitutes a methodological limitation. In eight cases, the same ^{18}F -fluoride PET/CT examination was used in both studies, with SUVmax independently recalculated according to study-specific analytical protocols. Although the studies addressed different research questions, the partial reuse of imaging data introduces some degree of non-independence between the cohorts, which should be acknowledged when interpreting the results. But there are several other limitations that warrant consideration when interpreting the findings of study IV.

First, the study was retrospective in design and based on clinically indicated PET/CT examinations. Although this reflects real-world diagnostic practice in patients with arthroplasties that are diagnostically challenging, it also introduces the risk of selection bias. The study population represents a subgroup in whom conventional diagnostic work-up was inconclusive, and the results may therefore not be directly generalisable to unselected arthroplasty populations or to routine screening settings.

Second, although the EBJIS criteria (McNally et al., 2021) provided the reference standard for infection classification, its status as a ‘gold standard’ is not without caveat. In the context of low-grade or culture-negative PJI, the risk of misclassification remains an inherent challenge that may have subtly skewed the diagnostic accuracy estimates for both tracers. Notably, by intentionally excluding imaging findings from the EBJIS classification, we successfully mitigated incorporation bias; however, this also highlights the inherent limitations of validating novel imaging against a composite standard that is itself subject to clinical interpretation (McNally et al., 2021).

Third, the study cohort was heterogeneous in implant design, fixation method, and time since index surgery. Although component-level analyses were employed to account for anatomical differences, the potential for residual confounding—driven by implant-specific geometry, baseline bone stock, and idiosyncratic remodelling patterns—cannot be entirely dismissed. Furthermore, the modest sample size within individual subgroups precluded robust stratified analyses, limiting the granularity of our conclusions regarding specific implant types.

Fourth, tracer uptake was quantified using SUVmax. Although this metric is favoured for its reproducibility and widespread clinical use, it remains inherently sensitive to technical factors, including scanner-specific characteristics, reconstruction algorithms, and partial volume effects—a limitation well-documented in PET/CT literature (Czernin et al., 2010; Even-Sapir et al., 2007). To mitigate this limitation, we used a single PET/CT system and a standardised imaging protocol. Nevertheless, the absolute SUVmax values

and exploratory thresholds identified in this study should be interpreted as institution-specific and may not be directly transferable to centres using different hardware or processing pipelines.

Fifth, the interpretability of PET/CT findings is inherently component-specific. We observed diminished diagnostic performance in certain anatomical regions, most notably the acetabular cups and femoral components of TKAs. These regional discrepancies likely arise from a complex interplay of prolonged physiological remodelling, implant-specific stress shielding, and technical hurdles—specifically metal artefacts and the relative sparsity of periprosthetic bone volume available for analysis. Hence, negative or equivocal results in these specific locations warrant a high degree of clinical caution to avoid false-negative interpretations.

Finally, although intra- and interobserver reliability for ^{18}F -FDG SUV_{max} measurements was generally robust, reproducibility fluctuated across specific components. This variability highlights that quantitative PET/CT interpretation remains contingent on clinical expertise and rigorous standardisation; consequently, simplified numerical thresholds cannot entirely replace qualitative assessment. Such findings align with existing literature on observer variability in PET/CT evaluation (Basu et al., 2014; Verberne et al., 2018) and reinforce the need for a nuanced, rather than purely algorithmic, diagnostic approach.

8 Conclusion and clinical implications

The studies comprising this thesis offer novel insights into the dynamics of periprosthetic bone remodelling, the efficacy of pharmacological intervention in modulating bone turnover, and the diagnostic utility of advanced molecular imaging following total joint arthroplasty. In non-osteoporotic cohorts undergoing uncemented THA, short-term denosumab treatment successfully attenuated early periprosthetic bone resorption and suppressed systemic biochemical markers of bone turnover. However, these biological effects proved transient and were not sustained at the five-year follow-up. This observation suggests that while potent antiresorptive therapy can temporarily decouple the remodelling process, it does not fundamentally or permanently alter the long-term trajectory of periprosthetic bone metabolism in patients with healthy baseline bone quality.

Following treatment discontinuation, a distinct rebound phenomenon was observed, characterised by a surge in biochemical bone turnover markers and a sharp upregulation of RANKL expression. Proteomic profiling identified a pronounced increase in systemic RANKL within the first year after denosumab treatment, peaking at three months, whereas TNFRSF9 was downregulated. The absence of consistent changes in other inflammatory markers suggests that this response is specifically metabolic rather than globally inflammatory. These findings indicate that RANKL upregulation—potentially mediated by reverse signalling mechanisms and the sequestration of osteomorphs (McDonald et al., 2021)—may drive the rapid reversal of bone preservation observed upon treatment discontinuation.

From a clinical perspective, administering two doses of denosumab to prevent periprosthetic bone loss following uncemented THA is not recommended based on the present results. The transient nature of the response and the subsequent rebound effect suggest that this abbreviated regimen lacks long-term efficacy. Whether prolonged treatment or sequential therapy with alternative antiresorptive agents can yield sustained benefits without increasing risk remains speculative; such strategies warrant rigorous evaluation in specifically powered clinical trials before they can be considered for routine practice.

Advanced metabolic imaging has emerged as a significant adjunct to conventional diagnostic pathways for evaluating painful arthroplasties.

Quantitative ¹⁸F-fluoride PET/CT demonstrated high diagnostic accuracy and excellent reproducibility for detecting implant loosening in the THA cup, THA femoral stem, and tibial TKA component. In contrast, diagnostic performance was reduced for the femoral TKA component. In a pragmatic clinical setting that included patients with both aseptic loosening and low-grade infection, the method proved feasible and relatively easy to implement. When PJI could be reliably excluded by other diagnostic means, diagnostic accuracy improved further, supporting the interpretation that increased ¹⁸F-fluoride uptake reflects altered bone turnover and mechanical adaptation rather than infection-specific pathology. Further prospective studies incorporating standardised intraoperative fixation assessment and longitudinal follow-up are required to validate these findings and elucidate the technical or physiological drivers of the reduced performance observed in femoral TKA components.

In clinically ambiguous cases, ¹⁸F-FDG PET/CT demonstrated superior diagnostic performance for PJI compared with ¹⁸F-fluoride PET/CT. This finding indicates the importance of inflammatory rather than purely osteoblastic signalling in infection and highlights that increased bone turnover alone is not specific for the underlying cause of implant failure. From a clinical standpoint, these results indicate that PET tracers are not interchangeable, and the underlying diagnostic question should guide tracer selection. While ¹⁸F-fluoride PET/CT should primarily be regarded as an imaging biomarker of periprosthetic bone metabolism and implant fixation, ¹⁸F-FDG PET/CT may serve as a complementary modality for evaluating suspected infection when conventional diagnostics are inconclusive.

Within this clinical context, mechanistic models of aseptic loosening provide a conceptual framework for interpreting the observed findings. Experimental evidence has demonstrated that mechanical instability, intraarticular pressure fluctuations, and high-velocity interfacial fluid flow can trigger inflammatory activation and osteoclast recruitment at the bone–implant interface— independent of wear particle generation. These mechanobiological pathways potentially elucidate early osteolytic responses and the pronounced individual variability in susceptibility to periprosthetic bone loss. However, the extent to which such mechanisms drive the progression of late-stage aseptic loosening in humans remains elusive. Furthermore, direct clinical evidence bridging experimental mechanobiology with longitudinal shifts in periprosthetic bone density, systemic biomarkers, and *in vivo* imaging markers remains sparse.

In summary, this thesis supports the view that periprosthetic bone is a dynamic, mechanically sensitive tissue in which pharmacological modulation, metabolic imaging, and inflammatory signalling interact in a complex,

multifactorial manner. While short-term antiresorptive therapy can transiently attenuate early periprosthetic bone loss following uncemented THA, it fails to confer lasting protection against remodelling. Conversely, tracer-specific PET/CT imaging provides distinct, pathophysiology-driven data that significantly enhances the diagnostic evaluation of painful hip and knee arthroplasties. Future research should focus on integrating imaging biomarkers with systemic markers, mechanical risk factors, and longitudinal clinical data to improve the prediction of implant failure, distinguish between mechanical, particle-induced, and infectious mechanisms, and identify specific patient cohorts who may benefit from targeted preventive or therapeutic interventions.

9 Sammanfattning på svenska

Denna avhandling behandlar periprostetisk benmetabolism vid höft- och knäproteser och bygger på fyra studier. Två studier undersöker denosumab och dess påverkan på benomsättning, medan två studier utvärderar avancerad PET/CT-baserad bilddiagnostik för att analysera benremodellering, implantatfixation och periprostetisk infektion.

Studie I analyserade den biologiska effekten av denosumab på inflammatoriska och benrelaterade signalvägar efter ocementerad total höftprotes (THA). Behandlingen gav en selektiv biologisk respons med ökad systemisk RANKL-nivå och samtidig nedreglering av TNFRSF9, utan bred aktivering av andra inflammatoriska markörer. Denna riktade påverkan på RANK-RANKL-axeln ger en möjlig förklaring till den ökning i benomsättning och den snabba periprostetiska benförlust som observerades efter utsättning av behandlingen.

Studie II utvärderade långtidseffekterna av två doser denosumab på periprostetisk benmineralhalt fem år efter THA. Trots initial dämpning av benförlusten under första året sågs inga kvarstående skillnader mellan behandlings- och placebogrupp vid fem år. Resultaten talar för att kortvarig anti-resorptiv behandling inte förändrar den långsiktiga, mekaniskt styrda benremodelleringen kring implantat och ifrågasätter den kliniska nyttan av behandlingen i denna patientgrupp.

Studie III undersökte den diagnostiska precisionen hos 18F-fluorid PET/CT för att identifiera aseptisk implantatlossning. Metoden visade hög diagnostisk träffsäkerhet och god reproducerbarhet för de flesta komponenter, särskilt vid höftproteser och i tibiakomponenten vid knäproteser. Däremot var prestandan lägre för femurkomponenten i knäproteser. Resultaten stödjer tolkningen att ökat fluoridupptag främst speglar förändrad benomsättning och mekanisk belastning snarare än infektion.

Studie IV jämförde 18F-FDG PET/CT och 18F-fluorid PET/CT vid misstänkt periprostetisk infektion, klassificerad enligt EBJIS-kriterier. FDG uppvisade överlag bättre diagnostisk förmåga än fluorid, med tydligast diskrimination i tibiakomponenten vid knäproteser och mer begränsad prestanda kring acetabularkomponenten. Den diagnostiska noggrannheten varierade mellan anatomiska regioner, och FDG visade genomgående hög negativ prediktiv

förmåga, vilket talar för en särskild roll i att utesluta infektion snarare än att bekräfta den. Sammantaget visar resultaten att FDG främst speglar inflammatorisk aktivitet, medan fluorid återspeglar benremodellering och mekanisk adaptation.

Sammanfattningsvis visar avhandlingen att periprostetiskt ben är en dynamisk och mekaniskt känslig vävnad där farmakologisk påverkan, inflammatorisk signalering och mekanisk belastning samverkar. Denosumab kan tillfälligt minska tidig benförlust men ger inga långsiktiga fördelar och kan följas av accelererad benomsättning efter utsättning. PET/CT-baserad metabol bilddiagnostik tillför däremot komplementär, biologiskt förankrad information som kan förbättra diagnostiken vid smärtsam protes. ¹⁸F-fluorid PET/CT är särskilt användbar för att påvisa mekanisk lossning, medan ¹⁸F-FDG PET/CT är mest värdefull för att utesluta infektion i diagnostiskt svårbedömda fall. Integrering av bilddiagnostik med kliniska, biomekaniska och biologiska markörer kan på sikt bidra till bättre prediktion av implantatsvikt och mer individualiserad behandling.

10 Acknowledgements

First and foremost, I wish to express my sincere gratitude to the **patients** whose clinical data contributed to the studies within this thesis. Their participation formed the essential foundation of this research and made these analyses possible.

I am deeply grateful to **Uppsala University** for providing a stimulating academic environment and for the privilege of pursuing doctoral studies alongside my clinical responsibilities. My thanks also go to **Akademiska sjukhuset** and **Region Uppsala** for supporting this research and providing the clinical infrastructure required to conduct these studies. The seamless integration of research and clinical practice has been vital to completing this work.

My deepest gratitude is extended to my main supervisor, **Professor Nils P. Hailer**, for his unwavering support throughout this doctoral project. His extensive scientific expertise, rigorous critical thinking, and commitment to high academic standards have been fundamental to both my development as a researcher and the quality of this thesis. I am particularly grateful for his ability to challenge assumptions, sharpen scientific arguments, and maintain a steadfast focus on clinically impactful research.

I also wish to thank **Professor Hans Mallmin** for his longstanding support and inspiration. He encouraged me early on to specialise in arthroplasty surgery—a decision that profoundly shaped my professional path. As the initiator of the DATA study, he laid the groundwork for much of the work presented here. His meticulous approach to research and insistence on precision have left a lasting imprint on my scientific practice.

My sincere thanks go to my co-supervisors: **Professor Jens Sörensen**, consultant in nuclear medicine, for his invaluable expertise and essential contributions to the PET/CT studies; **Associate Professor Stergios Lazarinis**, former Head of Department and long-standing clinical mentor, for his support, encouragement, and generosity as both a colleague and a dear friend; and **Anders Brüggemann**, my colleague in arthroplasty surgery, for his hands-on support and tireless practical assistance throughout the clinical and research phases of this work.

I am grateful to all my co-authors for their valuable contributions, collaboration, and constructive discussions, which were essential to the completion

of this thesis. Special thanks to **Eva Freyhult** (Study I) and **Tatevik Ghukasyan Lakić** (Study II) for their outstanding statistical support.

I would also like to acknowledge the leadership of **Marianne van Rooijen**, Hospital Director, who encouraged me to assume the role as Head of Department and always provided supportive and insightful counsel; her leadership remains a true inspiration. My thanks also go to **Henrik Olivero-Reinius**, Area Director, for his loyalty, trust, and genuine care, and to **Hans-Olov Hellström**, Deputy Hospital Director and orthopaedic surgeon, for his mentorship, guidance, and enduring support.

Special thanks are due to **Hanna Wistrand**, executive assistant, whose indispensable support with logistics, scheduling, and daily practicalities has been invaluable. I am also deeply grateful to **Viktor Näslund**, Deputy Head of Department, for stepping in to cover my responsibilities during the writing of this thesis, and to **Christian Carrwik** and the entire Clinic Management Team (**VLG**) for fostering the organisational conditions that made this work possible.

I want to thank **Catharina Strömstedt** and **Lena Karlsson** for their excellent research support, and **Arvid Johnsson** and **Nils Kraft**, medical students who contributed diligently to parts of Study III. My colleagues at the **Arthroplasty Section** deserve special thanks for their collaboration and support, in particular **Olof Nilsson** and **Jan Milbrink**. I am also grateful to all my **colleagues at the Department of Orthopaedics and Hand Surgery**—an incredibly dedicated group that has felt like an extended family. Your sense of community and shared commitment have meant more to me than I can express.

I would also like to thank **Professor Nick London**, with whom I completed a fellowship in Harrogate. His mentorship challenged me to become more independent and articulate as a surgeon, and his influence continues to shape my professional life.

I am forever grateful to **Jan Bonnerstig** and **Rolf Andersson**—both true role models—for laying the foundations of my training and for making me the orthopaedic surgeon I am today. This thesis is for you.

Financial support from **Skobranschens utvecklingsfond** is gratefully acknowledged.

My sincere thanks to **Leslie Shaps** for outstanding language editing—any remaining imperfections are entirely my own.

Beyond academia and clinical work, I wish to thank **Mikael Andersson**, a family friend and invaluable support, for help with everything from practical problem-solving at home to childcare. My sincere thanks also go to **Stig and Lena Granefjäll** for their generous support of my whole family and for taking

such wonderful care of Oswald as honorary grandparents. Warmest thanks to our newest family member, our loyal au pair, and cherished ‘big sister’, **Lara Bäni**.

I am deeply grateful to **Miriam Wadström**, colleague, close friend, and true partner in crime, for her unwavering support throughout my journey, and to **Pernilla and Tommy Roos**, our closest friends, who have followed me through life since our ‘Flygvapenungdom’ days, through every high and low. Pernilla, with rare courage and honesty, has also been the one to remind me that there is a world beyond research — and that life should be lived, not only studied.

I thank the rest of my family and dear friends for your constant patience and encouragement. My deepest gratitude goes to my beloved mother, **Gunhild Nyquist**, for her lifelong love and support; to my late father, **Claes Nyquist**, who is dearly missed but forever present in my heart and in the person I have become; and to my dearest mother-in-law, **Riitta Sköld**, for her warmth, kindness, and unwavering support to our family.

Finally, I thank **Fredrik and Sophie**, my precious children, for filling life with laughter, perspective, and constant reminders of what truly matters — and **Osvald**, our faithful companion, for his quiet loyalty and unconditional presence.

Last, and most importantly, I thank my husband, **Torbjörn**. My equal in both thought and silliness, my sharpest conversational partner, and the one who never fails to make me laugh — even in the midst of deadlines and footnotes. Thank you for keeping my feet on the ground while always standing beside me. Your wisdom, love, and unwavering support have carried me through this journey more than you know, and life with you is richer, lighter, and far more fun.

11 Use of Artificial Intelligence

During the preparation of this thesis, artificial intelligence tools based on large language models were used in a limited and supportive manner for language revision, clarity improvement, and academic text structuring. These tools were not used to generate scientific data, perform statistical analyses, conduct independent literature searches, interpret imaging, or produce scientific conclusions.

The study design, data acquisition, image evaluation, statistical analyses, and interpretation of results were conducted by the author and co-authors. All AI-assisted text was rigorously reviewed, revised, and verified by the author to ensure accuracy, factual correctness, and strict adherence to academic and ethical standards. The author assumes full responsibility for the entire content and integrity of this thesis.

Some figures were created and/or refined with the assistance of AI-based tools. All images are original and the copyright is held by the author unless other is stated. Relevant sources of inspiration are acknowledged where appropriate.

12 References

- Adesanya, O., Sprowson, A., Masters, J., & Hutchinson, C. (2015). Review of the role of dynamic 18F-NaF PET in diagnosing and distinguishing between septic and aseptic loosening in hip prosthesis. *J Orthop Surg Res, 10*, 5. <https://doi.org/10.1186/s13018-014-0147-7>
- Affatato, S. (2015). The history of total knee arthroplasty (TKA). In *Surgical Techniques in Total Knee Arthroplasty and Alternative Procedures* (pp. 3–16). Elsevier. <https://doi.org/10.1533/9781782420385.1.3>
- Anastasilakis, A. D., Polyzos, S. A., Makras, P., Aubry-Rozier, B., Kaouri, S., & Lamy, O. (2017). Clinical Features of 24 Patients with Rebound-Associated Vertebral Fractures After Denosumab Discontinuation: Systematic Review and Additional Cases. *Journal of Bone and Mineral Research: The Official Journal of the American Society for Bone and Mineral Research, 32*(6), 1291–1296. <https://doi.org/10.1002/jbmr.3110>
- Araz, M., Aras, G., & Kùçük, Ö. N. (2015). The role of 18F-NaF PET/CT in metastatic bone disease. *Journal of Bone Oncology, 4*(3), 92–97. <https://doi.org/10.1016/j.jbo.2015.08.002>
- Argenson, J.-N. A., Parratte, S., Ashour, A., Saintmard, B., & Aubaniac, J.-M. (2012). The outcome of rotating-platform total knee arthroplasty with cement at a minimum of ten years of follow-up. *Journal of Bone and Joint Surgery. American Volume, 94*(7), 638–644. <https://doi.org/10.2106/JBJS.K.00263>
- Aro, H. T. (2021). The potential use of denosumab in patients with arthroplasty. *The Lancet. Rheumatology, 3*(3), e165–e166. [https://doi.org/10.1016/S2665-9913\(20\)30447-1](https://doi.org/10.1016/S2665-9913(20)30447-1)
- Aro, H. T., Nazari-Farsani, S., Vuopio, M., Löyttyniemi, E., & Mattila, K. (2019). Effect of Denosumab on Femoral Periprosthetic BMD and Early Femoral Stem Subsidence in Postmenopausal Women Undergoing Cementless Total Hip Arthroplasty. *JBMR Plus, 3*(10), e10217. <https://doi.org/10.1002/jbm4.10217>
- Aspenberg, P., & Herbertsson, P. (1996). Periprosthetic bone resorption. Particles versus movement. *The Journal of Bone and Joint Surgery. British Volume, 78*(4), 641–646.
- Assarsson, E., Lundberg, M., Holmquist, G., Björkesten, J., Thorsen, S. B., Ekman, D., Eriksson, A., Rennel Dickens, E., Ohlsson, S., Edfeldt, G., Andersson, A.-C., Lindstedt, P., Stenvang, J., Gullberg, M., & Fredriksson, S. (2014). Homogenous 96-plex PEA immunoassay exhibiting high sensitivity, specificity, and excellent scalability. *PloS One, 9*(4), e95192. <https://doi.org/10.1371/journal.pone.0095192>
- Basu, S., Kwee, T. C., Saboury, B., Garino, J. P., Nelson, C. L., Zhuang, H., Parsons, M., Chen, W., Kumar, R., Salavati, A., Werner, T. J., & Alavi, A. (2014). FDG PET for diagnosing infection in hip and knee prostheses: Prospective study in 221 prostheses and subgroup comparison with combined (111) In-labelled leucocyte/(99m) Tc-sulfur colloid bone marrow imaging in 88 prostheses.

- Clinical Nuclear Medicine*, 39(7), 609–615.
<https://doi.org/10.1097/RLU.0000000000000464>
- Berding, G., Kirchhoff, T. D., Burchert, W., von der Hoff, J., Zeidler, H., Hundeshagen, H., & Knapp, W. H. (1998). [18F] fluoride PET indicates reduced bone formation in severe glucocorticoid-induced osteoporosis. *Nuklearmedizin. Nuclear Medicine*, 37(2), 76–79.
- Bernhardsson, M., Sandberg, O., Ressler, M., Kozirowski, J., Malmquist, J., & Aspenberg, P. (2018). Shining dead bone-cause for cautious interpretation of [(18)F] NaF PET scans. *Acta Orthop*, 89(1), 124–127. <https://doi.org/10.1080/17453674.2017.1372097>
- Bernstein, P., Beuthien-Baumann, B., Kotzerke, J., Hofheinz, F., Zessin, J., Stiehler, M., & Günther, K.-P. (2014). Periacetabular bone metabolism following hip revision surgery. PET-based evaluation of allograft osteointegration. *Nuklearmedizin. Nuclear Medicine*, 53(4), 147–154. <https://doi.org/10.3413/Nukmed-0607-13-06>
- Bijlsma, J. W., Berenbaum, F., & Lefeber, F. P. (2011). Osteoarthritis: An update with relevance for clinical practice. *The Lancet*, 377(9783), 2115–2126. [https://doi.org/10.1016/S0140-6736\(11\)60243-2](https://doi.org/10.1016/S0140-6736(11)60243-2)
- Black, D. M., Delmas, P. D., Eastell, R., Reid, I. R., Boonen, S., Cauley, J. A., Cosman, F., Lakatos, P., Leung, P. C., Man, Z., Mautalen, C., Mesenbrink, P., Hu, H., Caminis, J., Tong, K., Rosario-Jansen, T., Krasnow, J., Hue, T. F., Sellmeyer, D., ... HORIZON Pivotal Fracture Trial. (2007). Once-yearly zoledronic acid for treatment of postmenopausal osteoporosis. *The New England Journal of Medicine*, 356(18), 1809–1822. <https://doi.org/10.1056/NEJMoa067312>
- Blau, M., Nagler, W., & Bender, M. A. (1962). Fluorine-18: A new isotope for bone scanning. *Journal of Nuclear Medicine: Official Publication, Society of Nuclear Medicine*, 3, 332–334.
- Bodén, H. S. G., Sköldenberg, O. G., Salemyr, M. O. f, Lundberg, H.-J., & Adolphson, P. Y. (2006). Continuous bone loss around a tapered uncemented femoral stem: A long-term evaluation with DEXA. *Acta Orthopaedica*, 77(6), 877–885. <https://doi.org/10.1080/17453670610013169>
- Bolamperti, S., Villa, I., & Rubinacci, A. (2022). Bone remodeling: An operational process ensuring survival and bone mechanical competence. *Bone Research*, 10(1), 48. <https://doi.org/10.1038/s41413-022-00219-8>
- Bondeson, J., Blom, A. B., Wainwright, S., Hughes, C., Caterson, B., & van den Berg, W. B. (2010). The role of synovial macrophages and macrophage-produced mediators in driving inflammatory and destructive responses in osteoarthritis. *Arthritis and Rheumatism*, 62(3), 647–657. <https://doi.org/10.1002/art.27290>
- Bone, H. G., Bolognese, M. A., Yuen, C. K., Kendler, D. L., Miller, P. D., Yang, Y.-C., Grazette, L., San Martin, J., & Gallagher, J. C. (2011). Effects of Denosumab Treatment and Discontinuation on Bone Mineral Density and Bone Turnover Markers in Postmenopausal Women with Low Bone Mass. *The Journal of Clinical Endocrinology & Metabolism*, 96(4), 972–980. <https://doi.org/10.1210/jc.2010-1502>
- Bozic, K. J., Kamath, A. F., Ong, K., Lau, E., Kurtz, S., Chan, V., Vail, T. P., Rubash, H., & Berry, D. J. (2015). Comparative Epidemiology of Revision Arthroplasty: Failed THA Poses Greater Clinical and Economic Burdens Than Failed TKA. *Clinical Orthopaedics and Related Research*, 473(6), 2131–2138. <https://doi.org/10.1007/s11999-014-4078-8>
- Bratengeier, C., Bakker, A. D., Liszka, A., Schilcher, J., & Fahlgren, A. (2022). The release of osteoclast-stimulating factors on supraphysiological loading by

- osteoprogenitors coincides with expression of genes associated with inflammation and cytoskeletal arrangement. *Scientific Reports*, 12(1), 21578. <https://doi.org/10.1038/s41598-022-25567-7>
- Bratengeier, C., Liszka, A., Hoffman, J., Bakker, A. D., & Fahlgren, A. (2020). High shear stress amplitude in combination with prolonged stimulus duration determines induction of osteoclast formation by hematopoietic progenitor cells. *FASEB Journal: Official Publication of the Federation of American Societies for Experimental Biology*, 34(3), 3755–3772. <https://doi.org/10.1096/fj.201901458R>
- Brennan, F. M., & McInnes, I. B. (2008). Evidence that cytokines play a role in rheumatoid arthritis. *The Journal of Clinical Investigation*, 118(11), 3537–3545. <https://doi.org/10.1172/JCI36389>
- Brooker, A. F., Bowerman, J. W., Robinson, R. A., & Riley, L. H. J. (1973). Ectopic ossification following total hip replacement. Incidence and a method of classification. *The Journal of Bone and Joint Surgery. American Volume*, 55(8), 1629–1632.
- Buechel, F. F., & Pappas, M. J. (1986). The New Jersey Low-Contact-Stress Knee Replacement System: Biomechanical rationale and review of the first 123 cemented cases. *Archives of Orthopaedic and Traumatic Surgery. Archiv Fur Orthopadische Und Unfall-Chirurgie*, 105(4), 197–204. <https://doi.org/10.1007/BF00435480>
- Burger, E. H., & Klein-Nulend, J. (1999). Mechanotransduction in bone—Role of the lacuno-canalicular network. *FASEB Journal: Official Publication of the Federation of American Societies for Experimental Biology*, 13 Suppl, S101-112.
- Carver, W., Esch, A. M., Fowlkes, V., & Goldsmith, E. C. (2017). The Biomechanical Environment and Impact on Tissue Fibrosis. In B. Corradetti (Ed.), *The Immune Response to Implanted Materials and Devices* (pp. 169–188). Springer International Publishing. https://doi.org/10.1007/978-3-319-45433-7_9
- Cassuto, J., Folestad, A., Göthlin, J., Malchau, H., & Kärrholm, J. (2018). The key role of proinflammatory cytokines, matrix proteins, RANKL/OPG and Wnt/ β -catenin in bone healing of hip arthroplasty patients. *Bone*, 107, 66–77. <https://doi.org/10.1016/j.bone.2017.11.004>
- Charnley, J. (1960). Anchorage of the femoral head prosthesis to the shaft of the femur. *The Journal of Bone and Joint Surgery. British Volume*, 42-B, 28–30. <https://doi.org/10.1302/0301-620X.42B1.28>
- Chen, Q., Hu, C., Liu, Yanmei, Song, R., Zhu, W., Zhao, H., Nino, A., Zhang, F., & Liu, Yun. (2018). Pharmacokinetics, pharmacodynamics, safety, and tolerability of single-dose denosumab in healthy Chinese volunteers: A randomized, single-blind, placebo-controlled study. *PLoS One*, 13(6), e0197984. <https://doi.org/10.1371/journal.pone.0197984>
- Choe, H., Inaba, Y., Kobayashi, N., Ike, H., Aoki, C., Shizukuishi, K., Iwamoto, N., Yukizawa, Y., Ishida, T., Inoue, T., & Saito, T. (2011). Use of 18F-fluoride PET to determine the appropriate tissue sampling region for improved sensitivity of tissue examinations in cases of suspected periprosthetic infection after total hip arthroplasty. *Acta Orthop*, 82(4), 427–432. <https://doi.org/10.3109/17453674.2011.594232>
- Creutzig, H. (1976). Bone imaging after total replacement arthroplasty of the hip joint. A follow-up with different radiopharmaceuticals. *Eur J Nucl Med*, 1(3), 177–180.
- Cummings, S. R., Browner, W., Cummings, S. R., Black, D. M., Nevitt, M. C., Browner, W., Genant, H. K., Cauley, J., Ensrud, K., Scott, J., & Vogt, T. M.

- (1993). Bone density at various sites for prediction of hip fractures. *The Lancet*, 341(8837), 72–75. [https://doi.org/10.1016/0140-6736\(93\)92555-8](https://doi.org/10.1016/0140-6736(93)92555-8)
- Cummings, S. R., Ferrari, S., Eastell, R., Gilchrist, N., Jensen, J.-E. B., McClung, M., Roux, C., Törring, O., Valter, I., Wang, A. T., & Brown, J. P. (2018). Vertebral Fractures After Discontinuation of Denosumab: A Post Hoc Analysis of the Randomized Placebo-Controlled FREEDOM Trial and Its Extension. *Journal of Bone and Mineral Research: The Official Journal of the American Society for Bone and Mineral Research*, 33(2), 190–198. <https://doi.org/10.1002/jbmr.3337>
- Cummings, S. R., Martin, J. S., McClung, M. R., Siris, E. S., Eastell, R., Reid, I. R., Delmas, P., Zoog, H. B., Austin, M., Wang, A., Kutilek, S., Adami, S., Zanchetta, J., Libanati, C., Siddhanti, S., & Christiansen, C. (2009). Denosumab for Prevention of Fractures in Postmenopausal Women with Osteoporosis. *New England Journal of Medicine*, 361(8), 756–765. <https://doi.org/10.1056/NEJMoa0809493>
- Curtis, J. R., Arora, T., Liu, Y., Lin, T.-C., Spangler, L., Brunetti, V. C., Stad, R. K., McDermott, M., Bradbury, B. D., & Kim, M. (2024). Comparative effectiveness of denosumab vs alendronate among postmenopausal women with osteoporosis. *Journal of Bone and Mineral Research*, 39(7), 826–834. <https://doi.org/10.1093/jbmr/zjae079>
- Czermin, J., Satyamurthy, N., & Schiepers, C. (2010). Molecular mechanisms of bone 18F-NaF deposition. *J Nucl Med*, 51(12), 1826–1829. <https://doi.org/10.2967/jnumed.110.077933>
- Danielsson, L., & Lindberg, H. (1997). Prevalence of coxarthrosis in an urban population during four decades. *Clinical Orthopaedics and Related Research*, (342), 106–110.
- De Luca, G. M. R., & Habraken, J. B. A. (2022). Method to determine the statistical technical variability of SUV metrics. *EJNMMI Physics*, 9(1), 40. <https://doi.org/10.1186/s40658-022-00470-2>
- Delmas, P. D. (2008). Clinical potential of RANKL inhibition for the management of postmenopausal osteoporosis and other metabolic bone diseases. *Journal of Clinical Densitometry: The Official Journal of the International Society for Clinical Densitometry*, 11(2), 325–338. <https://doi.org/10.1016/j.jocd.2008.02.002>
- Delmas, P. D., Eastell, R., Garnero, P., Seibel, M. J., & Stepan, J. (2000). The Use of Biochemical Markers of Bone Turnover in Osteoporosis. *Osteoporosis International*, 11(0), S2–S17. <https://doi.org/10.1007/s001980070002>
- Digas, G., Kärrholm, J., & Thanner, J. (2006). Different loss of BMD using uncemented press-fit and whole polyethylene cups fixed with cement: Repeated DXA studies in 96 hips randomized to 3 types of fixation. *Acta Orthopaedica*, 77(2), 218–226. <https://doi.org/10.1080/17453670610045948>
- Duus, B. R., Boeckstyns, M., & Staeager, C. (1990). The natural course of radionuclide bone scanning in the evaluation of total knee replacement—A 2-year prospective study. *Clinical Radiology*, 41(5), 341–343. [https://doi.org/10.1016/s0009-9260\(05\)81699-x](https://doi.org/10.1016/s0009-9260(05)81699-x)
- Engl, C. A., Bobyn, J. D., & Glassman, A. H. (1987). Porous-coated hip replacement. The factors governing bone ingrowth, stress shielding, and clinical results. *The Journal of Bone and Joint Surgery. British Volume*, 69(1), 45–55. <https://doi.org/10.1302/0301-620X.69B1.3818732>
- Engl, C. A., McGovern, T. F., Bobyn, J. D., & Harris, W. H. (1992). A quantitative evaluation of periprosthetic bone-remodeling after cementless total hip

- arthroplasty. *The Journal of Bone and Joint Surgery. American Volume*, 74(7), 1009–1020.
- Even-Sapir, E., Mishani, E., Flusser, G., & Metser, U. (2007). 18F-Fluoride positron emission tomography and positron emission tomography/computed tomography. *Semin Nucl Med*, 37(6), 462–469. <https://doi.org/10.1053/j.semnuclmed.2007.07.002>
- Fahlgren, A., Bostrom, M. P. G., Yang, X., Johansson, L., Edlund, U., Agholme, F., & Aspenberg, P. (2010). Fluid pressure and flow as a cause of bone resorption. *Acta Orthopaedica*, 81(4), 508–516. <https://doi.org/10.3109/17453674.2010.504610>
- Fassio, A., Adami, G., Benini, C., Vantaggiato, E., Saag, K. G., Giollo, A., Lippolis, I., Viapiana, O., Idolazzi, L., Orsolini, G., Rossini, M., & Gatti, D. (2019). Changes in Dkk-1, sclerostin, and RANKL serum levels following discontinuation of long-term denosumab treatment in postmenopausal women. *Bone*, 123, 191–195. <https://doi.org/10.1016/j.bone.2019.03.019>
- Friedl, G., Radl, R., Stihsen, C., Rehak, P., Aigner, R., & Windhager, R. (2009). The effect of a single infusion of zoledronic acid on early implant migration in total hip arthroplasty. A randomized, double-blind, controlled trial. *The Journal of Bone and Joint Surgery. American Volume*, 91(2), 274–281. <https://doi.org/10.2106/JBJS.G.01193>
- Frost, H. M. (1987). Bone ‘mass’ and the ‘mechanostat’: A proposal. *The Anatomical Record*, 219(1), 1–9. <https://doi.org/10.1002/ar.1092190104>
- Frost, H. M. (1994). Wolff’s Law and bone’s structural adaptations to mechanical usage: An overview for clinicians. *The Angle Orthodontist*, 64(3), 175–188. [https://doi.org/10.1043/0003-3219\(1994\)064%3C0175:WLABSA%3E2.0.CO;2](https://doi.org/10.1043/0003-3219(1994)064%3C0175:WLABSA%3E2.0.CO;2)
- Frost, M. L., Moore, A. E., Siddique, M., Blake, G. M., Laurent, D., Borah, B., Schramm, U., Valentin, M.-A., Pellas, T. C., Marsden, P. K., Schleyer, P. J., & Fogelman, I. (2013). ¹⁸F-fluoride PET as a noninvasive imaging biomarker for determining treatment efficacy of bone active agents at the hip: A prospective, randomized, controlled clinical study. *Journal of Bone and Mineral Research: The Official Journal of the American Society for Bone and Mineral Research*, 28(6), 1337–1347. <https://doi.org/10.1002/jbmr.1862>
- Furlong, R. J., & Osborn, J. F. (1991). Fixation of hip prostheses by hydroxyapatite ceramic coatings. *The Journal of Bone and Joint Surgery. British Volume*, 73(5), 741–745. <https://doi.org/10.1302/0301-620X.73B5.1654336>
- Gallo, J., Goodman, S. B., Kontinen, Y. T., Wimmer, M. A., & Holinka, M. (2013). Osteolysis around total knee arthroplasty: A review of pathogenetic mechanisms. *Acta Biomater*, 9(9), 8046–8058. <https://doi.org/10.1016/j.actbio.2013.05.005>
- Gallo, J., Kaminek, P., Ticha, V., Rihakova, P., & Ditmar, R. (2002). Particle disease. A comprehensive theory of periprosthetic osteolysis: A review. *Biomed Pap Med Fac Univ Palacky Olomouc Czech Repub*, 146(2), 21–28.
- Geesink, R. G., de Groot, K., & Klein, C. P. (1987). Chemical implant fixation using hydroxyl-apatite coatings. The development of a human total hip prosthesis for chemical fixation to bone using hydroxyl-apatite coatings on titanium substrates. *Clinical Orthopaedics and Related Research*, (225), 147–170.
- Gelderman, S. J., Jutte, P. C., Boellaard, R., Ploegmakers, J. J. W., Vallez Garcia, D., Kampinga, G. A., Glaudemans, A., & Wouthuyzen-Bakker, M. (2018). (18)F-FDG-PET uptake in non-infected total hip prostheses. *Acta Orthop*, 89(6), 634–639. <https://doi.org/10.1080/17453674.2018.1525931>

- Gemmel, F., Van den Wyngaert, H., Love, C., Welling, M. M., Gemmel, P., & Palestro, C. J. (2012). Prosthetic joint infections: Radionuclide state-of-the-art imaging. *Eur J Nucl Med Mol Imaging*, 39(5), 892–909. <https://doi.org/10.1007/s00259-012-2062-7>
- Goldring, M. B., & Otero, M. (2011). Inflammation in osteoarthritis. *Current Opinion in Rheumatology*, 23(5), 471–478. <https://doi.org/10.1097/BOR.0b013e328349c2b1>
- Goodman, S. B., & Gallo, J. (2019). Periprosthetic Osteolysis: Mechanisms, Prevention and Treatment. *Journal of Clinical Medicine*, 8(12), 2091. <https://doi.org/10.3390/jcm8122091>
- Hallan, G., Lie, S. A., & Havelin, L. I. (2006). High wear rates and extensive osteolysis in 3 types of uncemented total hip arthroplasty: A review of the PCA, the Harris Galante and the Profile/Tri-Lock Plus arthroplasties with a minimum of 12 years median follow-up in 96 hips. *Acta Orthopaedica*, 77(4), 575–584. <https://doi.org/10.1080/17453670610012638>
- Harris, S. T., Watts, N. B., Genant, H. K., McKeever, C. D., Hangartner, T., Keller, M., Chesnut, C. H., Brown, J., Eriksen, E. F., Hoeseyni, M. S., Axelrod, D. W., & Miller, P. D. (1999). Effects of risedronate treatment on vertebral and non-vertebral fractures in women with postmenopausal osteoporosis: A randomized controlled trial. Vertebral Efficacy with Risedronate Therapy (VERT) Study Group. *JAMA*, 282(14), 1344–1352. <https://doi.org/10.1001/jama.282.14.1344>
- Harris, W. H. (1969). Traumatic arthritis of the hip after dislocation and acetabular fractures: Treatment by mold arthroplasty. An end-result study using a new method of result evaluation. *The Journal of Bone and Joint Surgery. American Volume*, 51(4), 737–755.
- Harris, W. H. (1995). The problem is osteolysis. *Clinical Orthopaedics and Related Research*, (311), 46–53.
- Hatzikotoulas, K., Southam, L., Stefansdottir, L., Boer, C. G., McDonald, M.-L., Pett, J. P., Park, Y.-C., Tuerlings, M., Mulders, R., Barysenka, A., Arruda, A. L., Tragante, V., Rocco, A., Bittner, N., Chen, S., Horn, S., Srinivasasainagendra, V., To, K., Katsoula, G., ... Zeggini, E. (2025). Translational genomics of osteoarthritis in 1,962,069 individuals. *Nature*, 641(8065), 1217–1224. <https://doi.org/10.1038/s41586-025-08771-z>
- Hu, M., Chen, G., Luo, L., & Shang, L. (2022). A Systematic Review and Meta-Analysis on the Accuracy of Fluorodeoxyglucose Positron Emission Tomography/Computerized Tomography for Diagnosing Periprosthetic Joint Infections. *Frontiers in Surgery*, 9, 698781. <https://doi.org/10.3389/fsurg.2022.698781>
- Huiskes, R. (1990). The various stress patterns of press-fit, ingrown, and cemented femoral stems. *Clinical Orthopaedics and Related Research*, (261), 27–38.
- Hunter, D. J., & Bierma-Zeinstra, S. (2019). Osteoarthritis. *The Lancet*, 393(10182), 1745–1759. [https://doi.org/10.1016/S0140-6736\(19\)30417-9](https://doi.org/10.1016/S0140-6736(19)30417-9)
- Insall, J. N., Lachiewicz, P. F., & Burstein, A. H. (1982). The posterior stabilized condylar prosthesis: A modification of the total condylar design. Two to four-year clinical experience. *The Journal of Bone and Joint Surgery. American Volume*, 64(9), 1317–1323.
- International Consensus Meeting 2025 ICM Istanbul*. (2025). https://www.icmortho.org/_files/ugd/34d74b_13778b1d82f9442784eadc4185af844b.pdf
- Jadvar, H., Desai, B., & Conti, P. S. (2015). Sodium 18F-fluoride PET/CT of bone, joint, and other disorders. *Semin Nucl Med*, 45(1), 58–65. <https://doi.org/10.1053/j.semnuclmed.2014.07.008>

- Kanakaris, N. K., & Giannoudis, P. V. (2015). Hip Heterotopic Ossification. In N. G. Lasanianos, N. K. Kanakaris, & P. V. Giannoudis (Eds), *Trauma and Orthopaedic Classifications* (pp. 425–427). Springer London. https://doi.org/10.1007/978-1-4471-6572-9_98
- Kanis, J. A. (1994). Assessment of fracture risk and its application to screening for postmenopausal osteoporosis: Synopsis of a WHO report. WHO Study Group. *Osteoporosis International: A Journal Established as Result of Cooperation between the European Foundation for Osteoporosis and the National Osteoporosis Foundation of the USA*, 4(6), 368–381. <https://doi.org/10.1007/BF01622200>
- Kärrholm, J., Herberts, P., Hultmark, P., Malchau, H., Nivbrant, B., & Thanner, J. (1997). Radiostereometry of hip prostheses. Review of methodology and clinical results. *Clinical Orthopaedics and Related Research*, (344), 94–110.
- Kellgren, J. H., & Lawrence, J. S. (1957). Radiological Assessment of Osteo-Arthrosis. *Annals of the Rheumatic Diseases*, 16(4), 494–502. <https://doi.org/10.1136/ard.16.4.494>
- Khan, M., Osman, K., Green, G., & Haddad, F. S. (2016). The epidemiology of failure in total knee arthroplasty: Avoiding your next revision. *The Bone & Joint Journal*, 98-B (1 Suppl A), 105–112. <https://doi.org/10.1302/0301-620X.98B1.36293>
- Kim, A. S., Girgis, C. M., & McDonald, M. M. (2022). Osteoclast Recycling and the Rebound Phenomenon Following Denosumab Discontinuation. *Current Osteoporosis Reports*, 20(6), 505–515. <https://doi.org/10.1007/s11914-022-00756-5>
- Kim, K., & Kim, S. J. (2021). Diagnostic role of PET or PET/CT for prosthetic joint infection: A systematic review and Meta-analysis. *Hellenic Journal of Nuclear Medicine*, 24(1), 83–93. <https://doi.org/10.1967/s002449912309>
- Kiran, M., Donnelly, T. D., Armstrong, C., Kapoor, B., Kumar, G., & Peter, V. (2019). Diagnostic utility of fluorodeoxyglucose positron emission tomography in prosthetic joint infection based on MSIS criteria. *The Bone & Joint Journal*, 101-B (8), 910–914. <https://doi.org/10.1302/0301-620X.101B8.BJJ-2018-0929.R2>
- Kiritopoulos, D., Nyström, A., Ullmark, G., Sörensen, J., Petrén-Mallmin, M., Milbrink, J., Hailer, N. P., & Mallmin, H. (2022). Denosumab prevents acetabular bone loss around an uncemented cup: Analysis of secondary outcomes in a randomized controlled trial. *Acta Orthopaedica*, 93, 709–720. <https://doi.org/10.2340/17453674.2022.4537>
- Kobayashi, N., Inaba, Y., Choe, H., Ike, H., Fujimaki, H., Tezuka, T., Hirata, Y., Tateishi, U., Inoue, T., & Saito, T. (2011). Use of F-18 fluoride PET to differentiate septic from aseptic loosening in total hip arthroplasty patients. *Clin Nucl Med*, 36(11), e156-61. <https://doi.org/10.1097/RLU.0b013e3182291ae7>
- Kobayashi, N., Inaba, Y., Uchiyama, M., Ike, H., Kubota, S., & Saito, T. (2016). Teriparatide Versus Alendronate for the Preservation of Bone Mineral Density After Total Hip Arthroplasty – A randomized Controlled Trial. *The Journal of Arthroplasty*, 31(1), 333–338. <https://doi.org/10.1016/j.arth.2015.07.017>
- Kong, Y. Y., Boyle, W. J., & Penninger, J. M. (1999). Osteoprotegerin ligand: A common link between osteoclastogenesis, lymph node formation and lymphocyte development. *Immunology and Cell Biology*, 77(2), 188–193. <https://doi.org/10.1046/j.1440-1711.1999.00815.x>
- Konishi, T., Shibusani, T., Okuda, K., Yoneyama, H., Moribe, R., Onoguchi, M., Nakajima, K., & Kinuya, S. (2021). Metal artifact reduction for improving

- quantitative SPECT/CT imaging. *Annals of Nuclear Medicine*, 35(3), 291–298. <https://doi.org/10.1007/s12149-020-01560-w>
- Koob, S., Gaertner, F. C., Jansen, T. R., Schmolders, J., Gravius, S., Strunk, H., Wirtz, D. C., & Essler, M. (2019). Diagnosis of peri-prosthetic loosening of total hip and knee arthroplasty using 18F-Fluoride PET/CT. *Oncotarget*, 10(22), 2203–2211. <https://doi.org/10.18632/oncotarget.26762>
- Kumar, R., Kumar, R., Kumar, V., & Malhotra, R. (2016a). Comparative analysis of dual-phase 18F-fluoride PET/CT and three phase bone scintigraphy in the evaluation of septic (or painful) hip prostheses: A prospective study. *J Orthop Sci*, 21(2), 205–210. <https://doi.org/10.1016/j.jos.2015.12.018>
- Kumar, R., Kumar, R., Kumar, V., & Malhotra, R. (2016b). Potential clinical implication of (18) F-FDG PET/CT in diagnosis of periprosthetic infection and its comparison with (18) F-Fluoride PET/CT. *J Med Imaging Radiat Oncol*, 60(3), 315–322. <https://doi.org/10.1111/1754-9485.12444>
- Kuo, T.-R., & Chen, C.-H. (2017). Bone biomarker for the clinical assessment of osteoporosis: Recent developments and future perspectives. *Biomarker Research*, 5(1), 18. <https://doi.org/10.1186/s40364-017-0097-4>
- Kurtz, S. M., Gawel, H. A., & Patel, J. D. (2011). History and Systematic Review of Wear and Osteolysis Outcomes for First-generation Highly Crosslinked Polyethylene. *Clinical Orthopaedics & Related Research*, 469(8), 2262–2277. <https://doi.org/10.1007/s11999-011-1872-4>
- Kwee, R. M., Broos, W. A., Brans, B., Walenkamp, G. H., Geurts, J., & Weijers, R. E. (2018). Added value of 18F-FDG PET/CT in diagnosing infected hip prosthesis. *Acta Radiol*, 59(5), 569–576. <https://doi.org/10.1177/0284185117726812>
- Kwee, R. M., & Kwee, T. C. (2020). 18F-FDG PET for Diagnosing Infections in Prosthetic Joints. *PET Clinics*, 15(2), 197–205. <https://doi.org/10.1016/j.cpet.2019.11.005>
- Lam, J., Takeshita, S., Barker, J. E., Kanagawa, O., Ross, F. P., & Teitelbaum, S. L. (2000). TNF- α induces osteoclastogenesis by direct stimulation of macrophages exposed to permissive levels of RANK ligand. *Journal of Clinical Investigation*, 106(12), 1481–1488. <https://doi.org/10.1172/JCI11176>
- Lamy, O., Gonzalez-Rodriguez, E., Stoll, D., Hans, D., & Aubry-Rozier, B. (2017). Severe Rebound-Associated Vertebral Fractures After Denosumab Discontinuation: 9 Clinical Cases Report. *The Journal of Clinical Endocrinology & Metabolism*, 102(2), 354–358. <https://doi.org/10.1210/jc.2016-3170>
- Lankinen, P. (2013). PET IMAGING OF OSTEOMYELITIS—Feasibility of 18F-FDG, 68Ga-chloride and 68Ga-DOTAVAP-P1 tracers in staphylococcal bone infections [PhD-thesis, University of Turku]. <https://www.utupub.fi/bitstream/handle/10024/90553/AnnalesD1076Lankinen.pdf?sequence=2>
- Lazarinis, S., Milbrink, J., Mattsson, P., Mallmin, H., & Hailer, N. P. (2014). Bone loss around a stable, partly threaded hydroxyapatite-coated cup: A prospective cohort study using RSA and DXA. *Hip International: The Journal of Clinical and Experimental Research on Hip Pathology and Therapy*, 24(2), 155–166. <https://doi.org/10.5301/hipint.5000104>
- Lekkerkerker, F., Kanis, J. A., Alsayed, N., Bouvenot, G., Burlet, N., Cahall, D., Chines, A., Delmas, P., Dreiser, R.-L., Ethgen, D., Hughes, N., Kaufman, J.-M., Korte, S., Kreutz, G., Laslop, A., Mitlak, B., Rabenda, V., Rizzoli, R., Santora, A., ... Group for the Respect of Ethics and Excellence in Science (GREES). (2007). Adherence to treatment of osteoporosis: A need for study. *Osteoporosis International: A Journal Established as Result of Cooperation between the European Foundation for Osteoporosis and the National*

- Osteoporosis Foundation of the USA*, 18(10), 1311–1317.
<https://doi.org/10.1007/s00198-007-0410-4>
- Liberman, U. A., Weiss, S. R., Bröll, J., Minne, H. W., Quan, H., Bell, N. H., Rodriguez-Portales, J., Downs, R. W., Dequeker, J., & Favus, M. (1995). Effect of oral alendronate on bone mineral density and the incidence of fractures in postmenopausal osteoporosis. The Alendronate Phase III Osteoporosis Treatment Study Group. *The New England Journal of Medicine*, 333(22), 1437–1443.
<https://doi.org/10.1056/NEJM199511303332201>
- Loharkar, S., & Basu, S. (2023). PET-Computed Tomography in Bone and Joint Infections. *PET Clinics*, 18(1), 49–69.
<https://doi.org/10.1016/j.cpet.2022.08.002>
- Lyles, K. W., Colón-Emeric, C. S., Magaziner, J. S., Adachi, J. D., Pieper, C. F., Mautalen, C., Hyldstrup, L., Recknor, C., Nordsletten, L., Moore, K. A., Lavecchia, C., Zhang, J., Mesenbrink, P., Hodgson, P. K., Abrams, K., Orloff, J. J., Horowitz, Z., Eriksen, E. F., Boonen, S., & HORIZON Recurrent Fracture Trial. (2007). Zoledronic acid and clinical fractures and mortality after hip fracture. *The New England Journal of Medicine*, 357(18), 1799–1809.
<https://doi.org/10.1056/NEJMoa074941>
- Martín-Pérez, M., Sánchez-Delgado, B., García-Poza, P., López-Álvarez, S., & Martín-Merino, E. (2025). Multiple vertebral fractures after antiosteoporotic medications discontinuation: A comparative study to evaluate the potential rebound effect of denosumab. *Bone*, 190, 117325.
<https://doi.org/10.1016/j.bone.2024.117325>
- Mayer-Wagner, S., Mayer, W., Maegerlein, S., Linke, R., Jansson, V., & Muller, P. E. (2010). Use of 18F-FDG-PET in the diagnosis of endoprosthetic loosening of knee and hip implants. *Arch Orthop Trauma Surg*, 130(10), 1231–1238.
<https://doi.org/10.1007/s00402-009-1000-z>
- Mayo, J. R. (1991). The high-resolution computed tomography technique. *Seminars in Roentgenology*, 26(2), 104–109. [https://doi.org/10.1016/0037-198X\(91\)90004-8](https://doi.org/10.1016/0037-198X(91)90004-8)
- McDonald, M. M., Khoo, W. H., Ng, P. Y., Xiao, Y., Zamerli, J., Thatcher, P., Kyaw, W., Pathmanandavel, K., Grootveld, A. K., Moran, I., Butt, D., Nguyen, A., Corr, A., Warren, S., Biro, M., Butterfield, N. C., Guilfoyle, S. E., Komla-Ebri, D., Dack, M. R. G., ... Phan, T. G. (2021). Osteoclasts recycle via osteomorphs during RANKL-stimulated bone resorption. *Cell*, 184(5), 1330-1347.e13.
<https://doi.org/10.1016/j.cell.2021.02.002>
- McNally, M., Sousa, R., Wouthuyzen-Bakker, M., Chen, A. F., Soriano, A., Vogely, H. C., Clauss, M., Higuera, C. A., & Trebše, R. (2021). The EBJIS definition of periprosthetic joint infection. *The Bone & Joint Journal*, 103-B (1), 18–25.
<https://doi.org/10.1302/0301-620X.103B1.BJJ-2020-1381.R1>
- Meneghini, R., & Hanssen, A. (2008). Cementless Fixation in Total Knee Arthroplasty – Past, Present, and Future. *Journal of Knee Surgery*, 21(04), 307–314.
<https://doi.org/10.1055/s-0030-1247837>
- Messa, C., Goodman, W. G., Hoh, C. K., Choi, Y., Nissenson, A. R., Salusky, I. B., Phelps, M. E., & Hawkins, R. A. (1993). Bone metabolic activity measured with positron emission tomography and [18F] fluoride ion in renal osteodystrophy: Correlation with bone histomorphometry. *J Clin Endocrinol Metab*, 77(4), 949–955. <https://doi.org/10.1210/jcem.77.4.8408470>
- Miller, P. D., Bolognese, M. A., Lewiecki, E. M., McClung, M. R., Ding, B., Austin, M., Liu, Y., & San Martin, J. (2008). Effect of denosumab on bone density and turnover in postmenopausal women with low bone mass after long-term continued, discontinued, and restarting of therapy: A randomized blinded phase 2

- clinical trial. *Bone*, 43(2), 222–229. <https://doi.org/10.1016/j.bone.2008.04.007>
- Mjöberg, B. (1994). Theories of wear and loosening in hip prostheses. Wear-induced loosening vs loosening-induced wear—A review. *Acta Orthopaedica Scandinavica*, 65(3), 361–371. <https://doi.org/10.3109/17453679408995473>
- Mjöberg, B. (1997). The theory of early loosening of hip prostheses. *Orthopedics*, 20(12), 1169–1175. <https://doi.org/10.3928/0147-7447-19971201-12>
- Mjöberg, B. (2018). Does particle disease really exist? *Acta Orthopaedica*, 89(1), 130–132. <https://doi.org/10.1080/17453674.2017.1373491>
- Mumme, T., Reinartz, P., Alfer, J., Müller-Rath, R., Buell, U., & Wirtz, D. C. (2005). Diagnostic values of positron emission tomography versus triple-phase bone scan in hip arthroplasty loosening. *Archives of Orthopaedic and Trauma Surgery*, 125(5), 322–329. <https://doi.org/10.1007/s00402-005-0810-x>
- Muren, O., Akbarian, E., Salemyr, M., Bodén, H., Eisler, T., Stark, A., & Sköldenberg, O. (2015). No effect of risedronate on femoral periprosthetic bone loss following total hip arthroplasty. A 4-year follow-up of 61 patients in a double-blind, randomized placebo-controlled trial. *Acta Orthopaedica*, 86(5), 569–574. <https://doi.org/10.3109/17453674.2015.1041846>
- Narayanan, P. (2013). Denosumab: A comprehensive review. *South Asian Journal of Cancer*, 2(4), 272–277. <https://doi.org/10.4103/2278-330X.119895>
- Nysted, M., Benum, P., Klaksvik, J., Foss, O., & Aamodt, A. (2011). Periprosthetic bone loss after insertion of an uncemented, customized femoral stem and an uncemented anatomical stem. A randomized DXA study with 5-year follow-up. *Acta Orthopaedica*, 82(4), 410–416. <https://doi.org/10.3109/17453674.2011.588860>
- Nyström, A., Kiritopoulos, D., Ullmark, G., Sörensen, J., Petrén-Mallmin, M., Milbrink, J., Hailer, N. P., & Mallmin, H. (2020). Denosumab Prevents Early Periprosthetic Bone Loss After Uncemented Total Hip Arthroplasty: Results from a Randomized Placebo-Controlled Clinical Trial. *Journal of Bone and Mineral Research*, 35(2), 239–247. <https://doi.org/10.1002/jbmr.3883>
- Ollivere, B., Wimhurst, J. A., Clark, I. M., & Donell, S. T. (2012). Current concepts in osteolysis. *The Journal of Bone and Joint Surgery. British Volume*, 94(1), 10–15. <https://doi.org/10.1302/0301-620X.94B1.28047>
- Olszta, M. J., Cheng, X., Jee, S. S., Kumar, R., Kim, Y.-Y., Kaufman, M. J., Douglas, E. P., & Gower, L. B. (2007). Bone structure and formation: A new perspective. *Materials Science and Engineering: R: Reports*, 58(3–5), 77–116. <https://doi.org/10.1016/j.mser.2007.05.001>
- Osaka, E., Okamura, Y., Yoshida, Y., Sugitani, M., & Tokuhashi, Y. (2019). Intra-articular ectopic ossification associated with denosumab administration for giant cell tumor of bone with intra-articular pathological fracture. *Journal of Orthopaedic Science: Official Journal of the Japanese Orthopaedic Association*, 24(3), 558–562. <https://doi.org/10.1016/j.jos.2016.12.026>
- Pozgan, U., Caglic, D., Rozman, B., Nagase, H., Turk, V., & Turk, B. (2010). Expression and activity profiling of selected cysteine cathepsins and matrix metalloproteinases in synovial fluids from patients with rheumatoid arthritis and osteoarthritis. *Biological Chemistry*, 391(5), 571–579. <https://doi.org/10.1515/BC.2010.035>
- Prasad, A. K., Tan, J. H. S., Bedair, H. S., Dawson-Bowling, S., & Hanna, S. A. (2020). Cemented vs. cementless fixation in primary total knee arthroplasty: A systematic review and meta-analysis. *EFORT Open Reviews*, 5(11), 793–798. <https://doi.org/10.1302/2058-5241.5.200030>

- Purdue, P. E., Koulouvaris, P., Potter, H. G., Nestor, B. J., & Sculco, T. P. (2007). The Cellular and Molecular Biology of Periprosthetic Osteolysis: *Clinical Orthopaedics and Related Research*, 454, 251–261. <https://doi.org/10.1097/01.blo.0000238813.95035.1b>
- Rabin, R., & Charro, F. D. (2001). EQ-SD: A measure of health status from the EuroQol Group. *Annals of Medicine*, 33(5), 337–343. <https://doi.org/10.3109/07853890109002087>
- Schiepers, C., Broos, P., Miserez, M., Bormans, G., & De Roo, M. (1998). Measurement of skeletal flow with positron emission tomography and 18F-fluoride in femoral head osteonecrosis. *Archives of Orthopaedic and Trauma Surgery*, 118(3), 131–135. <https://doi.org/10.1007/s004020050332>
- Schott, A. M., Cormier, C., Hans, D., Favier, F., Hausherr, E., Dargent-Molina, P., Delmas, P. D., Ribot, C., Sebert, J. L., Breart, G., & Meunier, P. J. (1998). How Hip and Whole-Body Bone Mineral Density Predict Hip Fracture in Elderly Women: The EPIDOS Prospective Study. *Osteoporosis International*, 8(3), 247–254. <https://doi.org/10.1007/s001980050061>
- Schwartz, A. M., Farley, K. X., Guild, G. N., & Bradbury, T. L. (2020). Projections and Epidemiology of Revision Hip and Knee Arthroplasty in the United States to 2030. *The Journal of Arthroplasty*, 35(6S), S79–S85. <https://doi.org/10.1016/j.arth.2020.02.030>
- Sheppard, A. J., Paravastu, S. S., Wojnowski, N. M., Osamor, C. C., Farhadi, F., Collins, M. T., & Saboury, B. (2023). Emerging Role of 18F-NaF PET/Computed Tomographic Imaging in Osteoporosis: A Potential Upgrade to the Osteoporosis Toolbox. *PET Clinics*, 18(1), 1–20. <https://doi.org/10.1016/j.cpet.2022.09.001>
- Shiers, L. G. (1954). Arthroplasty of the knee; preliminary report of new method. *The Journal of Bone and Joint Surgery. British Volume*, 36-B (4), 553–560. <https://doi.org/10.1302/0301-620X.36B4.553>
- Singh, J. A., Schleck, C., Harmsen, S., & Lewallen, D. (2016). Clinically important improvement thresholds for Harris Hip Score and its ability to predict revision risk after primary total hip arthroplasty. *BMC Musculoskeletal Disorders*, 17. <https://doi.org/10.1186/s12891-016-1106-8>
- Sköld, C., Kultima, K., Freyhult, E., Larsson, A., Gordh, T., Hailer, N. P., & Mallmin, H. (2022). Effects of denosumab treatment on the expression of receptor activator of nuclear kappa-B ligand (RANKL) and TNF-receptor TNFRSF9 after total hip arthroplasty—results from a randomized placebo-controlled clinical trial. *Osteoporosis International: A Journal Established as Result of Cooperation between the European Foundation for Osteoporosis and the National Osteoporosis Foundation of the USA*, 33(9), 1–8. <https://doi.org/10.1007/s00198-022-06423-w>
- Sköld, C., Sörensen, J., Brüggemann, A., & Hailer, N. P. (2025). Is 18 F-fluoride PET/CT an Accurate Tool to Diagnose Loosening After Total Joint Arthroplasty? *Clinical Orthopaedics and Related Research*, 483(3), 415–428. <https://doi.org/10.1097/CORR.0000000000003228>
- Sköldenberg, O. G., Bodén, H. S. G., Salemyr, M. O. F., Ahl, T. E., & Adolphson, P. Y. (2006). Periprosthetic proximal bone loss after uncemented hip arthroplasty is related to stem size: DXA measurements in 138 patients followed for 2-7 years. *Acta Orthopaedica*, 77(3), 386–392. <https://doi.org/10.1080/17453670610046307>
- Sköldenberg, O. G., Salemyr, M. O., Bodén, H. S., Ahl, T. E., & Adolphson, P. Y. (2011). The effect of weekly risedronate on periprosthetic bone resorption following total hip arthroplasty: A randomized, double-blind, placebo-controlled

- trial. *The Journal of Bone and Joint Surgery. American Volume*, 93(20), 1857–1864. <https://doi.org/10.2106/JBJS.J.01646>
- Skripitz, R., & Aspenberg, P. (2000). Pressure-induced periprosthetic osteolysis: A rat model. *Journal of Orthopaedic Research: Official Publication of the Orthopaedic Research Society*, 18(3), 481–484. <https://doi.org/10.1002/jor.1100180322>
- Söderman, P., & Malchau, H. (2001). Is the Harris hip score system useful to study the outcome of total hip replacement? *Clinical Orthopaedics and Related Research*, (384), 189–197. <https://doi.org/10.1097/00003086-200103000-00022>
- Sølling, A. S., Harsløf, T., & Langdahl, B. (2021). Treatment With Zoledronate Subsequent to Denosumab in Osteoporosis: A 2-Year Randomized Study. *Journal of Bone and Mineral Research: The Official Journal of the American Society for Bone and Mineral Research*, 36(7), 1245–1254. <https://doi.org/10.1002/jbmr.4305>
- Sommerfeldt, D. W., & Rubin, C. T. (2001). Biology of bone and how it orchestrates the form and function of the skeleton. *European Spine Journal: Official Publication of the European Spine Society, the European Spinal Deformity Society, and the European Section of the Cervical Spine Research Society*, 10 Suppl 2(Suppl 2), S86–95. <https://doi.org/10.1007/s005860100283>
- Son, H. J., Jeong, Y. J., Yoon, H. J., Wang, L., Kim, H. J., Park, J. H., & Kang, D. Y. (2016). Visual Pattern and Serial Quantitation of (18)F-Sodium Fluoride PET/CT in Asymptomatic Patients After Hip and Knee Arthroplasty. *Nucl Med Mol Imaging*, 50(4), 308–321. <https://doi.org/10.1007/s13139-016-0430-0>
- Sørensen, J., & Ullmark, G. (2009). PET scanning for evaluation of bone metabolism. *Acta Orthopaedica*, 80(6), 737–739. <https://doi.org/10.3109/17453670903487040>
- Sterner, T., Pink, R., Freudenberg, L., Jentzen, T., Quitmann, H., Bockisch, A., & Lör, F. (2007). The role of [18F] fluoride positron emission tomography in the early detection of aseptic loosening of total knee arthroplasty. *International Journal of Surgery*, 5(2), 99–104. <https://doi.org/10.1016/j.ijssu.2006.05.002>
- Stumpe, K. D. M., Nötzli, H. P., Zanetti, M., Kamel, E. M., Hany, T. F., Görres, G. W., von Schulthess, G. K., & Hodler, J. (2004). FDG PET for differentiation of infection and aseptic loosening in total hip replacements: Comparison with conventional radiography and three-phase bone scintigraphy. *Radiology*, 231(2), 333–341. <https://doi.org/10.1148/radiol.2312021596>
- Suh, D., Jo, W. L., Kim, S. C., Kim, Y. S., Kwon, S. Y., & Lim, Y. W. (2020). Comparative analysis of titanium coating on cobalt-chrome alloy in vitro and in vivo direct metal fabrication vs. Plasma spraying. *Journal of Orthopaedic Surgery and Research*, 15(1), 564. <https://doi.org/10.1186/s13018-020-02108-4>
- Sumner, D. R. (2015). Long-term implant fixation and stress-shielding in total hip replacement. *Journal of Biomechanics*, 48(5), 797–800. <https://doi.org/10.1016/j.jbiomech.2014.12.021>
- Sun, S. G., An Ma, B., Zhou, Y., Hua Zhang, M., & Yu Fan, Q. (2006). Effects of bone cement particles on the function of pseudocapsule-derived fibroblasts. *Acta Orthopaedica*, 77(2), 320–328. <https://doi.org/10.1080/17453670610046091>
- Suzuki, T., Sukezaki, F., Shibuki, T., Toyoshima, Y., Nagai, T., & Inagaki, K. (2018). Teriparatide Administration Increases Periprosthetic Bone Mineral Density After Total Knee Arthroplasty: A Prospective Study. *The Journal of Arthroplasty*, 33(1), 79–85. <https://doi.org/10.1016/j.arth.2017.07.026>

- Tabatabaei, M. S., & Ahmed, M. (2022). Enzyme-Linked Immunosorbent Assay (ELISA). *Methods in Molecular Biology (Clifton, N.J.)*, 2508, 115–134. https://doi.org/10.1007/978-1-0716-2376-3_10
- Temmerman, O. P. P., Raijmakers, P. G. H. M., Berkhof, J., Hoekstra, O. S., Teule, G. J. J., & Heyligers, I. C. (2005). Accuracy of diagnostic imaging techniques in the diagnosis of aseptic loosening of the femoral component of a hip prosthesis: A META-ANALYSIS. *The Journal of Bone and Joint Surgery. British Volume*, 87-B (6), 781–785. <https://doi.org/10.1302/0301-620X.87B6.15625>
- Thanner, J., Kärrholm, J., Malchau, H., & Herberts, P. (1999). Poor outcome of the PCA and Harris-Galante hip prostheses. Randomized study of 171 arthroplasties with 9-year follow-up. *Acta Orthopaedica Scandinavica*, 70(2), 155–162. <https://doi.org/10.3109/17453679909011255>
- Tsourdi, E., Langdahl, B., Cohen-Solal, M., Aubry-Rozier, B., Eriksen, E. F., Guañabens, N., Obermayer-Pietsch, B., Ralston, S. H., Eastell, R., & Zillikens, M. C. (2017). Discontinuation of Denosumab therapy for osteoporosis: A systematic review and position statement by ECTS. *Bone*, 105, 11–17. <https://doi.org/10.1016/j.bone.2017.08.003>
- Ullmark, G. (2020). Occult Hip Prosthetic Loosening Diagnosed by [18F] Fluoride-PET/CT. *Arthroplasty Today*, 6(3), 548–551. <https://doi.org/10.1016/j.artd.2020.06.003>
- Ullmark, G., Nilsson, O., Maripuu, E., & Sorensen, J. (2013). Analysis of bone mineralization on uncemented femoral stems by [18F]-fluoride-PET: a randomized clinical study of 16 hips in 8 patients. *Acta Orthop*, 84(2), 138–144. <https://doi.org/10.3109/17453674.2013.786632>
- Ullmark, G., Sorensen, J., Langstrom, B., & Nilsson, O. (2007). Bone regeneration 6 years after impaction bone grafting: A PET analysis. *Acta Orthop*, 78(2), 201–205. <https://doi.org/10.1080/17453670710013681>
- Ullmark, G., Sorensen, J., & Nilsson, O. (2009). Bone healing of severe acetabular defects after revision arthroplasty. *Acta Orthop*, 80(2), 179–183. <https://doi.org/10.3109/17453670902947416>
- Ullmark, G., Sorensen, J., & Nilsson, O. (2012). Analysis of bone formation on porous and calcium phosphate-coated acetabular cups: A randomised clinical [18F] fluoride PET study. *Hip Int*, 22(2), 172–178. <https://doi.org/10.5301/HIP.2012.9233>
- Ullmark, G., Sundgren, K., Milbrink, J., Nilsson, O., & Sorensen, J. (2011). Femoral Head Viability following Resurfacing Arthroplasty. A Clinical Positron Emission Tomography Study. *HIP International*, 21(1), 066–070. <https://doi.org/10.5301/hip.2011.6303>
- van Vliet, K. E., de Jong, V. M., Termaat, M. F., Schepers, T., van Eck-Smit, B. L. F., Goslings, J. C., & Schep, N. W. L. (2018). FDG-PET/CT for differentiating between aseptic and septic delayed union in the lower extremity. *Archives of Orthopaedic and Trauma Surgery*, 138(2), 189–194. <https://doi.org/10.1007/s00402-017-2806-8>
- Venesmaa, P. K., Kröger, H. P., Miettinen, H. J., Jurvelin, J. S., Suomalainen, O. T., & Alhava, E. M. (2001). Alendronate reduces periprosthetic bone loss after uncemented primary total hip arthroplasty: A prospective randomized study. *Journal of Bone and Mineral Research: The Official Journal of the American Society for Bone and Mineral Research*, 16(11), 2126–2131. <https://doi.org/10.1359/jbmr.2001.16.11.2126>
- Verberne, S. J., Temmerman, O. P. P., Vuong, B. H., & Raijmakers, P. G. (2018). Fluorodeoxyglucose positron emission tomography imaging for diagnosing

- periprosthetic hip infection: The importance of diagnostic criteria. *Int Orthop*, 42(9), 2025–2034. <https://doi.org/10.1007/s00264-018-3931-x>
- Vlad, S. C., Neogi, T., Aliabadi, P., Fontes, J. D. T., & Felson, D. T. (2011). No association between markers of inflammation and osteoarthritis of the hands and knees. *The Journal of Rheumatology*, 38(8), 1665–1670. <https://doi.org/10.3899/jrheum.100971>
- Walldius, B. (1957). Arthroplasty of the knee using an endoprosthesis. *Acta Orthopaedica Scandinavica. Supplementum*, 24, 1–112. <https://doi.org/10.3109/ort.1957.28.suppl-24.01>
- Wang, Y., Li, Y., Han, L., Wang, J., Zhang, C., Qi, E., Zhang, D., Zhang, X., Huan, Y., & Tian, J. (2022). 18F-FDG and 68 Ga-FAPI PET/CT for the evaluation of periprosthetic joint infection and aseptic loosening in rabbit models. *BMC Musculoskeletal Disorders*, 23(1), 592. <https://doi.org/10.1186/s12891-022-05537-w>
- W-Dahl, A., Kärrholm, J., Rogmark, C., Johansson, O., Thorén, A., Ighani Arani, P., Mohaddes, M., & Rolfson, O. (2025). *SAR - Swedish Arthroplasty Register. Annual report 2025* (p. 316). https://registercentrum.blob.core.windows.net/slr/r/Ledprotesregistret-A-rsrapport-2025_1-2-8P7uE2KKW.pdf
- Winkler, D. G. (2003). Osteocyte control of bone formation via sclerostin, a novel BMP antagonist. *The EMBO Journal*, 22(23), 6267–6276. <https://doi.org/10.1093/emboj/cdg599>
- Yamasaki, S., Masuhara, K., Yamaguchi, K., Nakai, T., Fuji, T., & Seino, Y. (2007). Risedronate reduces postoperative bone resorption after cementless total hip arthroplasty. *Osteoporosis International: A Journal Established as Result of Cooperation between the European Foundation for Osteoporosis and the National Osteoporosis Foundation of the USA*, 18(7), 1009–1015. <https://doi.org/10.1007/s00198-007-0339-7>

Acta Universitatis Upsaliensis

Digital Comprehensive Summaries of Uppsala Dissertations from the Faculty of Medicine 2235

Editor: The Dean of the Faculty of Medicine

A doctoral dissertation from the Faculty of Medicine, Uppsala University, is usually a summary of a number of papers. A few copies of the complete dissertation are kept at major Swedish research libraries, while the summary alone is distributed internationally through the series Digital Comprehensive Summaries of Uppsala Dissertations from the Faculty of Medicine. (Prior to January, 2005, the series was published under the title “Comprehensive Summaries of Uppsala Dissertations from the Faculty of Medicine”.)

Distribution: publications.uu.se
urn:nbn:se:uu:diva-580203



ACTA UNIVERSITATIS
UPSALIENSIS
2026